Spring 2020

Exosomes in Transmission and Blocking of Arthropod-Borne Flaviviral Infection and Pathogenesis

Wenshuo Zhou
Old Dominion University, zhouwenshuobiology@gmail.com

EXOSOMES IN TRANSMISSION AND BLOCKING OF ARTHROPOD-BORNE FLAVIVIRAL INFECTION AND PATHOGENESIS

by

Wenshuo Zhou

B.E. August 2011, China Pharmaceutical University, China

A Dissertation Submitted to the Faculty of
Old Dominion University in Partial Fulfilment of the
Requirements for the degree of

DOCTOR OF PHILOSOPHY

BIOMEDICAL SCIENCES

OLD DOMINION UNIVERSITY
March 2020

Approved by:

Hameeda Sultana (Director)

Girish Neelakanta (Member)

Emilia Oleszak (Member)

Willy Wriggers (Member)

ABSTRACT

EXOSOMES IN TRANSMISSION AND BLOCKING OF ARTHROPOD-BORNE FLAVIVIRAL INFECTION AND PATHOGENESIS

Wenshuo Zhou
Old Dominion University, 2020
Director: Dr. Hameeda Sultana

Vector-borne diseases (VBDs) are human illnesses that are transmitted by vectors such as ticks, mosquitoes, and fleas. These arthropods transmit infectious pathogens such as viruses, protozoa, and bacteria, to humans during their blood-feeding. According to the estimation of the WHO, billions of people are affected by VBDs worldwide, and about 700,000 deaths are reported annually. Currently, very few reliable VBDs control approaches and vaccines available to treat various VBDs. Additionally, approaches to control arthropod' proliferation and migration are difficult to develop. Furthermore, molecular determinants and mechanisms for the transmission are poorly understood. This work describes two studies identifying the novel role for exosomes in facilitating transmission of viral infectious material and viral infections.

The first study focused on tick-borne pathogen transmission via exosomes derived from several different cell types. The conclusions suggested that exosomes could protect full-length viral RNA genomes, and viral proteins from host immune surveillance. The results showed the exosomes assistance in the transmission of viral materials from infected cells to naïve cells leading to active viral replication in the recipient cells. The exosomal viral materials were highly infectious and replicative in

recipient cells. However, treatment with GW4869, a commercial inhibitor for neutral Sphingomyelinases that mediated-exosome formation and release, resulted in reduced viral transmission via exosomes and affected the viral replication in recipient cells. These findings suggested a novel and promising therapeutic approach to block exosome-mediated viral transmission from arthropods to humans.

The second study demonstrated mosquito-borne arboviruses used exosomes for dissemination and infection of recipient vertebrate host cells as well. Results showed that ZIKV uses exosomes as mediators of viral transmission, and readily infected these neuronal cells. Neuronal exosomes enclosed both ZIKV viral RNA and proteins inside. Furthermore, the results addressed ZIKV induced both activity and gene expression of neutral Sphingomyelinase (nSMase)-2/SMPD3, a critical molecule regulates the formation and release of exosomes. The silencing of SMPD3 in neuronal cells resulted in decreased viral burden and dissemination via exosomes. Overall, this research elucidated that ZIKV mediated SMPD3 activity in cortical neurons for its infection and transmission through exosomes, perhaps caused severe neuronal death that result in neurological manifestations.

This manuscript is dedicated to my parents Liren Zhou and Ying Qu.
To my supportive and amazing girlfriend Lindsay Park.

ACKNOWLEDGMENTS

This project would not have been finished without the assistance and support of many people. I would like to express my sincere and highest respect and appreciation to my principal mentor and committee chair, Dr. Hameeda Sultana, for giving me the opportunity to study and perform research in the U.S and providing me all the assistance and guidance through my entire Ph.D. program. She continually showed me how to be a talented young researcher/scientist who should be full of enthusiasm, willing to take scientific adventures, and novel ideas. Her teaching skills, characteristics of hardworking, wisdom of knowledge, approaches of thinking, and solving problems, and achievements of managing labs have always inspired me. I have learned from her how to be a productive researcher with dedication and persistence. I appreciate all her efforts, time, ideas, patience, and funding that she has contributed to the past six years of my Ph.D. study. Without her assistance and guidance, I could not have finished this dissertation.

I would like to express my respect and appreciation to my co-mentor, Dr. Girish Neelakanta as well who has also contributed lots of precious scientific inputs to my research. By taking his graduate courses, I have gained an abundant of knowledge on Vector-borne disease, Microbiology, and Biotechnology. His level of thinking, professionalism, and experimental skills impressed me so much that all these memories should be my best examples to learn and follow.

Furthermore, I would like to thank my committee members, Drs. Emilia Oleszak and Willy Wriggers, for providing valuable suggestions on this academic work and for offering assistance on all my requirements, including structure courses, candidacy exam and prospectus writing throughout this Ph.D. dissertation.

I would acknowledge to all the assistance, valuable discussion, suggestions, relaxing happy time from all my colleagues, Drs. Ashish Vora, Vikas Taank, and other Ph.D. candidates Shovan Dutta and Supreet Khanal, Postdoctoral fellows Drs. Ellango Ramasamy, Waqas Ahmed and others, new Ph.D. students Ashkan Roozitalab and Mackenzie Tardif, Master students Pravesh Regmi and Jeremy Turck. They are all my friends and family members and have helped me so much in the past six years with no

hesitating encouragement, inspiration, and support, which made it much easier for me to complete this doctoral degree at old Dominion University.

My sincere acknowledgments should also go to Old Dominion University, Startup funds from Old Dominion University to Drs. Sultana and Neelakanta. The department of Biological Sciences provided me all the fantastic structural courses, advanced lab facilities, incredible research atmosphere, and professional, excellent mentors. My greatest appreciations go to the Department of Biological of Sciences and Drs. Sultana and Neelakanta for providing me with Dominion scholar research assistantship and teaching assistantship. I have learned a lot from teaching the undergraduates, and I have obtained great training from this precious teaching experience. I had a very unforgettable time with all the smart undergraduate students. These scholar assistantships have provided financial means as well to sustain me completing my graduate program.

An enormous late debt and gratitude are owed to my late father, Liren Zhou, who was so proud of me, dreamed of attending my graduation ceremony but just passed away just several months before my dissertation. Thanks a lot, to my late father that he had taught me how to be responsible, honest, patient, brave, earnest, and how to be a gentleman. My deepest appreciations go to my late father for providing me with a warm, lovely, comfortable home filled with good memories, positive influence, and happiness. It has been really an honor to be my father's son, I am so proud of my late father, and I would be proud forever. My heart will continually beat for him, and I would work harder in my future in order to be the man that he expected me to be. I promise I would be stronger, more successful and more talented to peace my late father in paradise. Great gratitude is also owed to my mother, Ying Qu, who loves and supports me unconditionally and incredibly. My life-partner, Lindsay Park, made many sacrifices to support the completion of my Ph.D. degree. She brings lots of happiness, hopes, and encouragement to me, especially after my father passing away, the darkest time in my life. Also, my thanks go to all my friends, such as my roommates, Yichao Yang and Anji Chen, and the graduate students from other departments who have supported me a lot throughout my entire Ph.D. program.

ABBREVIATIONS

Ab	Antibody
Am. Ticks	*Amblyomma maculatum* ticks
ATCC	American Type Culture Collection
BBB	Blood-Brain Barrier
CD molecules	Cluster of differentiation molecules
CDC	Centers for Disease Control and Prevention
CNS	Central Nervous system
Cryo-EM	Cryo-electron microscopy
DAPI	4′,6-diamidino-2-phenylindole
DENV	Dengue virus
DG	Density gradient
ELISA	Enzyme-Linked Immunosorbent Assay
EVs	Extracellular Vesicles
GAPDH	Glyceraldehyde-3-Phosphate Dehydrogenase
GBS	Guillain-Barré Syndrome
GFAP	Glial Fibrillary Acidic Protein
HCV	Hepatitis C virus
HIV	Human Immunodeficiency Virus
HSP	Heat Shock Protein
HUVEC	Human Vascular Endothelial Cells
Is. Ticks	*Ixodes scapularis* ticks
LGTV	Langat virus
LIV	Louping ill virus
MAP-2	Microtubule Associated Protein 2
MOI	Multiplicity of Infection
MTT	3-(4,5-dimethylthiazol-2-yl)-2,5-diphenyltetrazolium bromide
MVBs	Multi-Vesicular Bodies
NPCs	Neuronal precursor cells
p.i.	Post-infection

p.t.	Post-treatment
PHEIC	Public Health Emergency of International Concern
PNS	Peripheral Nervous System
POWV	Powassan virus
QRT-PCR	Quantitative Real-Time Polymerase Chain Reaction
SG	Salivary Gland
SIT	Sterile Insect Technique
SMPD3	Sphingomyelin phosphodiesterase 3
TBEV	Tick-borne encephalitis virus
TEM	Transmission electron microscope
UT	Untreated
VBDs	Vector-borne diseases
WHO	World Health Organization
WNV	West Nile Virus
ZIKV	Zika Virus

TABLE OF CONTENTS

Page

LIST OF FIGURES

CHAPTER 1

INTRODUCTION AND BACKGROUND

1.1 VECTOR-BORNE DISEASES

Vector-borne diseases (VBDs) are human illnesses that are transmitted by arthropods such as ticks, mosquitoes, fleas, sandflies, lice, and tsetse flies that are carrying viruses, bacteria, and parasites (Feinleib, 2001; Roberts and Janovy, 2009). Many deadliest VBDs such as malaria, dengue, yellow fever, Japanese encephalitis cause almost one million deaths annually. According to WHO 2019 reports, in over 128 countries, more than 3.9 billion people are at the risk of dengue infection (WHO, 2019). Malaria causes more than half a million deaths per year all over the world. VBDs account for more than 17% of all known infectious diseases' cases (WHO, 2019). VBDs distribution is determined by various factors such as environmental and social factors, global travel and trade, lacking medical knowledge in developing counties, complex demography and poverty, and mutations in pathogens caused by climate change and human activities (Feinleib, 2001; Roberts and Janovy, 2009). All these factors contribute to an unstable, uncertain situation to control, prevent, and estimate VBDs. Additionally, pathogen transmission is hard and complicated to predict. Many people die annually due to vector-borne diseases all over the world (WHO, 2004) (Figure 1).

Vectors

A vector is defined as an agent that carries and disseminates infectious pathogens to another living organism. Arthropods such as mosquitoes, ticks, flies, fleas, and mites are the major group of vectors for pathogens (Patz et al., 1996; Schmidt et al., 2013) These vectors can transmit specific pathogens to other hosts, especially humans by biting and blood-feeding. Vectors can transmit infectious pathogens to the host by releasing their infectious saliva, feces, and directly poking into host bloodstream (Patz et al., 1996; Schmidt et al., 2013). The most well-known vectors are ticks and mosquitoes that can carry dangerous pathogens such as *Plasmodium falciparum*,

DENV, ZIKV (mosquitoes), and POWV, TBEV, and *Borrelia* (ticks). Figure 2 shows the major vectors and their specific pathogens. These vectors have several life stages; for example, ticks have four morphological stages, egg, larva, nymph and adult (Stanek et al., 1986); Mosquitoes have four life stages as well, egg, larva, pupa, and adult (Crans, 2004). Ticks need blood meals to develop to the next life cycle stage. However, adult female ticks and mosquitoes both need to feed on blood to lay eggs.

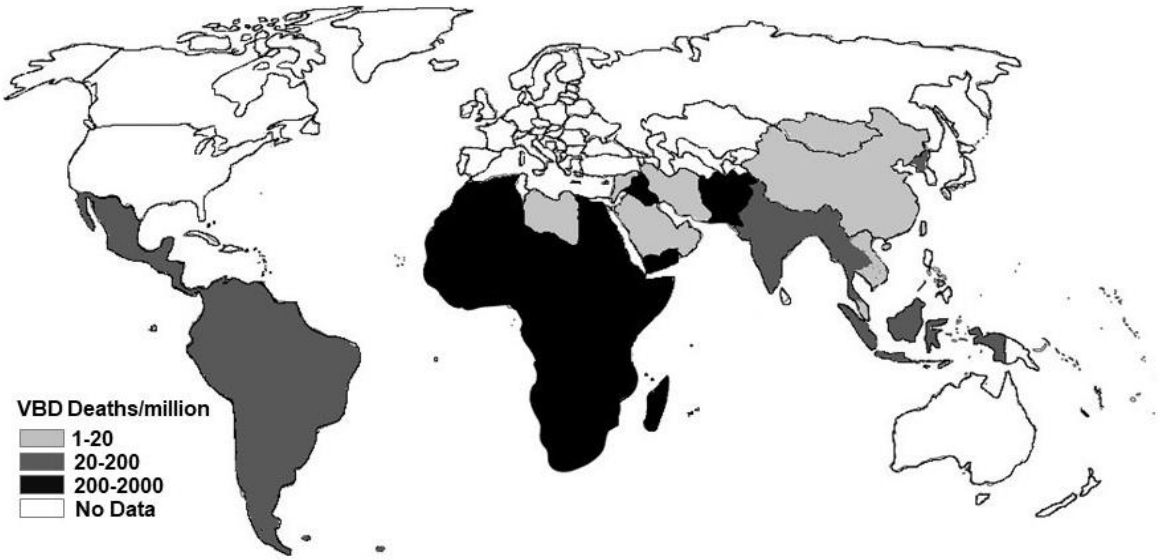

Figure 1. Deaths from Vector-Borne Disease

The image showed the distribution of deaths from VBDs all over the world. Africa, southeast and southwest Asia and south America indicate more burden of deaths caused by VBDs. The image was adapted from “Malaria control: the power of integrated action”, a report of The Health and Environment Linkages Initiative, a part of the WHO (https://www.who.int/heli/risks/vectors/malariacontrol/en/).

Ticks

There are more than 850 ticks’ existing that are divided into two broad groups: hard ticks and soft ticks (Arthur, 1962; Jongejan and Uilenberg, 2004; Sonenshine and Roe, 2013). In the United States, there are several main ticks that transmit several pathogens

to humans. *Ixodes scapularis*, also referred to as black-legged ticks, are distributed across the Eastern United States (CDC, 2019). They transmit *Borrelia burgdorferi* and *B. mayonii* that cause Lyme disease, *Anaplasma phagocytophilum*, the agent of human granulocytic anaplasmosis, POWV and TBEV that cause Powassan virus disease and encephalitis. *Amblyomma americanum*, also known as lone star ticks, are widely distributed in the southeastern United States. These ticks transmit *Ehrlichia chaffeensis,* the agent of human ehrlichiosis, Heartland virus, the agent of Heartland virus disease, and Bourbon virus, the agent of Bourbon virus disease. *Dermacentor*

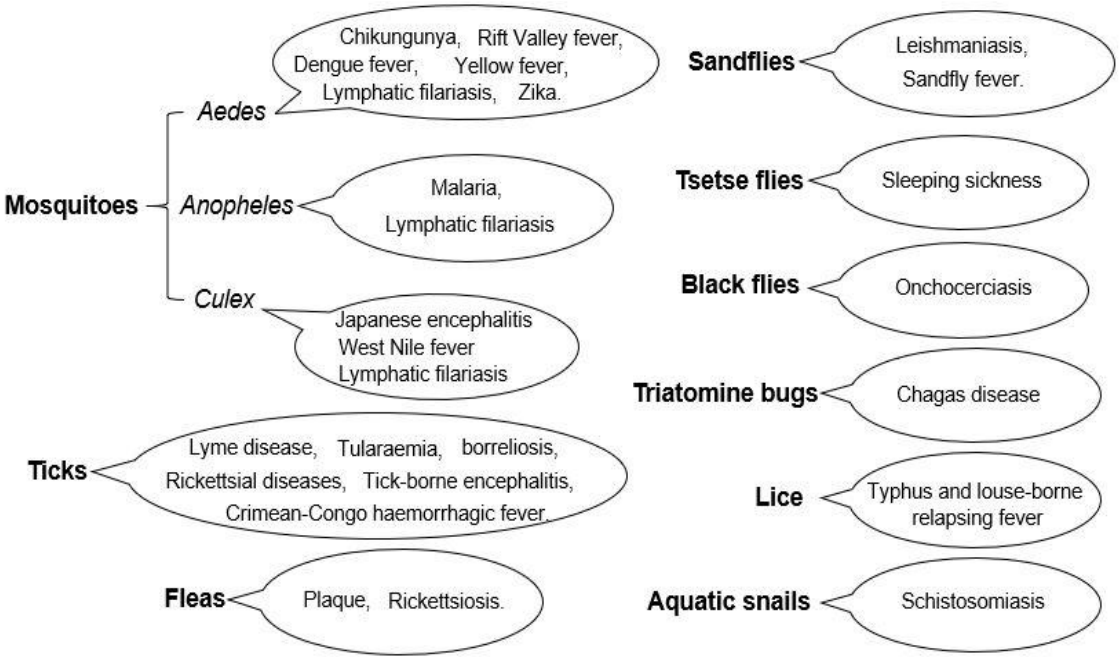

Figure 2. Main Vectors and Vector-Borne Diseases

Some of the important vector-borne diseases and vectors were shown. Ticks and mosquitoes are the most common vectors that can transmit several pathogens, causing lethal diseases in humans. The information shown in this figure was collected from the WHO's website on main vectors and vector-borne diseases (https://www.who.int/news-room/fact sheets/detail/vector-borne-diseases).

variabilis, also called American dog ticks, are distributed east of the Rocky Mountains. These ticks transmit *Rickettsia rickettsia*, the agent of Rocky Mountain spotted fever.

Other common ticks' species like *Rhipicephalus sanguineus*, *Ixodes cookie, Amblyomma maculatum, Dermacentor andersoni,* and *Ixodes pacificus* are widely distributed in the United States as well (Arthur, 1962; Jongejan and Uilenberg, 2004; Sonenshine and Roe, 2013).

Mosquitoes

There are 3,500 species mosquitoes living on earth, and morphologically, they consist of a slender segmented body, one pair of wings, three pairs of long legs, and an elongated mouthpart (Bates, 1949; Clements, 1992; Becker et al., 2010). The four life cycle stages in mosquitoes are egg, larva, pupa, and adult. Upon a blood meal, female mosquitos' mate and lay eggs on the water surface. The eggs hatch into larva that can feed on aquatic algae or organic material and molt into a pupa. Adult mosquitoes emerge from the pupa. Female mosquitoes feed on blood in need of protein and iron to produce eggs. Female mosquitoes take blood meals by poking through host skin using their tube-like mouthparts. Mosquitoes can feed on various vertebrate hosts such as mammals, birds, and amphibians but sometimes on fish, which is an invertebrate. Mosquitoes spit saliva onto the host during the bite and blood-feeding (Bates, 1949; Clements, 1992; Becker et al., 2010). If an infected mosquito took a blood meal, the infectious organism is disseminated through mosquito's saliva to host blood, resulting in the infection in the host. That is the reason why mosquitoes are considered as a most dangerous disease-causing vector. Several VBDs are transmitted by mosquitoes, including *P.falciparum*, yellow fever, Chikungunya, Zika, Dengue and West Nile disease. Annually, many people die from mosquito-borne disease infection. Several well-known mosquito species that are also primary pathogen vectors are introduced below.

Aedes aegypti is the primary vector that transmits several tropical fevers causing pathogens, including Dengue fever, Zika fever, yellow fever, and Chikungunya fever (Black IV et al., 2002; Nene et al., 2007). These mosquitoes originated from Africa. They can be recognized by white markings on their legs and they are distributed in tropical, subtropical, and temperate regions throughout the world. *Aedes aegypti* mosquitoes prefer to feed at dusk and dawn time, indoors and shady areas, or

on a cloudy day. For seeking a blood meal, *Aedes aegypti* can detect and attracted to chemical compounds such as ammonia, lactic acid, and carbon dioxide that are emitted by mammals (Bates, 1949; Clements, 1992; Becker et al., 2010).

Another well-known mosquito species is *Aedes albopictus*, also known as tiger mosquito (striking white and black pattern) or forest mosquito that is native to the tropical and subtropical areas of Southeast Asia. This kind of mosquitoes is about 2 to 10 mm length, and male is 20% smaller than female. Adults mosquitoes vary in size and this depends on several optimal conditions including the density of larval population, food supply, the environment near breeding water, their predators, and local climate. Recently, this species has spread to many other countries and areas through the transport of goods and travels. They fly and feed in day-time but sometimes at dusk and dawn as well. Since this species is more closely associated with humans, it has become a significant pest in human communities. Epidemiologically, *Aedes albopictus* is an important pathogen vector as well since it can transmit many infectious organisms that cause yellow fever, dengue fever, Chikungunya fever and, Wolbachia infection. In addition, this vector is capable of hosting and transmitting Zika virus to humans (Black IV et al., 2002; Nene et al., 2007).

Culex, also called house mosquito, is the most common type in the United States. This group includes *Culex Pipiens* and *Culex restuans Theobald.* This pale brown with white stripes mosquito is usually found near remaining polluted water or leftover water such as a birdbath, pet dishes, and storm drains. The female mosquito can lay about 400 eggs, and it typically takes 10 to 14 days to hatch or longer depending on the weather. *Culex* can also transmit a variety of viruses and parasites to humans (Nasci et al., 2001). Additionally, *Culex quinquefasciatus*, also called southern mosquito, is another mosquito that shares similar physical and behavioral characters with *Culex.* They are mid-night feeders and the primary vector of the St. Louis encephalitis virus and West Nile virus (Nasci et al., 2001).

Vector Control

Vector control is a significant approach for controlling some specific pathogens or the only way for protecting humans from several deadly infectious organisms such as ZIKV,

DENV, and WNV that, by far, there is no effective cure. It is a method to limit or eradicate vectors that transmit pathogens to humans and animals. Several methods have been used that show effectiveness in this approach; These methods are divided into four approaches, habitat and environment control, reducing contact, chemical control and biological control (Organization, 2006, 2012; Golding et al., 2015). Habitat and environment control mean reducing or removing the habitats or potential breeding areas of vectors, for example, removing polluted water or rubbish area that can breed mosquitoes and mowing grass for reducing tick bite. These can reduce the opportunity for mosquitoes and ticks spreading diseases to humans via saliva and feces. Reducing contact means decreasing chances for exposure to infectious vectors, subsequently affecting pathogen transmission. For example, it could be done by installing bed nets, window screens, or wear more protective clothing. All these can significantly reduce the contact with infectious vectors. Insecticides, larvicides, repellents, rodenticides and lethal ovitraps have been used for chemical control (Organization, 2006, 2012; Golding et al., 2015). Application of insecticides to walls and bed nets, spraying repellents on human skin, treating leftover water where larvae may breed with larvicides, and pesticides for vectors have been promoted and proved by the WHO to be highly effective. The last approach is biological control, which means the use of vector predators, such as introducing fishes that eat mosquito larvae, using bacterial toxins or botanical compounds to kill vectors. This approach has been proved significantly reducing the risks of vector-borne disease infection. Recently, a new pest control method has been developed that could effectively reduce the infection of mosquito-borne diseases (Organization, 2006, 2012; Golding et al., 2015). This method is called the sterile insect technique (SIT) (Vreysen et al., 2000). This is an environmentally friendly insect pest control method that involves radiation on a target pest, breeding in a mass-rearing and sterilization, followed by releasing the sterile males by air over defined area systematically and widely. SIT-engineering males mate with females resulting in no production of offspring and a reduction of the pest population. This technology has many advantages. The sterile insects are not self-replicating, so they can’t be established in nature, and the SIT doesn’t introduce any invading species into the local ecosystem which makes this method safe and friendly to the environment

(Vreysen et al., 2000). Furthermore, after using this technique, a significant reduction in crop and livestock production loss has been observed. This method is different from the classical vector control and has been proved to be efficient and successful in the past 60 years that was applied in six continents. This technique also has some disadvantages, such as a) radiation, transport and treatment of releasing insects can reduce male mating efficiency and, b) breeding sterile insect generation from mass-rearing and irradiation require very careful process to avoid releasing unexpected sterile insects. In addition, gender separation is hard, and it is uncertain whether the sterile male is competitive to wild-type males. In general, SIT is economically and environmentally beneficial in many regions all over the world on saving billions of dollars annually (Vreysen et al., 2000).

However, although these approaches have been proved to be effective to some extent, the high cost for these treatments make it very difficult for developing countries to proceed with these measures. Less developed countries may have more zones to treat due to poverty, lack of knowledge and education in the population, and awareness of vector-borne diseases and information on effective treatment. Infectious vectors transported from these areas to the other parts of the world via the transport of goods and international travel are hard to be controlled. This may also impact the vector control measures in developed areas.

1.2 EXOSOMES

Exosomes are small membranous extracellular microvesicles with the size ranging from 30 nm to 250 nm, which are of endocytic origin formed in the late endosomal compartments (as multivesicular bodies; MVBs) (Mellman, 1996; Fevrier and Raposo, 2004; Couzin, 2005; Keller et al., 2006; Raposo and Stoorvogel, 2013). Exosomes are produced from most eukaryotic cells. They have biological lipid bilayer membrane structure that gained from cells by exocytosis into a biological fluid such as blood, urine, saliva, and cerebrospinal fluid. Initially, exosomes were considered as garbage bins to discard unwanted cellular components. However, other studies showed that exosomes are mere cell debris, apoptotic blebs, and signs of cell death (Mellman, 1996; Keller et al., 2006; Raposo and Stoorvogel, 2013). Recent studies have suggested that

exosomes could play significant roles for the intercellular communication process and are therapeutic targets for neurological disorders, cancer, and autoimmune diseases. Exosomes derived from several different cells have been shown to function as signaling related vesicles, transporting cell-specific collections of several proteins such as cytoskeletal protein (actin, myosin, and tubulin), heat shock proteins (HSPs), cytokines and tetraspanin domain containing family proteins, lipids, and nucleic acids such as DNA, RNA and microRNA (Thery et al., 2002; Alvarez et al., 2012; Xiao et al., 2012; Schageman et al., 2013; Villarroya-Beltri et al., 2014; Schey et al., 2015). Due to the presence of lipid bilayer membrane structure, exosomes derived from one cell can easily merge with other cells through the circulatory system and exchange contents from the inside or luminal part of exosomes. Exosomes can transfer messages over longer distances for e.g., between different tissues or multiple organs (Fevrier and Raposo, 2004; Ohno et al., 2013; Zhang et al., 2015; Ding et al., 2018). Recently, our studies have shown that exosomes serve as modes of arthropod-borne *flavivirus*' transmission from ticks and mosquitoes to humans and disseminate viral RNA and proteins among different types of cells (Zhou et al., 2018a).

Due to their small size and instability under normal laboratory conditions, exosome isolation needs to strictly follow ultracentrifugation protocol under cold temperature, which has been standardized by expert exosome researchers. After isolation, exosome samples should be processed for Western blots and probing for exosomal biomarkers such as CD9, CD63, CD81, HSP 70, Flotillin, and Alix (Keller et al., 2007; Baietti et al., 2012; Lin et al., 2015), followed by Micro scoping detection (TEM and Cryo-EM are recommended). Figure 3 shows the Cryo-EM image of exosomes derived from murine cortical neurons.

Studies have also shown that exosomes are vesicles of transmission for a variety of microorganisms and some pathogens use exosomes to manipulate local microenvironments (Bobrie et al., 2011; Dreux et al., 2012; Ohno et al., 2013). As an example, malaria parasites, *Plasmodium falciparum*, use exosomes for communication between infected red blood cells (Regev-Rudzki et al., 2013). Hepatitis C virus (HCV), an enveloped RNA virus, associates with exosomes isolated from cell culture supernatants and from infected patients (Bukong et al., 2014; Liu et al., 2014).

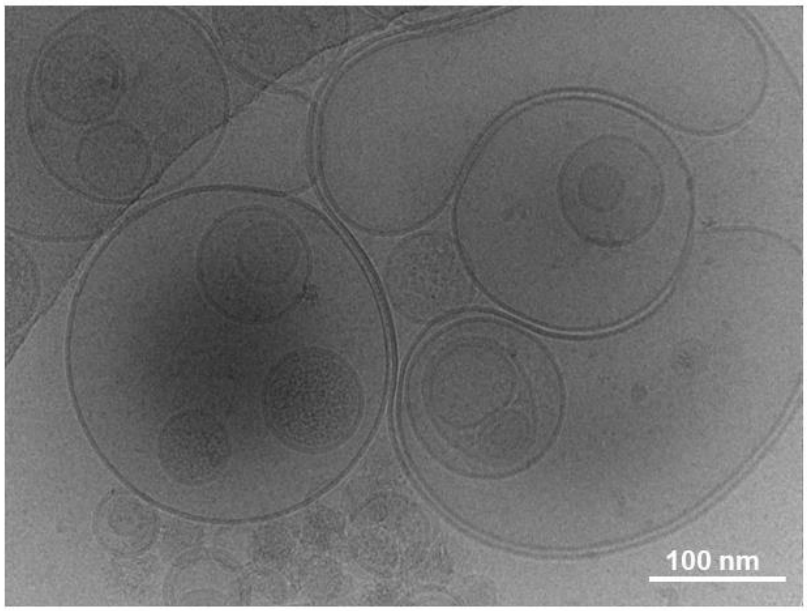

Figure 3. **Cryo-EM Image Shows Exosomes from Murine Cortical Neuronal Cells**
The image showed exosomes in a variety of sizes with a bilayer membrane structure. Cortical neuronal cells were isolated from pregnant C57BL/6 female mice E16 days embryo. Exosomes were isolated by ultracentrifugation from supernatant collected from 5 days cortical neuronal cell culture. Scale bar indicates 100 nm.

1.3 LANGAT VIRUS (LGTV)

Langat virus (LGTV, strain TP-21) was first isolated in Malaysia and Thailand in 1955 from *Ixodes granulatus* ticks from the forest. It is considered as a model pathogen closely related to tick-borne encephalitis virus (TBEV) and is used as a biosafety level 2 (BSL2) pathogen to study pathogenesis of TBEV (Mellman, 1996; Labuda and Randolph, 1999; Nuttall and Labuda, 2003b), due to its 74% similarity in its genome with TBEV. LGTV is about 50 nm particle, belongs to the *Flaviviridae* family, with 11 Kb positive-sense single-stranded RNA genome (Smith, 1956; Gritsun et al., 2003; Rumyantsev et al., 2006). *Ixodes* ticks transmit several other *flaviviruses,* including Powassan virus (POWV), tick-borne encephalitis virus (TBEV), and Louping ill virus (LIV).

In nature, LGTV can infect rodents but not humans, although it shares more than 74% nucleotides similarity with TBEV (Smith, 1956; Gritsun et al., 2003; Rumyantsev et al., 2006). Under laboratory conditions, LGTV is barely virulent for adult mice and primates. Till now, there is no good evidence showing LGTV causing any disease in humans. However, antibodies against LGTV can be detectable in the sera of local people in the Malaysian region. Compare to TBEV, LGTV is non-virulent to humans. LGTV induces antibodies in humans and has significant homology in its genome with TBEV. All these features suggest LGTV could be an ideal candidate for developing a vaccine against TBEV (Shapoval et al., 1989). LGTV has been widely used in many research laboratories as a substitute for TBEV.

1.4 ZIKA VIRUS (ZIKV)

Zika virus is a mosquito-borne positive-sense single-stranded RNA *Flavivirus* transmitted by *Aedes* mosquitoes, basically *A. aegypti* and *A. albopictus* (Wang et al., 2017a). People first isolated this virus from a forest of Uganda in Africa called “Zika” in 1947, and that is where the virus name came from (Russo and Beltrao-Braga, 2017; van den Pol et al., 2017b; Wang et al., 2017a). It is highly like its other members of the *Flavivirus* family such as Dengue virus (DENV), West Nile virus (WNV), Yellow Fever virus (YFV), and Japanese Encephalitis virus (JEV). Zika virus’ 10 kilobases genome encodes three structural proteins and seven non-structural proteins, making a 40-50 nm virion. Originally it was endemic in Africa and Asia; however, it has spread out to the Americas, leading to the Zika virus outbreak in 2015 to 2016 (Brasil et al., 2016; Schuler-Faccini, 2016). *Aedes* mosquitoes release saliva and feces on our skin when they are biting and feeding for blood meals. The direct contact with infected mosquito saliva and feces will transmit the virus to keratinocytes at the wound site. Then this blood-borne virus will spread through the cell to cell transmission and via the circulatory system through bloodstream (Brasil et al., 2016; Schuler-Faccini, 2016). Zika virus infects the placental cells after it crosses the placental barrier (Campos et al., 2015; Musso et al., 2015).

Most infected people don’t develop strong symptoms, but some will show up symptoms such as red eyes, headache, rash, joint pain, muscle pain and fever which

are shown in Figure 4. ZIKV infection has been shown to affect both the Central Nervous System (CNS) and the Peripheral Nervous System (PNS) and is associated with severe neurological complications. In some immoral scenarios, it will result in severe Guillain-Barre Syndrome (GBS) but eventually, people will recover back (Faizan et al., 2016; Oh et al., 2017b; Russo and Beltrao-Braga, 2017; van den Pol et al., 2017b; Wang et al., 2017a). However, the significant reason that people become panicked from the Zika virus is that pregnant women are highly vulnerable to the infection. Zika virus can transmit through the placental barrier and infect human

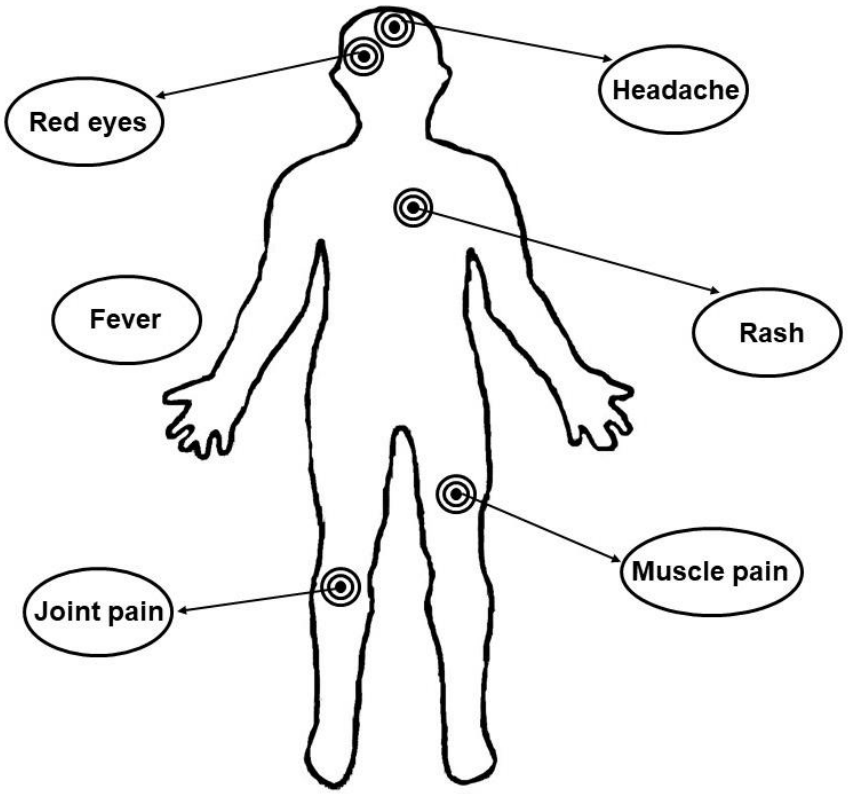

Figure 4. **Human Zika Virus Infection Symptoms**

The image showed several symptoms on different parts of the human body after ZIKV infection. The image was adapted from the CDC's website on the topic of the Zika overview (https://www.cdc.gov/zika/about/overview.html).

fetus, killing the primary stem cells of fetal brains, resulting in the smaller size of heads termed as microcephaly. Microcephaly, a less studied neurodevelopmental disorder is a marked reduction in brain size and intellectual disability with defective cell proliferation and severe death of cortical progenitor cells and their neuronal progeny. Because of the severity of microcephaly, babies will suffer different problems due to underdeveloped brains. These problems include intellectual disability, problems with movement, and balance, difficulties with talking, sitting and walking, hearing loss and vision problems. Undoubtedly, all these make Zika virus infection as a disaster to mothers and families. Due to its harmfulness to humans, research on the Zika virus is significantly important and meaningful. Figure 5 shows the world map with areas for the risk of ZIKV.

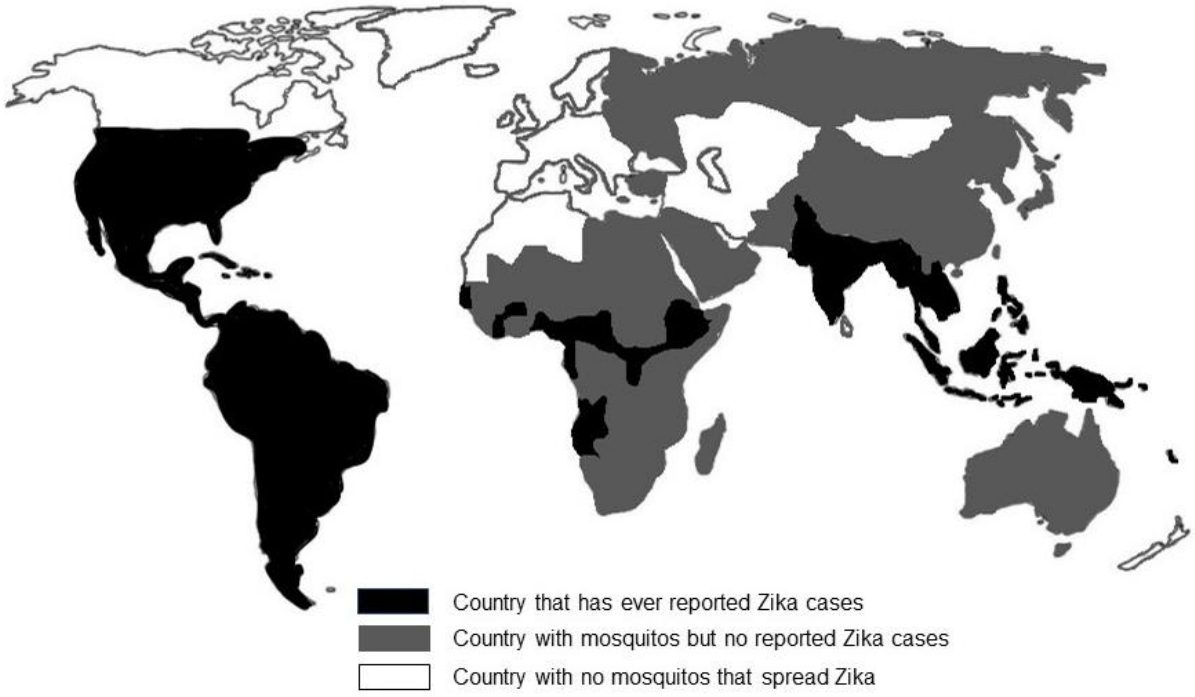

Figure 5. World Map of Areas with Risk of Zika

The image showed areas with a risk of ZIKV infection. Americas, Southeast and Southwest Asia and some regions in Africa are under high risk of ZIKV infection. The image was adapted from the CDC's website on Zika travel information (https://wwwnc.cdc.gov/travel/page/zika-travel-information).

1.5 SPHINGOMYELIN PHOSPHODIESTERASE 3 (SMPD3)

Neutral sphingomyelinase, also known as sphingomyelin phosphodiesterase or SMase, is a hydrolase enzyme that is involved in sphingolipid metabolism reaction (Aslan et al., 2014a; Aslan et al., 2014b; Albi et al., 2019). It belongs to DNase I family and its function is to break down sphingomyelin lipid into phosphocholine and ceramide, which is the major pathway for ceramides responding to cellular stress. SMases are divided into five types: Lysosomal acid SMase, Secreted zinc-dependent acid SMase, Magnesium-independent neutral SMase, Magnesium-dependent neutral SMase and Alkaline SMase (Jung et al., 2000; Hannun and Obeid, 2002; Ago et al., 2006). They are divided into different families according to their cation dependence and pH optima of actin. The lysosomal acidic SMase and the magnesium-dependent neutral SMase are considered as major candidates for producing ceramide and dealing with cell stress (Jung et al., 2000; Hannun and Obeid, 2002; Ago et al., 2006).

Sphingomyelin Phosphodiesterase 3 (SMPD3), also called Neutral Sphingomyelinase II or nSMase II is a key enzyme for catalyzing the hydrolysis of sphingomyelin to form ceramide and phosphocholine (Miyauchi et al., 2017). Ceramide can mediate lots of cellular functions such as apoptosis, growth arrest, cellular stress responses and exosome-mediated intercellular communication. SMPD3 is a protein-coding gene that is associated with some diseases such as Deafness, Autosomal Recessive and Gaucher Disease, Type III and it is involved in Sphingolipid metabolism and TNF signaling pathways.

CHAPTER 2

EXOSOMES SERVE AS NOVEL MODES OF TICK-BORNE *FLAVIVIRUS* TRANSMISSION FROM ARTHROPOD TO HUMAN CELLS AND FACILITATES DISSEMINATION OF VIRAL RNA AND PROTEINS TO VERTEBRATE NEURONAL CELLS

2.1 INTRODUCTION

Recently, the function of exosomes has been emphasized in significant medical and clinical research on cancer and autoimmune diseases and they are now considered as novel therapeutic targets for neurological disorders such as Parkinson's disease (Kooijmans et al., 2012; Pant et al., 2012; Vader et al., 2014). Over the past decade, exosomes have been given potential biological significance by identifying a variety of their specific roles (Keller et al., 2006; Pant et al., 2012; Raposo and Stoorvogel, 2013; Apte-Sengupta et al., 2014). Exosomes are released into circulation after their fusion with the plasma membrane and these vesicles would serve as mediators of molecular transmission (Keller et al., 2006; Thery et al., 2006; Bobrie et al., 2011; Colombo et al., 2014). Recent conclusions of HCV transmission through hepatic exosomes establish infection provides new perception into hepatitis drug development (Greenhill, 2013; Cosset and Dreux, 2014). Exosomes also charge in the transfer of immuno-stimulatory viral RNA from HCV-infected cells to co-cultured plasmacytoid dendritic cells (Dreux et al., 2012). Besides, exosomes speed up the receptor-independent transmission of replication-competent HCV viral RNA that was discovered to be in complex with Ago2-miR122- HSP90 in HCV-infected individuals or infected hepatocytes (Bukong et al., 2014). Interestingly, exosomes have been shown to perform dual roles in the

transmission of Hepatitis A virus (HAV) and HCV, thereby evading antibody-mediated immune responses (Longatti, 2015). Several studies have suggested exosomes as important mediators in HIV-1 pathogenesis (Arenaccio et al., 2014; Madison and Okeoma, 2015). Exosome secreted HIV Nef protein has been proved to trigger apoptosis in CD4 + T cells; also, the Gag p17 coding RNA is also marked to the exosomes (Lenassi et al., 2010; Columba Cabezas and Federico, 2013). HIV-infected cell-derived exosomes have been revealed to contain the TAR (Trans-Activation Response Element) miRNA that facilitates the production of pro-inflammatory cytokines (Narayanan et al., 2013; Sampey et al., 2016). Moreover, a recent but very highlighting study showed that uninfected cell-derived exosome activates the transcription of HIV-1 in the latent stage (Barclay et al., 2017).

Ixodes ticks transmit several viruses belonging to the family *Flaviviridae* such as tick-borne encephalitis virus (TBEV), Powassan virus (POWV) and Langat virus (LGTV) (Randolph et al., 1996; Labuda et al., 1996; Labuda and Randolph, 1999; Nuttall and Labuda, 2003a). LGTV is considered as a model biosafety level 2 (BSL2) pathogen to study the pathogenesis of TBEV, due to their significant genome homology with the later virus. Transmission modes of these arthropod-borne *flaviviruses* (with positive-sense single-stranded RNA) are still poorly understood (Liu et al., 2014). For the first time, it was noted that arthropod exosomes facilitate the transmission of *flavivirus* RNA and proteins from tick to human cells (Zhou et al., 2018). The data demonstrated that cells from the medically important vector, *Ixodes scapularis* tick, secreted exosomes that mediated transmission of tickborne LGTV RNA and proteins from arthropod to human cells (Zhou et al., 2018). In addition, the presence of abundant amounts of LGTV RNA and proteins in exosomes isolated from arthropod and neuronal cells was noted. It was also found that LGTV-infected tick cell-derived exosomes were capable of transmigrating and infecting naive human skin keratinocytes (the initial barrier lining the human cells that come in contact during bites from infected ticks) and human vascular endothelial cells (HUVEC) (the barrier that comes in contact during arthropod blood-feeding) (Zhou et al., 2018). The data showed that vertebrate exosomes mediate the transmission of tick-borne LGTV RNA and proteins from infected brain microvascular endothelial cells (a component of the blood-brain barrier; BBB) to neuronal cells. In

addition, it has been demonstrated that exosomes containing tick-borne LGTV and mosquito-borne West Nile virus (WNV) facilitate the transmission of viral RNA and proteins from one neuronal cell to others, suggesting their novel role in neuropathogenesis (Zhou et al., 2018). Dihydrochloride hydrate, GW4869 (a selective and commercial inhibitor for neutral sphingomyelinase; N-SMase, an enzyme that regulates formation and release of exosomes), hampered LGTV loads in exosomes and inhibited the transmission of viral RNA and proteins in not only arthropods' but also vertebrate host cells (Zhou et al., 2018). Overall, this study suggests that exosomes are the mediators for transmission of arthropod-borne *flavivirus* RNA and proteins from arthropod to the vertebrate host, along with promoting the dissemination of this infectious viral material within the vertebrate host, including allowing neuro-invasion and neuropathogenesis in the Central Nervous System (CNS) by a crossing of BBB cells.

2.2 RESULTS

Detection of Tick Cell-Derived Exosomes by Cryo-EM and Western Blot

Cryo-Electron Microscopy (cryo-EM) performed on tick cell-derived exosomal fractions showed the presence of purified arthropod exosomes with the size in diameter from 30 to 250 nm (Figure 6A), the same as exosomes isolated from mammalian cells (Fevrier and Raposo, 2004; Couzin, 2005; Keller et al., 2006). Exosomes isolated from arthropod cells showed a heterogeneous population of vesicles in the cryo-EM analysis (Zhou et al., 2018). In order to understand such heterogeneity in the exosome population, quantitative analysis was done using images collected from both uninfected and LGTV-infected tick cell-derived exosomes. Counting of exosomes per image showed a higher number of exosomes in LGTV-infected (n = 14) in comparison to the uninfected (n = 27) group (Figure 6B). It was noted that the majority of the exosomes were of sizes between 50 to 100 nm in both uninfected and infected fractions (Figures 6C and 6D). However, exosomes of other sizes 100 to 150 nm and 150 to 200 nm were evenly spread in infected preparation when compared to the uninfected preparation (Figures 6C and 6D). Fewer vesicles from sizes of 200 to 250 nm were marginally more in uninfected (10.1%) in comparison to the infected group (6.5%) (Zhou et al., 2018). The large exosomes were very few in number and were from 0 to 1.5% in both the uninfected and infected groups (Figures 6C and 6D). This data suggested that LGTV-infection (72 h p.i.) might enhance the production and release of exosomes (Zhou et al., 2018). The OptiPrep (DG-Exo-iso) method (Tauro et al., 2012) purified various sizes of exosomes in six different fractions. Immunoblotting analysis (with highly cross-reactive 4G2 monoclonal antibody that identified the viral Envelope (E)- protein) of these fractions (20 µl) proved the presence of LGTV E-protein in all six fractions but enriched lots of E-protein were present in fractions four and five in comparison to the other fractions (Figure 6E). These results were connected with the size analysis data (Figures 6B-6D). Enhanced detection of LGTV-E protein in fractions four may correspond to the 50 to 100 nm (fraction 4) size exosomes that are in a higher population (Figure 6E). As expected, E-protein in the fractions from uninfected control was not detectable. Total cell lysates (20 µg) from uninfected and LGTV-infected fractions were used as internal

controls to compare the amounts of E-protein in the 20 µl of different fractions (Figure 6E). The PonceauS images showing the protein profile served as control (Figure 6E).

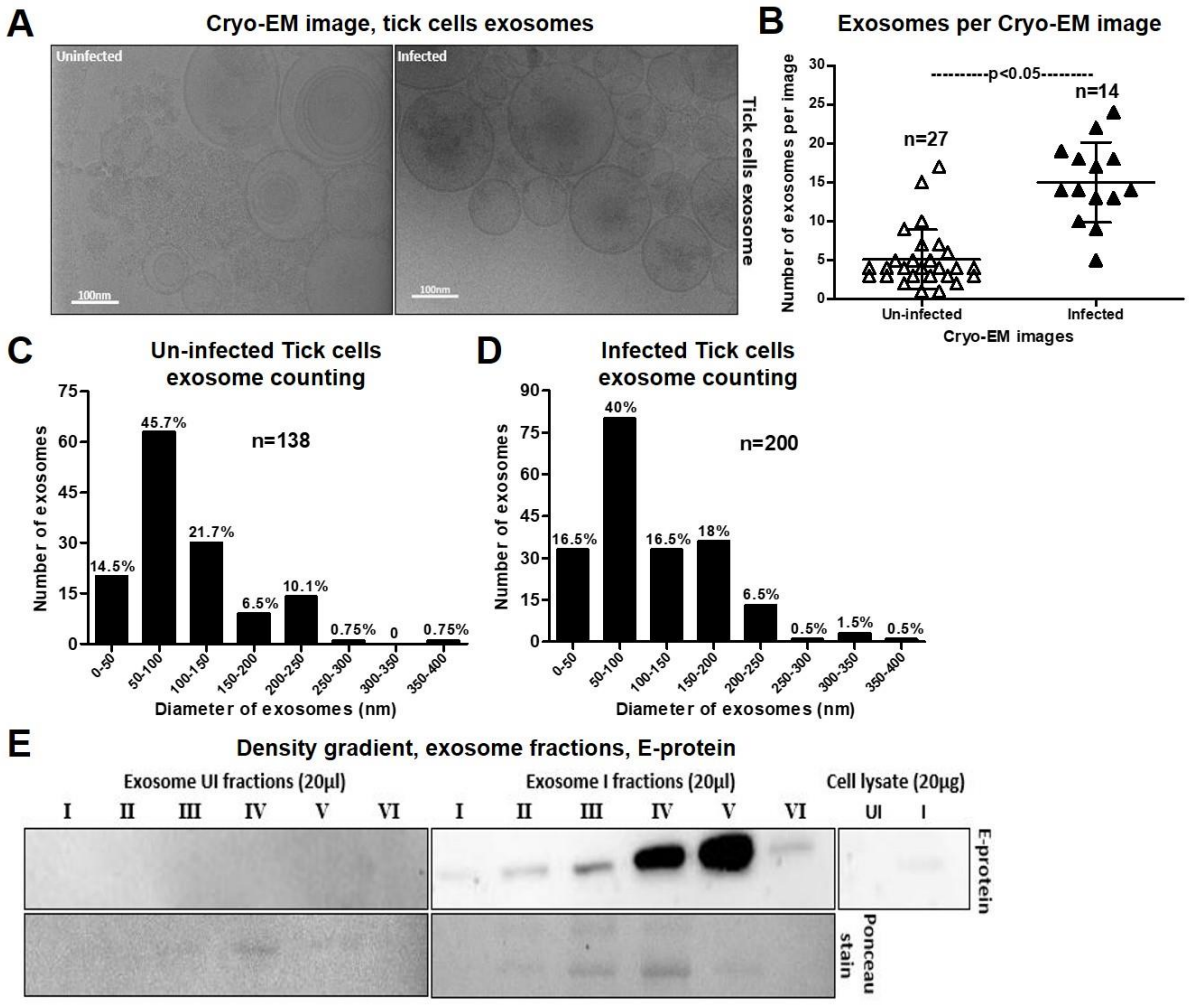

Figure 6. Cryo-EM Images and Western Blot Show Exosomes Derived from Un-infected and LGTV Infected Tick Cells

(A) Cryo-EM images showed exosomes derived from uninfected and LGTV-infected (MOI 1; 72 h p.i.), ISE6 tick cells. Scale bar indicates 100nm.

(B) A comparison of exosome numbers per cryo-EM image from uninfected and infected groups.

(C-D) Quantification of diameter or sizes for heterogenous population of exosomes from uninfected or LGTV- infected tick cell-derived exosomes.

(E) DG-Exos showed the presence of LGTV envelope protein in fractions 1 to 6.

This figure was adapted from the published journal article (Zhou et al., 2018).

Tick Cell-Derived Exosomes Containing Viral RNA and Exosomes are Infectious

Quantitative Real-Time PCR (QRT-PCR) analysis revealed the presence of LGTV total RNA in exosomes isolated from infected tick cells (Figure 7A). The replication numbers of viral RNA in LGTV-infected (72 h p.i.) exosomes derived tick cells is shown in (Figure 7B). Furthermore, the presence of both positive and negative sense LGTV RNA strands in tick cells-derived exosomes (Figure 7C) was also determined. LGTV RNA was also perceptible in exosomes from tick cells cultured and infected in exosome-depleted FBS medium (with no cross-contaminating bovine exosomes presence in regular commercial FBS), further indicating the presence of viral RNA in tick cell-derived exosomes (Figure 7D). During the isolation of tick exosomes, pellets (exosomes fraction) and supernatant fraction (collected after pelleting exosomes and before PBS wash; See Figure 8) was tested in plaque assays to determine the infectivity and replication of LGTV RNA and titers as described in methods. Plaque assays carried out with the tick cell-derived exosome pellet fractions formed plaques at dilutions of 1:10 and 1:100 that were too many to count, and around 20 to 22 plaques at a dilution of 1:1000 (Figures 7E-7G). No plaques were visible in plates where Vero cells were treated with the supernatant fractions at any trial dilutions (Figures 7E-7G). Plaque assays demonstrated the presence of infectious LGTV RNA or proteins in infected exosomes that resulted in high loads of LGTV in Vero cells (6.6×10^4 pfu/ml) and developed formation of viral plaques. Plaque assays further verified that tick cell-derived exosomes contain LGTV RNA and proteins capable of replication and forming viable plaques that are extremely infectious to mammalian cells (Figures 7E-7G). No viral plaques detected after treatment with the supernatant fraction (depleted of exosomes) suggests the presence of abundant amounts of LGTV RNA and proteins in exosomes (Figures 7E-7G).

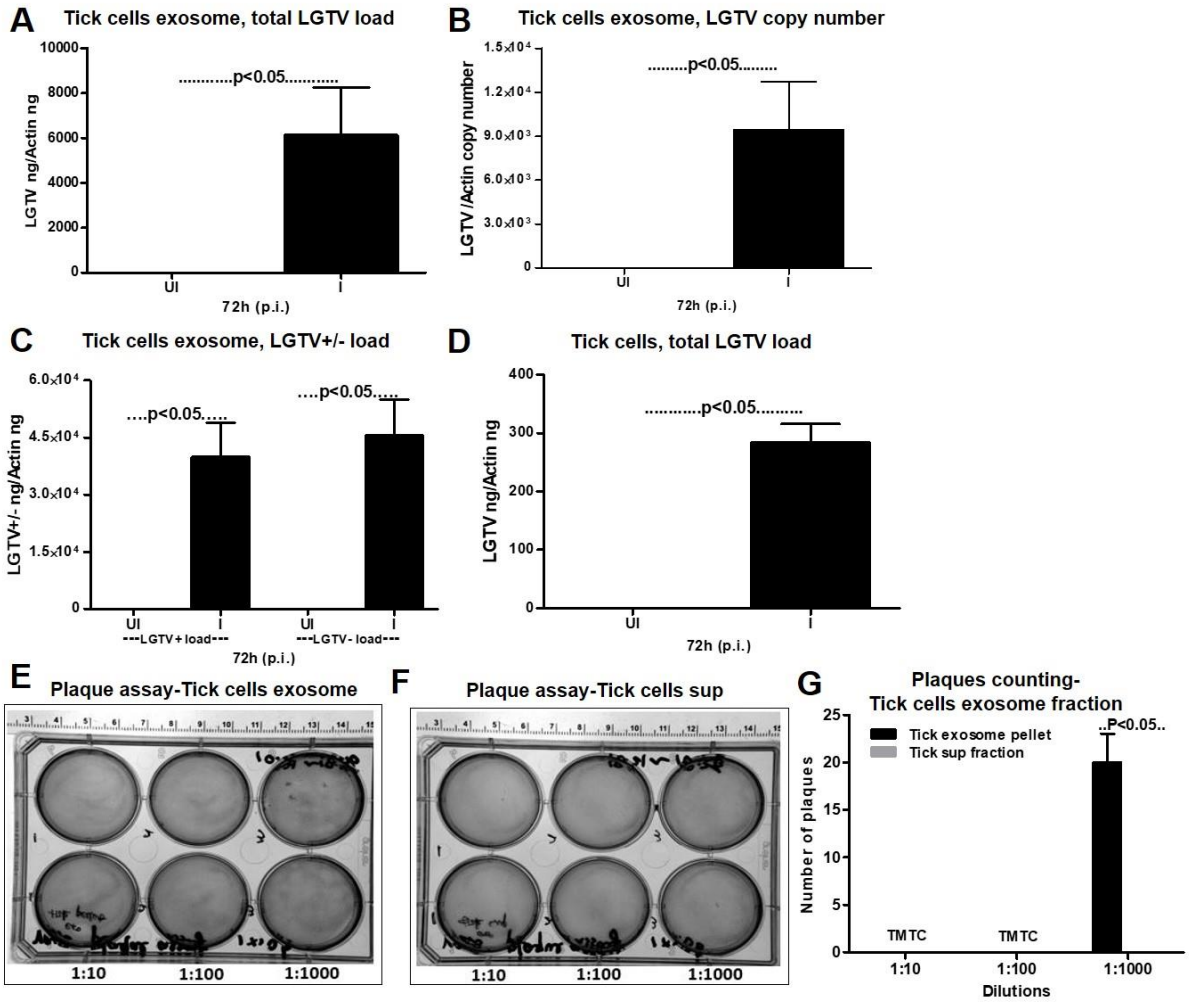

Figure 7. Arthropod Exosomes Contain Infectious LGTV RNA and Exosomes Form Plaques

(A) QRT-PCR analysis showed total LGTV loads.

(B) The copy number of LGTV RNA.

(C) The levels of LGTV positive-sense strand and negative-sense strand in exosomes isolated from tick cells at 72 h (p.i.), Uninfected cells serve as a control.

(D) QRT-PCR analysis showed LGTV total loads from LGTV infected tick cells at 72 h p.i. (5 x 10^6 tick cells, infected with 1 MOI of LGTV). Cells were grown in commercially exosome-free FBS medium. LGTV transcript levels were normalized to tick *beta-actin*.

(E-F) Plaque assays performed with different dilutions (1:10, 1:100, 1:1000) of exosomes fraction or corresponding different volumes (600, 60, 6 µl) of supernatant fractions prepared from tick cells. The rulers at the top determines scale for the represented plaque assays.

(G) Quantitative assessment of the number of plaques in exosomal and supernatant fractions was shown. TMTC indicates “too many to count”.

This figure was adapted from the published journal article (Zhou et al., 2018).

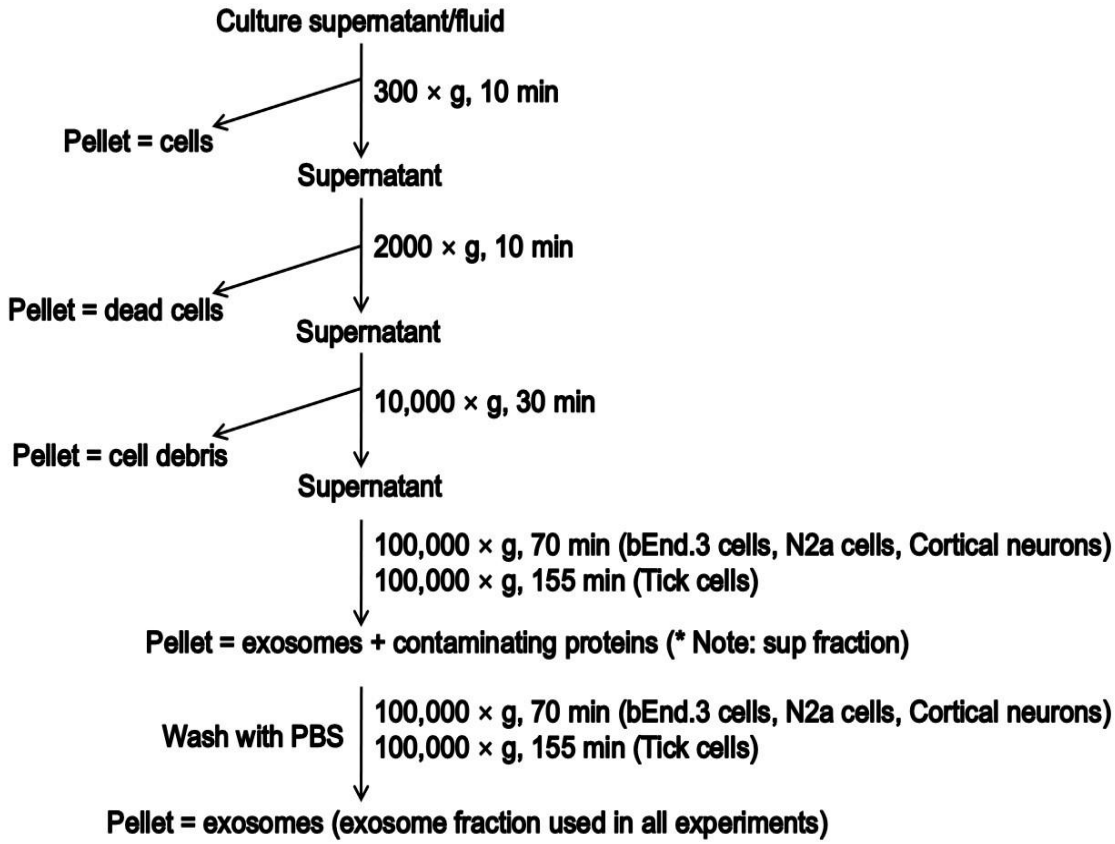

Figure 8. Schematic Representation of the Method Used for Exosomes Isolation from Different Cells

Cell culture supernatant/fluid was spun at 300 g for 10 min to remove floating cells, and supernatant fraction was collected. The supernatant was spun at 2000 g for 10 min to remove dead cells, and the resulting supernatant fraction was collected and spun again at 10, 000 g for 30 min to remove any remaining cell debris. The supernatant fraction collected from the previous step was spun at 100, 000 g for 70 min (for bEnd.3 cells, N2a cells, cortical neurons) or for 155 min (for tick cells) in an ultracentrifugation unit. Supernatants resulted after the above longer spin step were used in all the experiments as supernatant fractions. The exosomes containing pellet fraction was washed in ice-cold PBS and spun at 100, 000 g for 70 min (for bEnd.3 cells, N2a cells or cortical neurons) or for 155 min (for tick cells). The pellet resulted after this wash was considered as exosome fraction in all the experiments. The exosome pellet/fraction was either dissolved in PBS (for performing re-infection, plaque or trans-well assays, Native PAGE and 4G2-antibody-beads-binding assay), or in RNA lysis buffer (for total RNA extractions) or in modified RIPA buffer for protein extractions. This figure was reproduced from the published journal article (Zhou et al., 2018).

Tick Cell Exosomes Contain Viral Proteins inside the Luminal Region

The presence of LGTV E-protein in tick cells-derived exosomes was further recognized by SDS-PAGE followed by immunoblotting with 4G2 antibody (Figure 9A). More E-protein loads were detected (at ~50kDa) in total cell lysates in comparison to exosomal fractions (Figure 9A). Immunoblotting with monoclonal anti-LGTV NS1 (Clone 6E11) antibody (obtained from BEI resources) also pointed out that NS1 presents in both tick cell-derived exosomes and total cell lysates (Figure 9A). Remarkably, the presence of tick HSP70 (heat-shock cognate protein 70, a specific exosomal marker in mammalian cells) in exosomal lysates had been detected (Figure 9A). Presumably, due to a low amount in cell lysates, no HSP70 was detected in the tested condition (Figure 9A). Total protein lysates prepared from the same batch of uninfected or LGTV-infected tick cell-derived exosomes or from whole tick cells served as a loading control for all immunoblots (Figure 9A). In addition, native-PAGE followed by immunoblotting with 4G2 antibody, showed higher levels of LGTV E-protein (at <250kDa; in native state) in Triton-X-100 (a detergent that lyses the exosomal lipid bilayer membranes) treated exosomes (30 min, RT) with in comparison to the exosomes treated for three rounds of freeze-thaw cycle (1 h, at -80°C) or the MOCK group (untreated exosomes) held at 4°C (Figure 9B). Total protein lysates generated from uninfected or LGTV-infected tick cell-derived exosomes with same treatments served as controls in this immunoblotting analysis (Figure 9B). The treatment with Proteinase K (0.5 µg/µl or 50 µg/ml, 15 min at 37°C) suggested working concentrations (50 to 100 µg/ml) that digested all proteins (Figure 9C). In untreated infected samples, E-protein was detected. However, no E-protein was detected in Proteinase K-treated infected samples. Uninfected samples either treated or untreated served as internal controls (Figure 9C). The Ponceau S stained blot proved no proteins detected in both infected and uninfected proteinase K-treated samples (Figure 9C). Detection of LGTV E-protein inside exosomes (but not outside from PBS suspensions) was further performed with E-protein-4G2-antibody-beads binding assay as described in methods. No significant ($P>0.05$) differences in viral loads were obtained in LGTV-infected (72 h p.i.) exosomes that were either, untreated, or treated with 4G2 antibody (that binds to LGTV E-protein) or relevant isotype antibody that served as control (Figure 9D). Similar results were obtained with

LGTV-infected exosomal fractions that derived from GW4869 inhibitor-treated tick cells (of 72 h p.i.) (Figure 9D). Native-PAGE and the beads assay clearly suggested that exosomes contain viral RNA and proteins inside exosomes. To further evaluate if viral E-protein was indeed inside the exosomes, the protease-resistance assay was performed with Proteinase K that basically digest proteins in all biological specimens. Overall, these results suggested that the majority of the LGTV RNA and proteins escape from tick cells via exosomes which could mediate not only LGTV transmission and infection, but also possibly other closely related viruses such as TBEV and POWV.

Human Keratinocytes were Infected by Tick Cell-Derived Exosomes and Viral RNA Presences was Detected in Exosomes but not in the Supernatant

The LGTV infection kinetics of HaCaT cells showed no difference between all three-time points, demonstrating that instead of holding viral replication inside of these cells, HaCaT cells prefer to free of viral material by releasing exosome to neighboring cells (Figure 10A). Tick cell-derived exosomes and the relative fraction supernatant (after exosome ultracentrifugation isolation) were treated on HaCaT cells. The results showed that the majority of viral RNA was present in exosomes but not in the supernatant. This data suggests that viral RNA is concentrated in exosomes, and very few exosomes may remain in the supernatant fraction after isolation (Figure 10B). The finding of exosomes derived from HaCaT cells re-infecting HaCaT cells indicated that the exosomes of HaCaT cells were also infectious. However, the relative supernatant was not very infectious since the load is invisible. The reason could be that very few exosomes remain in the supernatant. These observations prove again that the majority of viral RNA was present in the exosomes and not in the supernatant (Figure 10C). Trans-well assay mimicked the process of how exosomes assist viral infectious material comes across the human skin barrier and infects human keratinocytes. Tick cells derived exosomes pass through the membrane between upper and lower chambers, and then infected naïve HaCaT cells growing on the lower chamber of the plate. With the use of exosome inhibitor, exosomes production and virus load were inhibited, demonstrating again that exosomes assist virus transmission between cell types.

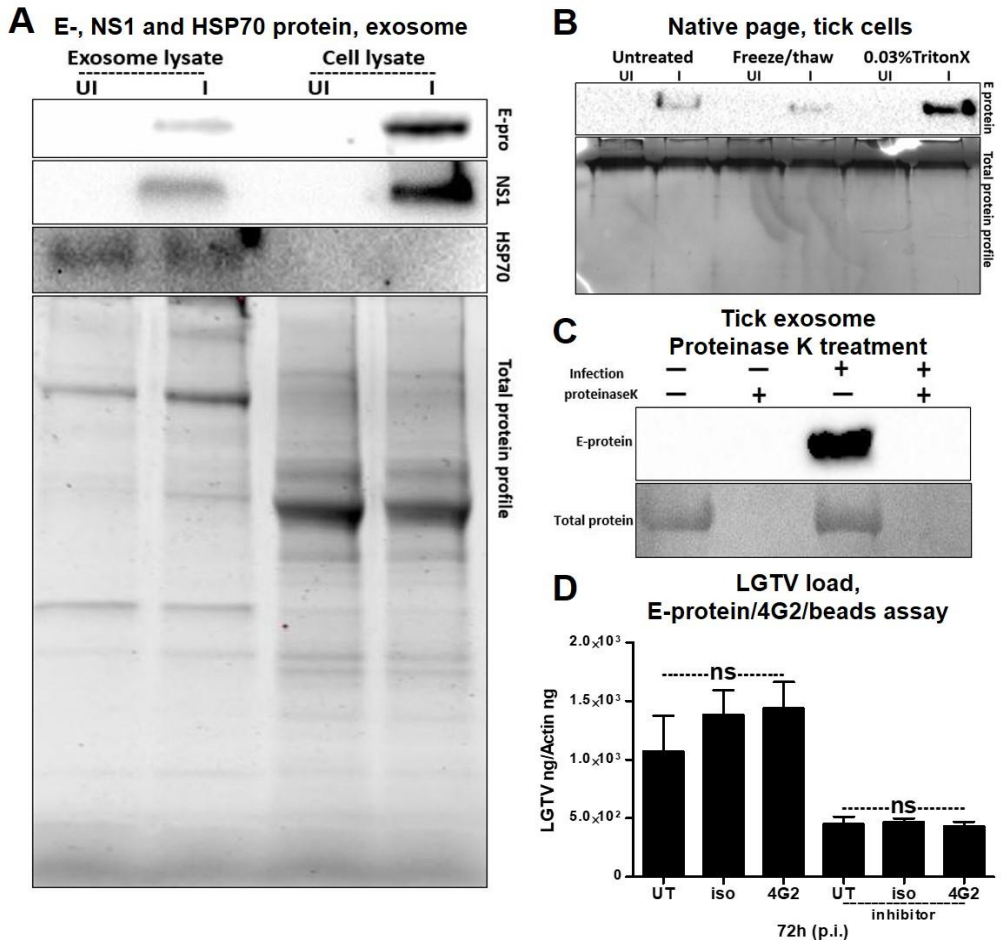

Figure 9. Arthropod Exosomes Contain LGTV Proteins Inside

(A) Immunoblotting analysis showed the detection of LGTV E-glycoprotein and viral NS1 protein in exosome fraction and total lysates from the cells prepared from uninfected (UI) or infected (I) tick cells at 72 h (p.i.). Uninfected samples and total protein profiles serve as controls.

(B) Native-PAGE followed by immunoblotting analysis showed the presence of E-protein from LGTV-infected (MOI 1; 72 h p.i.) or uninfected tick cell-derived exosomes treated with Triton-X-100 (0.03%), or freeze-thaw cycles (3 times freezing at -80°C for 1 h each cycle) or untreated samples held on ice. Coomassie-stained gel showed the total protein profiles that serve as a loading control.

(C) Immunoblot gel image showed the levels of E-protein or total protein loads (Ponceau stained) in LGTV-infected tick cell-derived exosomes treated with proteinase K (50 µg/ml, 15 min, 37°C).

(D) Antibody-beads binding assay performed on LGTV infected (MOI 1) tick cell-derived exosomes (collected from tick cells either untreated or treated with GW4869; 5 µM, exosome inhibitor) showed no differences in Langat-E protein loads between 4G2, isotype, and untreated samples.

This figure was adapted from the published journal article (Zhou et al., 2018).

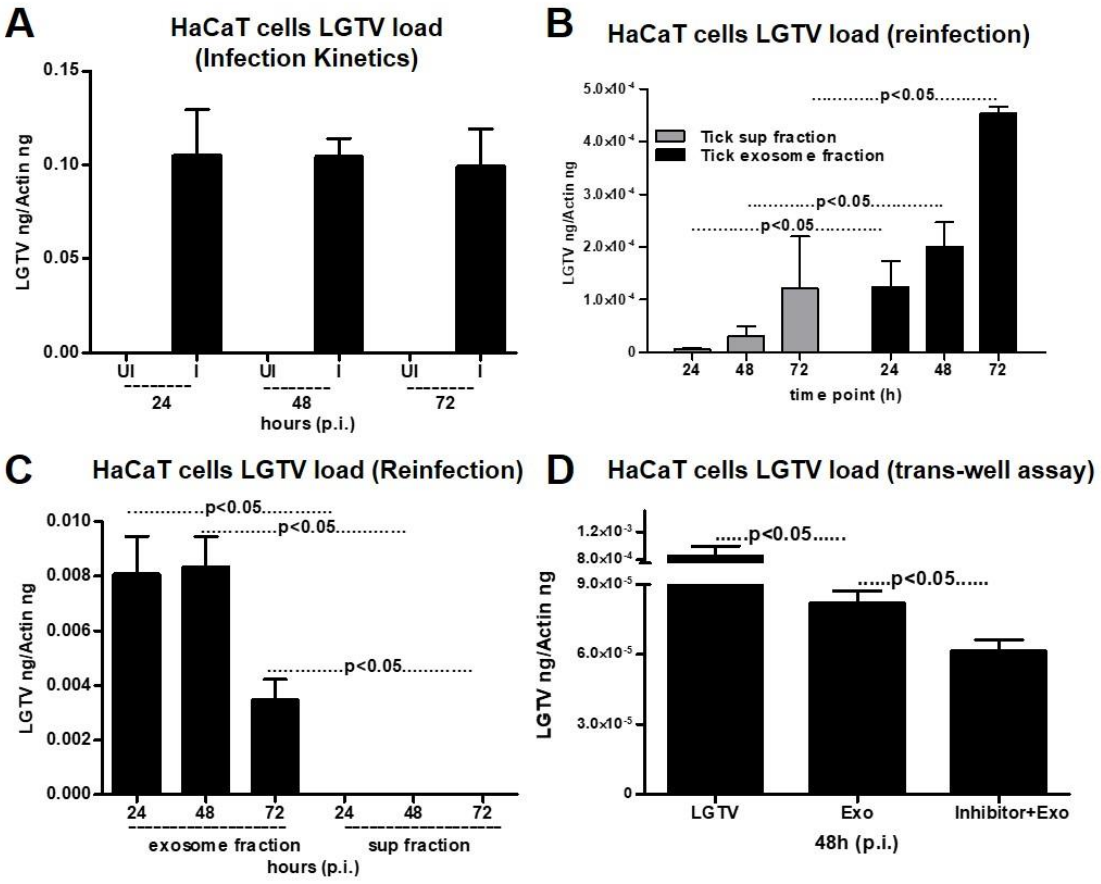

Figure 10. Exosomes Derived from Tick Cells and HaCaT Cells are more Infectious to Human Keratinocytes

(A) QRT-PCR analysis showed the levels of LGTV in HaCaT cells at different time points (24, 48, and 72 h p.i.). LGTV (6 MOI) was used to infect 1 x 10^5 HaCaT cells.

(B) Viral re-infection kinetics as determined by the presence of total LGTV loads in HaCaT cells (1 x 10^5 cells) at different time points treated with exosomes (20 µl) or supernatant fractions (400 µl) prepared from 72 h p.i. LGTV-infected tick cells were shown.

(C) Viral re-infection kinetics as determined by the presence of LGTV in HaCaT cells (1 x 10^5 cells at 24, 48, and 72 h p.i.) infected by treatment with exosome (20 µl) or supernatant (400 µl) fractions prepared from 72 h p.i. LGTV-infected tick cells that were seeded in exosome-free FBS medium were shown.

(D) Viral loads at 48 h p.i. was determined by the presence of LGTV in a trans-well assay performed with tick cells (1 x 10^5, upper chamber) or HaCaT cells (1 x 10^5, lower chamber) treated with tick exosome fraction (20 µl, upper chamber) for 4 h in the presence or absence of 5 µM exosome inhibitor GW4869. Tick cells infected with LGTV laboratory stocks were used as controls. LGTV transcript levels were normalized to human *beta-actin*. P values were determined by the Student's two-tail *t*-test. This figure was adapted from the published journal article (Zhou et al., 2018).

Human Vascular Endothelial Cells (HUVEC) were Infected by LGTV and Exosomes Assisted Viral RNA Transmitted from Brain Endothelial Cells to Neuronal Cells

The data also showed that LGTV (laboratory viral stocks, generated from Vero cells) was able to infect human vascular endothelial (HUVEC) cells with no changes in viral loads at 24 h p.i. in comparison to later time points (48 and 72 h p.i.) (Figure 11A). HUVEC cells treated with exosomes-carrying-LGTV showed magnificently ($P<0.05$) increased viral loads at 48 h p.i. in comparison to the supernatant fractions treated cells, suggested that LGTV RNA is concentrated in exosomes (Figure 11B). Due to the transmission to vertebrate host, arthropod-borne neurotropic encephalitis viruses were noticed to first reproduced in the blood and peripheral organs (spleen and liver), cross the Blood-Brain Barrier (BBB) and invade the CNS (Chambers and Diamond, 2003; Samuel and Diamond, 2006). Mouse brain-microvascular endothelial cells (bEnd.3 cells; that served as the BBB) was used to address if infectious viral RNA and proteins are transmitted to neurons by the mediation of bEnd.3 cell-derived exosomes. LGTV rapidly infected and replicated in bEnd.3 cells at all the time points (48 and 72 h p.i.) (Figure 12A). Furthermore, it was shown that the viral loads in brain endothelial cells were not impressively different over the infection period as revealed by the viral loads at much later time points (96 and 120 h p.i.) (Figure 12B). QRT-PCR analysis revealed significantly ($P<0.05$) increased viral burden and replication numbers in exosomes derived from bEnd.3 cells at 24 h p.i. in comparison to the other checking points (48, 72, 96 and 120 h p.i.) (Figures 11C and Figure 12C). Higher loads of LGTV positive and negative sense RNA strands were found at 24 and 48 h p.i., in comparison to the other tested time points (72, 96 and 120 h p.i.) (Figure 11D). LGTV infected and replicated in neuronal cells (mouse N2a cells) in a time-dependent manner with a peak infection at 72 h p.i. (Figure 12D). N2a cells were infected later with bEnd.3 cell-derived exosomes collected at different time points (24 and 48 h p.i.). The bEnd.3 cells derived exosomes containing viral RNA and proteins were tested to be infectious to N2a cells with a peak level of infection, which is observed with exosomes derived from endothelial cells at 48 h (p.i.) (Figure 11E). N2a cells treated with supernatant fractions (collected at the indicated time points) derived from endothelial cells resulted in significantly ($P<0.05$)

less viral loads in comparison to the treatments with exosome fractions isolated from the bEnd.3 cells (Figure 11E). Trans-well assays performed with exosomes isolated from LGTV-infected-brain endothelial cells indicated the transmission of viral RNA and proteins from bEnd.3 cells (plated in upper chamber) to uninfected/naive N2a cells split in the lower plate (Figure 11F). The presence of exosome inhibitor significantly reduced transmission of infectious viral RNA from bEnd.3 cell-derived exosomes to N2a cells (Figure 11F). Infection of bEnd.3 cells with 6 MOI virus stocks showed the transmission of LGTV to N2a cells (by crossing the membrane barriers in trans-well plates) and served as a control in this assay (Figure 11F). These results suggested that exosomes derived from brain-endothelial cells were perhaps the mediators of BBB permeability (crossing of infectious exosomes from infected-endothelial cells lining the BBB and transmission to the neuronal cells) that may stimulate neuro-invasion of tick-borne viruses such as LGTV, TBEV, and POWV.

Exosomes Derived from Un-infected and LGTV-Infected Neuronal Cells were Successfully Isolated and Characterized by Cryo-EM Images and Western Blot Analysis

Upon entry into the brain, tick-borne neuro-invasive viruses (such as TBEV) infect neuronal cells. To investigate if exosomes mediate viruses' transmission within the brain from one neuronal cell to another; N2a cells were infected with LGTV. The presence of purified exosome with the size range of 30 to 250 nm in diameter derived from neuronal cell was observed with Cryo-EM (Figure 13A), much the same to exosomes isolated from tick cells. Parallel to arthropod exosomes, neuronal cell-derived exosomes also showed a heterogeneous population of vesicles. In a very coincident way, quantitative analysis was done depending on cryo-EM images collected from both uninfected and LGTV-infected N2a cell-derived exosomes. Counting of exosomes per image indicated a bigger number of exosomes in LGTV-infected (n = 13) cells in comparison to the uninfected (n = 9) group (Figure 13B). This result suggested that LGTV-infection (72 h p.i.) possibly, enhance the formation and release of exosomes. Majority of these exosomes were also varying from 50 to 100 nm in both uninfected and infected groups (Figures 13C and 13D). Smaller sizes of exosomes (0 to 50 nm) were of slightly higher

percentages in the infected exosomes when compared to the uninfected group (Figures 13C and 13D). Fewer vesicles from sizes of 150 to 200 nm (9 to 11%) or 200 to 250 nm (6.3%) were observed in both infected and uninfected preparations.

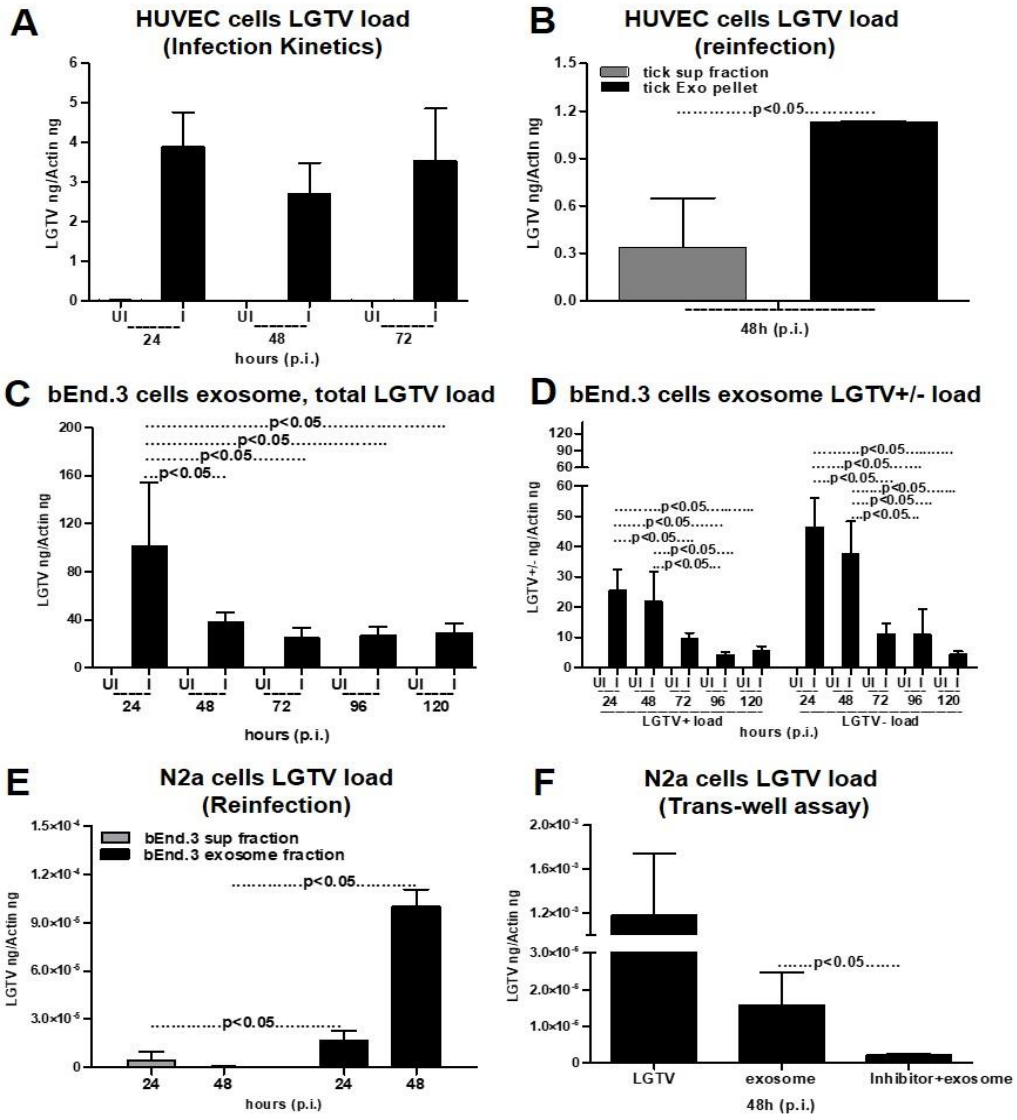

Figure 11. **Human Endothelial Cells are Infected by LGTV and Endothelial Cell-Derived Exosomes Mediate Transmission of LGTV RNA from bEnd.3 Cells to N2a Neuronal Cells**

(A) QRT-PCR analysis showed the levels of LGTV in HUVEC cells at different time points.

(B) Infection of HUVEC cells with infectious tick cell exosomes or supernatant fractions showed the LGTV loads at 48 h p.i.

(C) QRT-PCR analysis showed the total LGTV loads in bEnd.3 cells (1 x 10^5 cells, LGTV, MOI 6).

(D) QRT-PCR analysis showed the levels of LGTV positive-sense strand or negative-sense strand in exosomes isolated from bEnd.3 cells at different time points (24, 48, 72, 96, and 120 h p.i.).
(E) Viral loads were determined after 24 h p.i. by the presence of LGTV in N2a cells (1 x 10^5) treated with LGTV containing exosomes (20 µl) or supernatant (400 µl) fractions prepared from bEnd.3 cells.
(F) Viral loads at 48 h p.i. of N2a cells (lower chamber) as determined by the presence of LGTV in a trans-well assay performed with 1x 10^5 of bEnd.3 cells treated with 20 µl brain endothelial cell-derived exosomes (upper chamber) for 4 h in the presence or absence of exosome inhibitor (5 µM) (upper chamber) or infected with LGTV laboratory virus stocks were shown.
This figure was reproduced from the published journal article (Zhou et al., 2018).

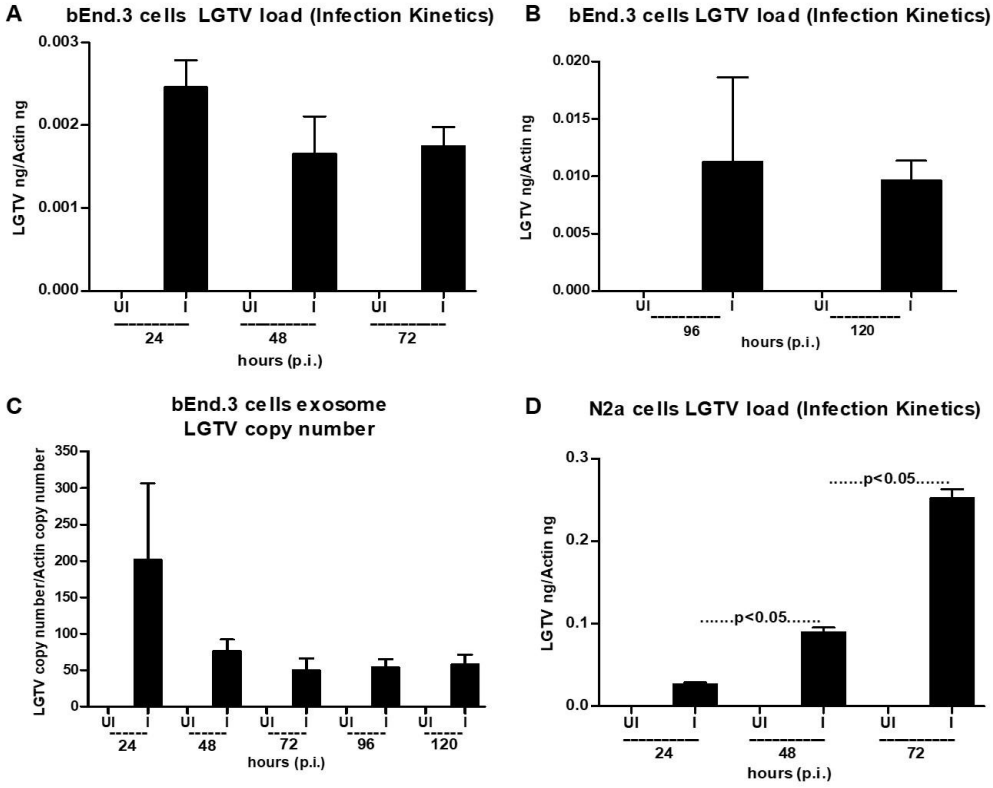

Figure 12. LGTV Infection Kinetics in bEnd.3 and N2a Cells

(A-B) QRT-PCR analysis showed the levels of LGTV in bEnd.3 cells (24, 48, 72, 96, and 120 h p.i.).
(C) The LGTV copy numbers at different time points (24, 48, 72, 96, and 120 h p.i.) were shown for bEnd.3 cells (1 x 10^5 cells, LGTV, MOI 6).
(D) Infection kinetics with increasing LGTV loads in N2a cells (1 x 10^5 cells, LGTV, MOI 6) was shown. UI indicates uninfected, and I indicate LGTV-infected. LGTV transcript levels were normalized to mouse *beta-actin*. P values were determined by the Student's two-tailed *t*-test.
This figure was adapted from the published journal article (Zhou et al., 2018).

Less than 1% of larger vesicles (sizes of 250 to 350 nm) were found in infected group (Figures 13C and 13D). The OptiPrep density gradient (that separates exosomes from viruses and large micro-vesicles) yielded purified exosomes into six different fractions of different sizes. Immunoblotting analysis (using 4G2 antibody) of these fractions (20 µl) elucidated the presence of LGTV E-protein in all fractions but concentrated amounts of E-protein were present in fractions 4 and 5 in comparison to the other fractions (Figure 13E**).** E-protein was not detected in the fractions from uninfected control. The cell lysates (20 µg) from uninfected and infected preparations were used as controls to compare the amounts of E-protein detected in the different fractions volume (Figure 13E). Immunoblotting with anti-HSP70 antibody detected enriched amounts of HSP70 (exosomal marker) in the 4th fraction of both uninfected and infected samples (Figure 13E). HSP70 levels were also found in 3 and 5 of infected fractions but not in uninfected fractions (Figure 13E). Besides the HSP70, it had also been analyzed the CD9 (another exosomal marker) levels in uninfected and infected fractions. CD9 was detected in all six of the uninfected fractions in a boosting manner, with higher levels in fractions 4 and 5 (Figure 13E). However, CD9 was detected in 2 to 5 of infected fractions with higher-level detection in fractions 3 and 4 (Figure 13E). It was intriguing to aware that LGTV E-protein was enhanced in similar exosomal fractions (fractions 3 to 5) that had more concentrated HSP70 and CD9 protein, suggesting that infectious exosomes in fraction 4 have higher levels of exosomal markers. OptiPrep DG-isolation of exosomes using 0.1 µm filter (culture supernatants were filtered to condense volume, any molecule smaller than 5 KDa would filter away) detected E-protein also in fraction 4, suggesting that these infectious exosomes have sizes of 50 to 100 nm (Figure 13E). This result also connected with the quantitative analysis from cryo-EM images. For the curiosity to know where to do the intact LGTV particles present on the parallel gradients, OptiPrep DG-isolation was performed with the laboratory stocks of LGTV (prepared in Vero cells, collected after 7 to 14 days post-infection and stored at -80^{o}C). It was recognized as a differential pattern in E-protein loads when density gradients were performed with LGTV-infected exosomal fractions from N2a cells (Figure 13E) or with LGTV laboratory stocks containing viruses (Figure 13F). An enhanced E- protein signal was obtained in fraction 6 (indicating the presence of virions in this fraction) and not in fraction 5.

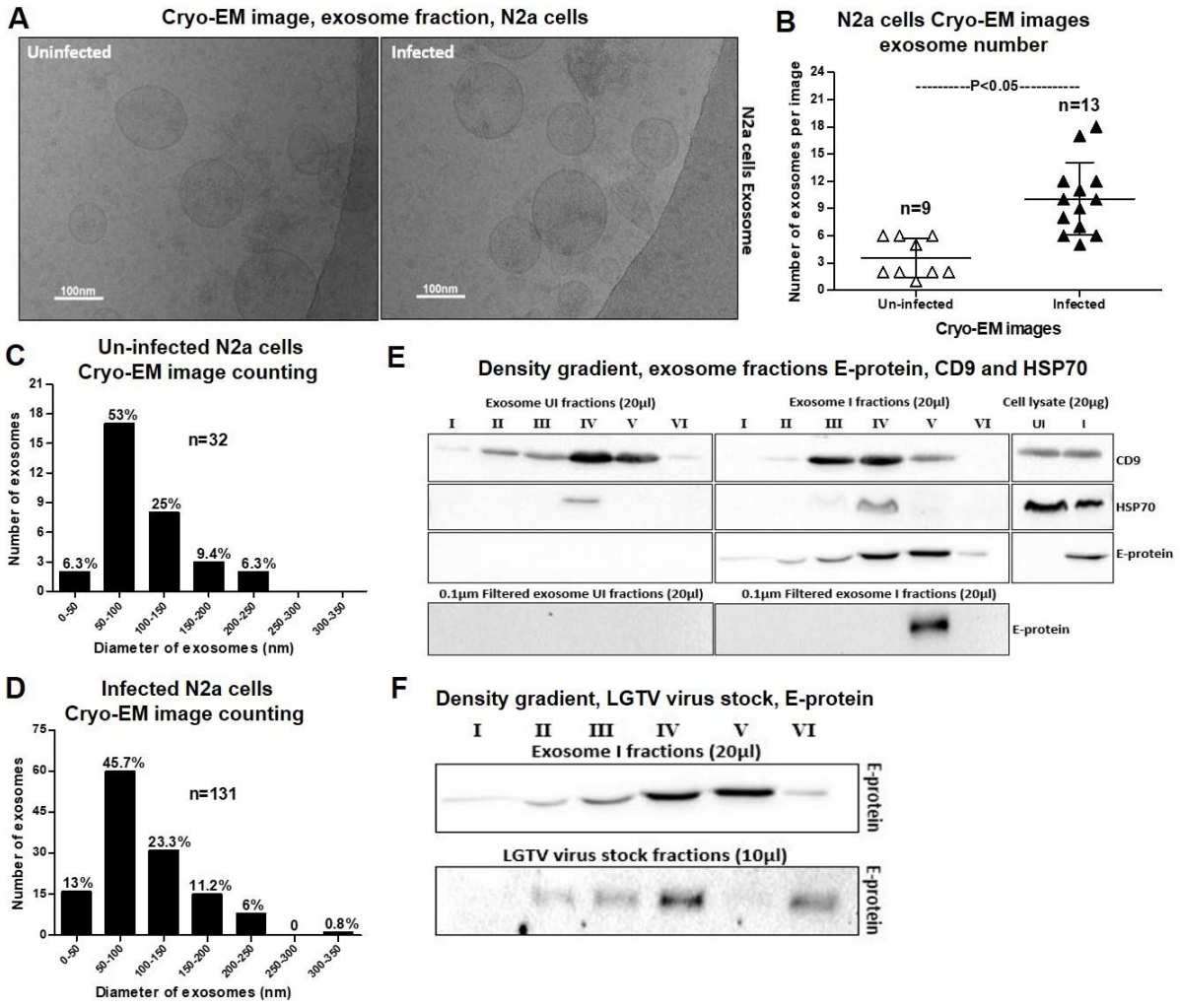

Figure 13. Exosomes Derived from Un-infected and Infected Neuronal Cells are Detected by Cryo-EM and Western Blot

(A) Cryo-EM images showed exosomes isolated from uninfected and LGTV-infected (MOI 6; 72 h p.i.) N2a cells (1 x 10^7). Scale bar indicates 100nm.

(B) A comparison of exosome numbers per image from uninfected and infected groups was shown.

(C-D) Quantification of diameter or sizes for heterogenous population of exosomes from uninfected or LGTV- infected N2a cell-derived exosomes.

(E) DG-Exos showed the presence of enhanced LGTV envelope protein loads in fractions 1 to 6. Fractions 3 to 5 showed enriched amounts of exosomal markers CD9 and HSP70. E-protein was detected in fraction 5 in 0.1 µm filtered samples that processed for OptiPrep DG-isolation.

(F) E-protein was detected in OptiPrep DG-isolated fractions from laboratory virus stocks.

This figure was adapted from the published journal article (Zhou et al., 2018).

Detection of E-protein in fractions 4, 3 and 2 from the laboratory virus stock suggested the presence of infectious exosomes containing viral E-protein (Figure 13F). This exciting result indicated that the viral stocks are not just the virions only but also are perhaps infectious exosomes mixtures carrying viral E-protein.

Neuronal Cell Exosomes Contain Infectious Viral RNA and Proteins

LGTV infected exosomes derived from N2a cells were collected at different time points (of 24, 48, 72 h p.i.) and evaluated for viral loads. QRT-PCR analysis disclosed an increased total viral RNA load and replication numbers at 72 h p.i. in comparison to the other measured time points (of 24 and 48 h p.i.) (Figures 14A and 14B). Both positive- and negative-sense viral RNA were detected with higher levels in the exosomes derived from N2a cells at 72 h p.i. in comparison to the other tested time points (Figure 14C). Immunoblotting analysis further indicated LGTV E-protein presented in the N2a cell-derived exosomes (Figure 14D). The E-protein loads were one- to two-fold higher in total lysates when compared with the exosomal lysates derived from N2a cells (Figure 14D). The smaller molecular mass of LGTV E protein was found in exosomes in comparison to the total lysates (Figure 14D), suggesting a possible de-glycosylation of the viral E protein in neuronal cell-derived exosomes. Similar de-glycosylation of the viral E protein in immunoblots performed on laboratory virus stocks was recorded (Figure 14E). A high level of CD9 was detected in the LGTV-infected exosomes, comparing to uninfected control and the LGTV-infected or uninfected N2a cells from total cell lysates low levels CD9 expression (Figure 14D). Total protein lysates in the immunoblotting served as a loading control (Figure 14D).

Neuronal Cell-derived Exosomes Contain Infectious Viral RNA and Proteins inside the Luminal Region

Next, studies were performed to address the possibility that viral RNA is perhaps binding to the outside of the exosomes and may be transmitted to the recipient cells. In order to test this possibility, freshly prepared LGTV-infected (72 h p.i.)- N2a cell-derived exosomes were treated with RNase A (5 µg/ml, for 15 min, at 37°C). No differences in

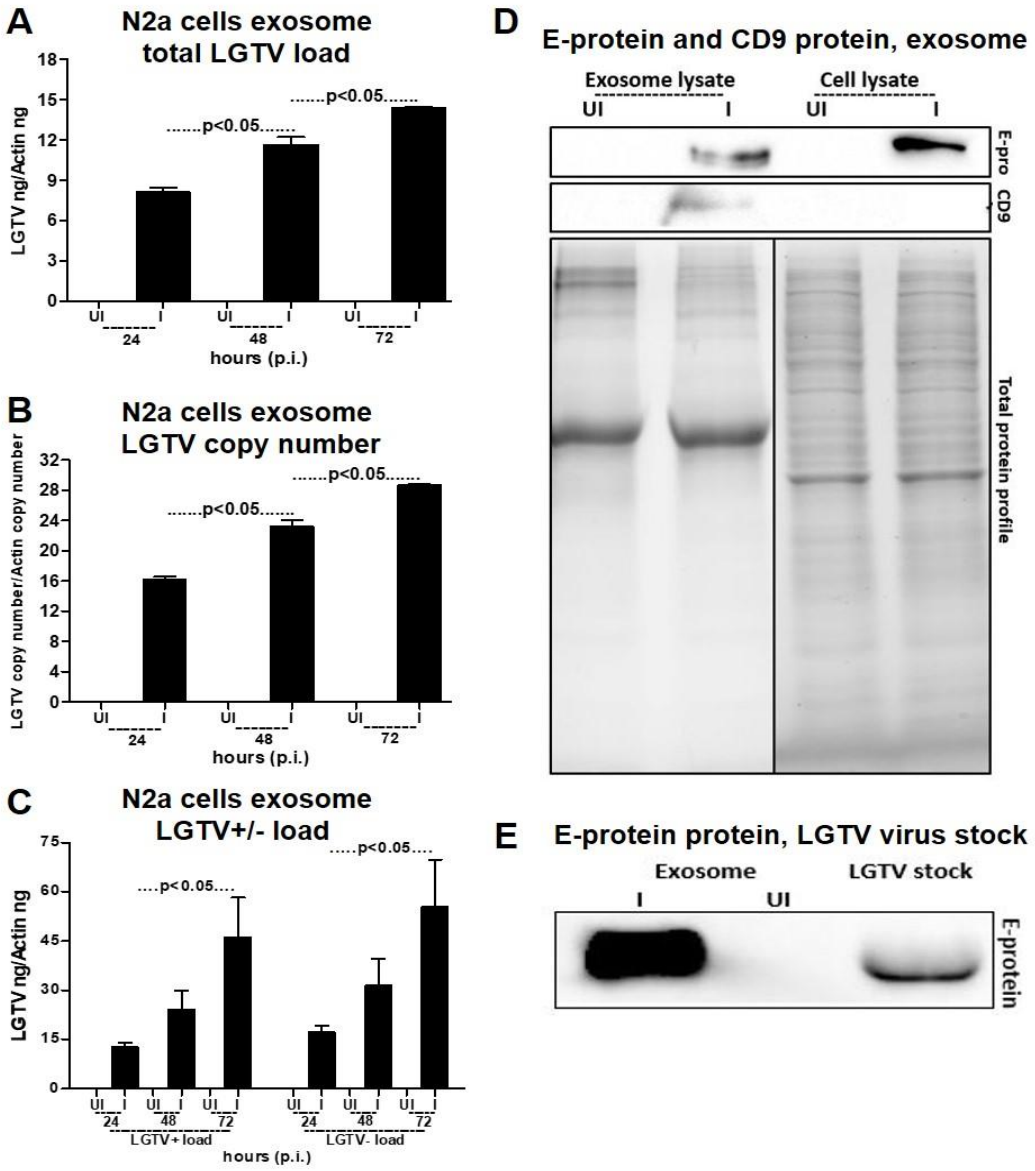

Figure 14. **Detection of LGTV RNA and Proteins in Exosomes Isolated from N2a Cell Line**

(A) QRT-PCR analysis showed the levels of total LGTV loads in exosomes derived from N2a cells.

(B) QRT-PCR analysis showed the copy numbers of LGTV in exosomes derived from N2a cells.

(C) QRT-PCR analysis showed the levels of LGTV positive-sense or negative-sense strand loads in exosomes isolated from N2a cells. N2a (1 x 10^5) cells were infected with 6 MOI of LGTV.

(D) Immunoblotting analysis showed the detection of LGTV E glycoprotein and mammalian exosomal marker CD9 in exosome fractions and total lysates from whole cells prepared at 48 h p.i. from 2 x 10^6 uninfected (UI) or infected (I) N2a cells. Stain-free gels showed the total protein profiles that serve as the loading control.

(E) Immunoblot analysis showed E-protein in de-glycosylated form from laboratory virus stocks.

This figure was adapted from the published journal article (Zhou et al., 2018).

LGTV loads from infected treated or untreated groups was observed (Figure 15A). The uninfected group treated with RNase A was kept as an internal control (Figure 15A). In addition, exosomes isolated from LGTV-infected N2a cells were treated, with Triton-X-100 (0.1%; for 45 min, at RT), or with RNase A (5 µg/ml, for 15 min, at 37°C). QRT-PCR analysis showed that exosomes treated with either Triton-X-100 RNase A has lower LGTV loads in comparison to untreated exosomes (Figure 15B). Enhanced levels of LGTV- E protein in neuronal exosomes treated with Triton-X-100 (0.03%; for 30 min, RT) in comparison to the exosomes treated after freeze-thaw cycle (thrice frozen and thawed at -80°C) or untreated exosomes held at 4°C was detected by native-PAGE followed by immunoblotting with 4G2 antibody (Figure 15C). E-protein was detected at higher molecular mass (<250kDa) in neuronal exosomes when samples were processed for native-PAGE analysis under non-reducing and non-denaturation conditions. Detection of NS1 protein in independent samples at the similar molecular mass suggests presence of other LGTV proteins or polyprotein in exosomes (Figure 15C). Exosomes derived from uninfected N2a cells served as control (Figure 15C). Total protein lysates prepared from uninfected or LGTV-infected neuronal cell-derived exosomes after freeze-thaw or Triton-X-100 treatments or untreated samples served as loading control (Figure 15C). ELISA corroborate results of the native-PAGE, where higher loads of LGTV E-protein were detected when exosomes were treated with 0.1% of Triton-X-100 in comparison to untreated exosomal fractions (Figure 15D). Lower level of E-protein in LGTV-infected untreated neuronal exosomes was considered as background signal due to non-specific antibody binding (Figure 15D). Furthermore, the presence of E-protein inside neuronal exosomes by a 4G2-antibody-coated bead-binding assay (as described in methods) was performed (Figure 15E). No significant ($P>0.05$) differences in viral loads were observed in LGTV-infected (72 h p.i.) neuronal exosome samples that were untreated/treated with either 4G2 antibody or isotype control antibody (Figure 15E). GW4869 inhibitor treated exosomes from LGTV-infected neuronal cells collected at 72 h p.i., followed by treatments with either 4G2 or isotype control also showed no significant ($P>0.05$) differences in viral load in comparison to untreated samples (Figure 15E). However, a significant decrease in LGTV loads were observed in the inhibitor treated group in comparison to no-inhibitor treated group

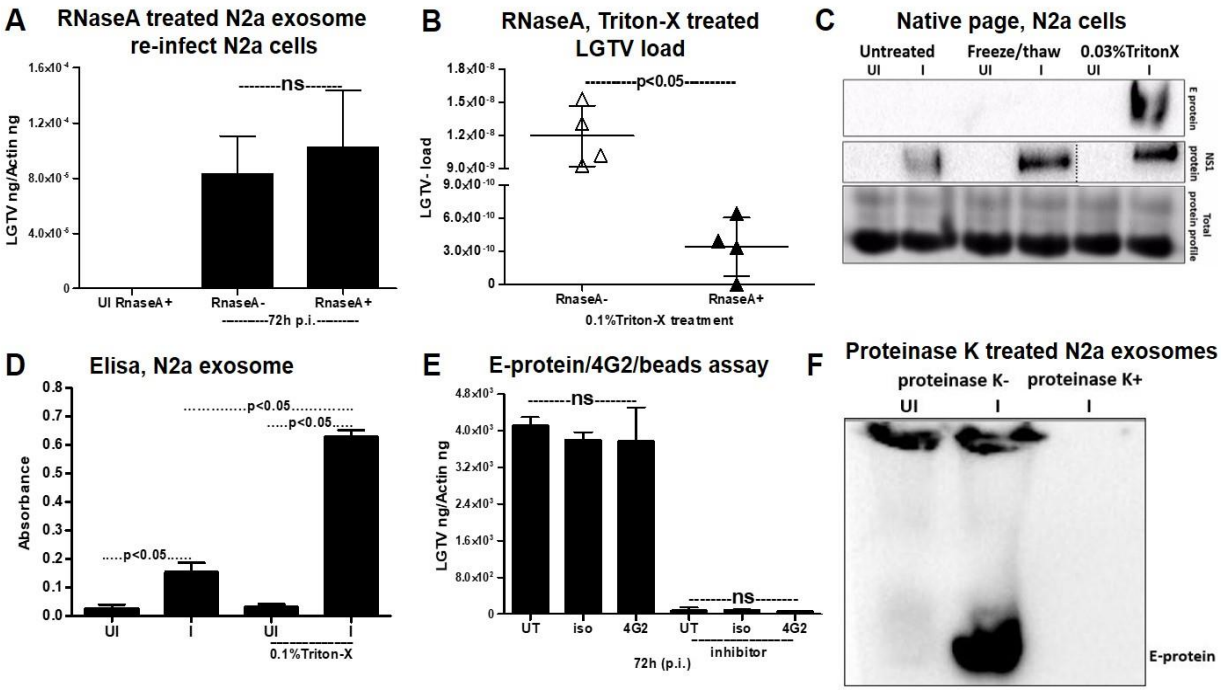

Figure 15. **Exosomes Derived from N2a Cell Line Contains LGTV RNA and Proteins Inside**

(A) The LGTV loads of the treatment of LGTV-infected (72 h p.i.) N2a cell-derived exosomes with RNase A were shown. The uninfected samples treated with RNase A serve as a control.

(B) QRT-PCR analysis showed the LGTV loads in N2a cell-derived exosomes treated with Triton-X-100, followed by RNase A.

(C) Native-PAGE followed by immunoblotting analysis showed the presence of LGTV E- and NS1 proteins from LGTV-infected (MOI 1; 72 h p.i.) or uninfected N2a cell-derived exosomes treated with Triton-X-100 (0.03%), or freeze-thaw cycles or untreated, held on ice. Coomassie-stained gel image showed total protein profiles that serve as a loading control.

(D) ELISA performed on uninfected or LGTV-infected (MOI 6; 72 h p.i.) N2a cell-derived exosomes either untreated or treated with Triton-X-100 (0.1%).

(E) Antibody-beads binding assay performed on infected (MOI 1, 72 h p.i.) N2a cell-derived exosomes (collected from N2a cells either untreated or treated with GW4869; 5 μM, exosome inhibitor) showed no differences in LGTV-E protein loads between 4G2, isotype, and untreated groups.

(F) Immunoblotting analysis showed the E-protein of infected N2a cell-derived exosomes treated with proteinase K (100 μg/μl, 15 min, 37°C). The uninfected but untreated groups serve as a control.

This figure was adapted from the published journal article (Zhou et al., 2018).

(Figure 15E).In addition, treatment with Proteinase K (100 µg/µl, 15 min at 37°C) indicated that all proteins on the exosomes surface might have been digested, thereby, lysing the vesicles and allowing degradation of the exosomal luminal proteins (Figure 15F). E-protein was detected in infected- untreated samples but not in treated samples. Untreated, uninfected samples served as internal controls (Figure 15F). The Ponceau S stained blot showed no proteins upon Proteinase K treatment (Figure 15F).

Exosomes Derived from N2a Cells Contained Viral RNA and Proteins and these Exosomes were Infectious and allowed Viral Replication

Moreover, plaque assays validated that LGTV-infected N2a cell-derived exosomes enclosed infectious viral RNA, with a magnificently higher number of plaques, depending on the evidence of infection with exosome fractions in comparison to the one with supernatant' (Figures 16A and 16B). In addition, infectious exosomes containing LGTV RNA and proteins derived from N2a cells at different time points (24, 48, 72 h p.i.) were able to re-infecting naive N2a cells (Figure 16C). A significantly higher level of viral burden was detected in LGTV containing-exosomes derived from freshly infected N2a collected from 48 or 72 h (p.i.) in comparison to the infection with exosome fractions prepared from 24 h p.i. time points (Figure 16C). Re-infection with supernatant fractions elucidated undetectable levels of LGTV (Figure 16C). A marginal amount of viral load from re-infection kinetics were observed upon incubations with LGTV-infected N2a cell-derived exosomes generated using commercial exosome isolation kit reagent (Figure 16D).

WNV Viral RNA was also Detected in Exosomes

To investigate, whether mosquito-borne *flaviviruses* such as WNV viral RNA is present in exosomes as well, mouse N2a cells were co-incubated with WNV. Viral infection kinetics indicated that WNV rapidly infected N2a cells with increased viremia at 72 h p.i. (Figure 17A). Also, exosomes derived from WNV-infected N2a cells showed a viral infection peak at 72 h p.i. (Figure 17B), suggesting that WNV RNA might also serve exosome as a transmission mediator.

Exosome-Mediated Viral Transmission is Clathrin-Dependent

N2a cells were treated (4 h) with 5 µg of 4G2 monoclonal antibody, followed by infection with exosomes derived from LGTV-infected (72 h p.i.) N2a cells to test whether treatment with 4G2 antibody affects viral transmission. No differences were found in antibody treated or untreated preparations (Figure 17C). Then, it was determined if exosome mediated-viral transmission is receptor-dependent process and requires clathrin-mediated endocytosis. N2a cells were treated with clathrin specific inhibitor (Pitstop-2; 30 µM and 15 min) and infected these clathrin-inhibitor treated cells

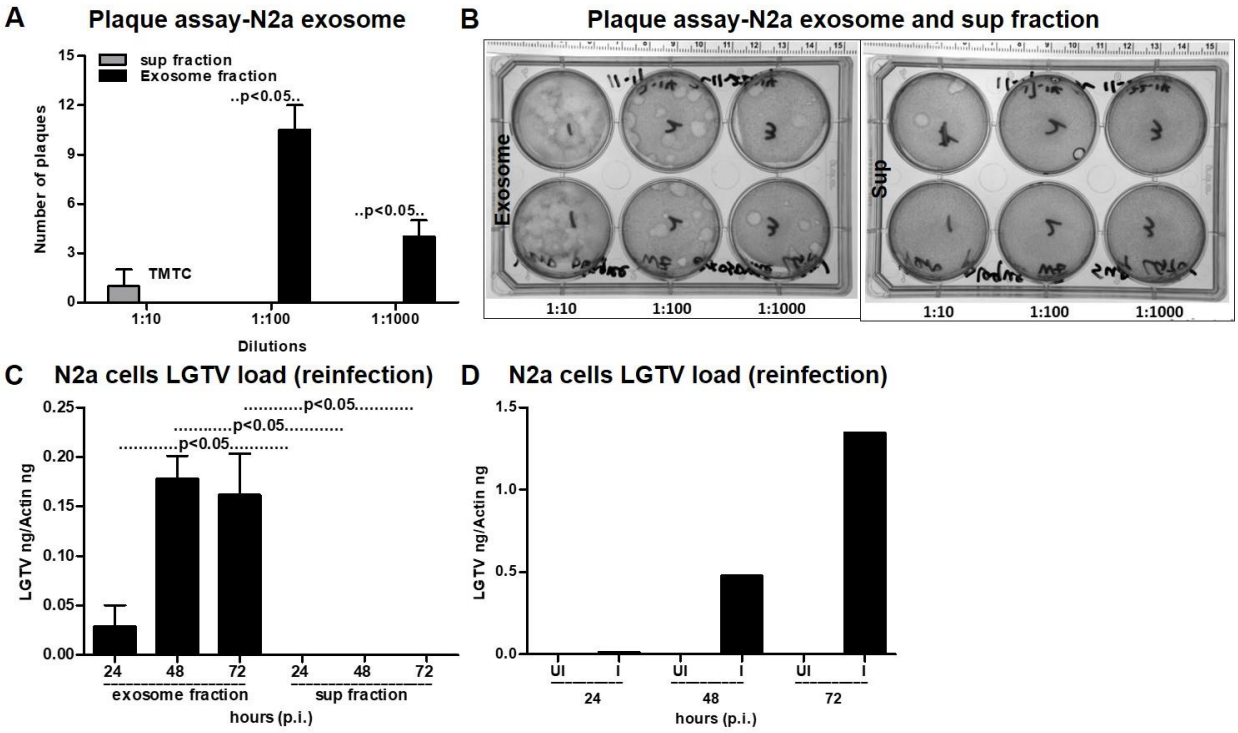

Figure 16. Exosomes Derived from N2a Cells that Contains LGTV RNA and Proteins are Infectious and Replicable

(A) Quantitative assessment of the number of plaques from exosomal and supernatant fractions was shown. TMTC indicates “too many to count”.

(B) Plaque assays performed with different dilutions (1:10, 1:100, 1:1000) of exosome pellet or corresponding different volumes (600, 60, 6 µl) of supernatant fractions prepared from LGTV-infected N2a cells. The rulers at the top determined the scale for the plaques.

(C) QRT-PCR analysis for the LGTV loads in fresh N2a (1 x 10^5) cells at 24 h p.i., infected with

exosomes (20 µl) or supernatant (400 µl) fractions prepared from 24, 48 and 72 h p.i.
(D) QRT-PCR analysis of the infection of naïve neuronal N2a cells (1 x 10^5 cells) collected at 24 h p.i. with exosome (20 µl) fractions prepared from LGTV-infected N2a cells (from 24, 48 and 72 h p.i.) or uninfected cells showed the presence of LGTV RNA in infected cells.
This figure was adapted from the published journal article (Zhou et al., 2018).

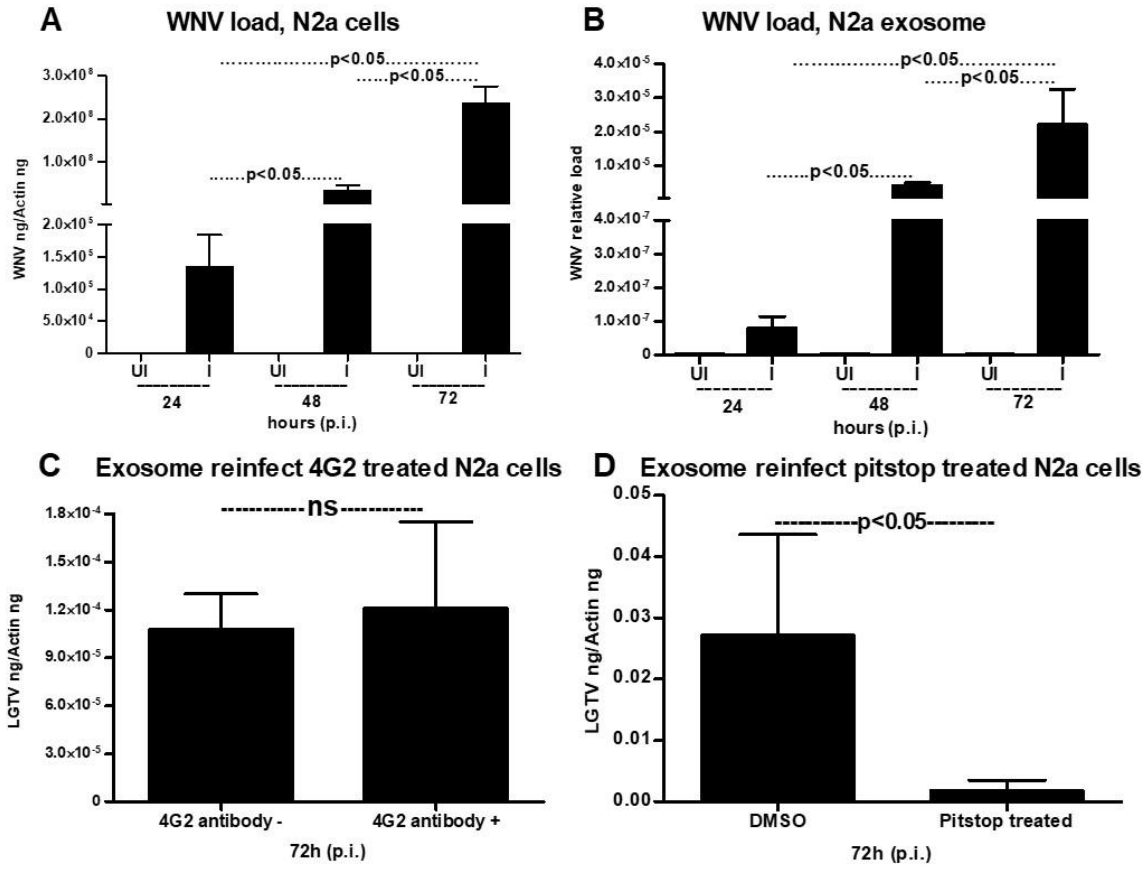

Figure 17. WNV Viral RNA Presents in Exosomes Transmission of LGTV through Infectious Exosome to Naïve Cells is Clathrin Dependent

(A-B) QRT-PCR analysis showed the infection kinetics with WNV (MOI 5) at different times (24, 48, 72 h) p.i., in N2a cells and N2a cell-derived exosomes. WNV E- gene transcript levels were normalized to mouse *beta-actin*.
(C) QRT-PCR analysis showed the LGTV loads in N2a cells treated with a 4G2 antibody (5 µg for 4 h). Infected but untreated sample was served as a control.
(D) QRT-PCR analysis showed the LGTV loads in N2a cells treated with Pitstop-2 clathrin inhibitor (treated 30 µM for 15 min at 37°C) and infected with LGTV-containing (72 h p.i.) N2a cell-derived

exosomes. The infected and DMSO-treated group was served as control. LGTV transcript levels were normalized to mouse *beta-actin*. P values were determined by the Student's two-tail *t*-test.
This figure was adapted from the published journal article (Zhou et al., 2018).

with infectious (LGTV; 72 h p.i.) exosomes derived from N2a cells. A significant ($P<0.05$) reduction in LGTV loads (72 h p.i.) in Pitstop-2 treated cells in comparison to the DMSO (vehicle) treated controls (Figure 17D) was noted. These results suggested that exosome-mediated LGTV transmission to naive cells via receptor-dependent endocytosis that requires clathrin.

Exosome Inhibitor GW4869 Reduced Viral Loads and Transmission

Using GW4869 exosome-inhibitor at different concentrations (1, 5 and 10 μM) significantly ($P<0.05$) depressed LGTV loads in exosomes (from N2a cells) in comparison to DMSO-treated controls (Figure 18A). Furthermore, exosomes isolated from inhibitor-treated (1 μM) N2a cells were magnificently hampered re-infection of naive N2a cells in comparison to DMSO-treated control (Figure 18B). In addition, it has been proved that exosomes derived from N2a cells that pre-treated with 5 μM inhibitor, then followed with LGTV infection, had significantly lower viral loads in comparison to exosomes isolated from cells post-treated with inhibitor after infection (Figure 18C). Whereas, viral loads in exosomes were significantly deducted in N2a cells in spite of pre- or post-inhibitor treatment in comparison to the LGTV infection performed with 5 MOI laboratory viral stocks (Figure 18C). Plaque assays performed with exosomes derived from LGTV infected N2a cells DMSO-treated group yielded significantly increased number of plaques in comparison to the group's with exosomes isolated from inhibitor-treated (Figures 18D and 18E). Also, plaque assays performed with exosome preparations from N2a cells revealed the viral titers for both N2a 1 μM-inhibitor treated group (2.3×10^3 pfu/ml) and N2a-DMSO control group (8×10^3 pfu/ml). The GW4869 inhibitor effects on LGTV viral particles from virus stocks were also measured. Immunoblotting with 4G2 antibody showed no differences in 5 or 10 μM exosome inhibitor treated (4 h) groups, in comparison to the DMSO control (Figure 18F).

Infectious Viral RNA and Proteins were Transmitted from One Neuronal Cell to Others via Exosomes

To investigate whether exosomes serve as the mediators of viral transmission from one neuronal cell to another, LGTV infections were executed on primary neuronal cultures of murine cortical neurons (isolated from female mice's embryonic day E16 brains, as described in methods). Infection of cortical neurons with LGTV (MOI 4) showed kinetics of LGTV infection in a time dependent manna with increased viral burden at 72 to 96 h p.i. (Figure 19A). QRT-PCR analysis revealed magnificently ($P<0.05$) increased LGTV loads and replication numbers in exosomes derived from murine cortical neurons at 72 h (p.i.), comparing to other tested time points exosomes preparations (of 24 and 48 h p.i.) (Figures 19B and 19C). Furthermore, higher loads of LGTV positive- and negative-sense RNA strands have been detected, suggesting the presence of both viral genomes in the LGTV infected neuronal cells derived exosomes (Figure 19D). Immunoblotting elucidated plentiful LGTV E-protein amounts (2 to 3 folds) in exosomes derived from cortical neurons in comparison to the loads found in total cell lysates (Figure 20A). Like N2a cells, possibly de-glycosylated LGTV E protein (with low molecular mass) was again, detected in exosomes derived from cortical neurons in comparison to the total cell lysates (with high molecular mass) isolated from cortical neurons (Figure 20A). Remarkable levels of CD9 (exosomal marker) were detected in the LGTV-infected cortical neurons derived exosomes and in total cell lysates in comparison to their alternatively uninfected controls (Figure 20A). Furthermore, levels of CD9 were dramatically enhanced in exosomes from LGTV-infected cortical neuronal cells in comparison to the levels in total cell lysates (Figure 20A), suggesting that LGTV infection may facilitate the enrichment of CD9 in neuronal cells derived exosomes. Also, exosomes from LGTV infected cortical neurons resulted in higher amounts of CD9 in comparison to the N2a cell-derived exosomes enclosing LGTV (Figures 14D and 20A). Total protein profiles were considered as loading control in the immunoblotting analysis (Figure 20A). Immunoblotting showed the presence of NS1 in both exosomes' and in total cell lysates preparations, suggesting that exosomes from cortical neurons contain LGTV proteins (Figure 20B).

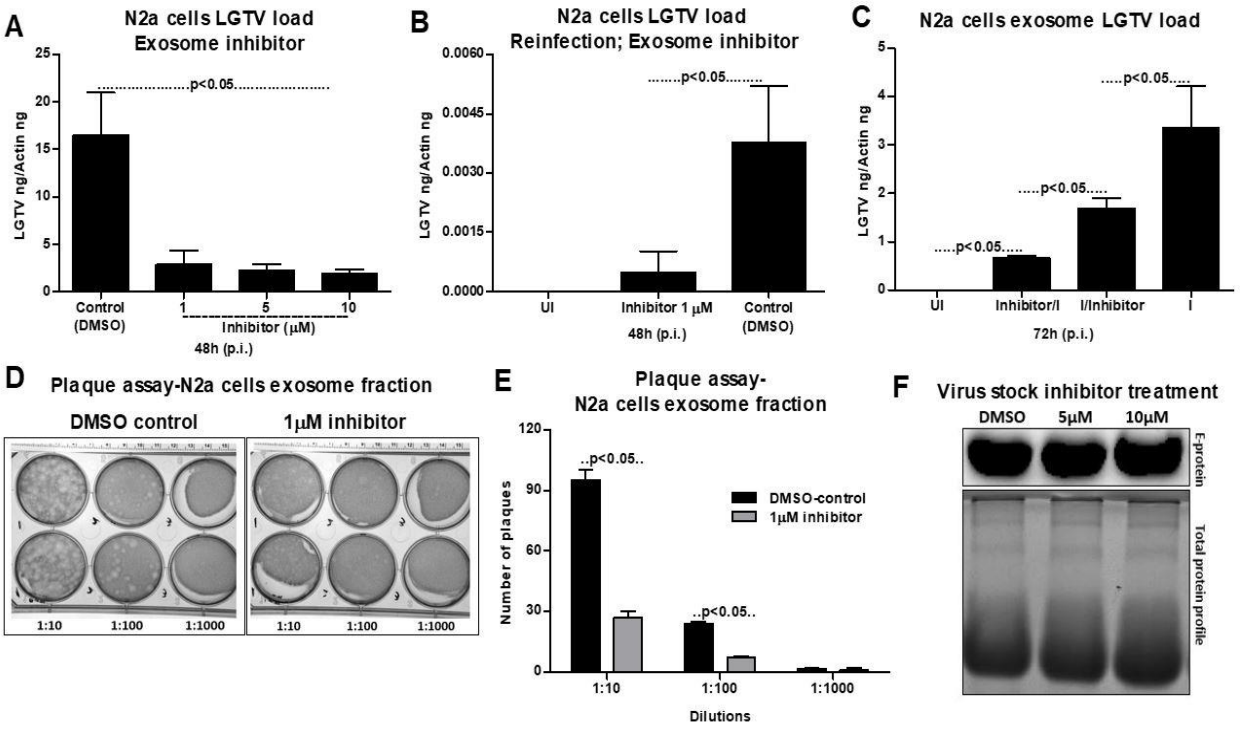

Figure 18. Treatment of Neuronal N2a Cells with Exosome Inhibitor Affects LGTV Infection, if Treated either before or after Infection

(A) QRT-PCR analysis showed the levels of LGTV in exosomes isolated from N2a cells at 48 h p.i. in the presence of exosomes-inhibitor at different concentrations (1, 5, 10 μM). 1 x 10^5 N2a cells were pre-treated with inhibitor for 4 h followed by infection with LGTV (6 MOI). Exosomes isolated from N2a cells treated with DMSO served as a loading control.

(B) The levels of LGTV in N2a cells at 48 h p.i., infected by treatment with exosomes (20 μl) isolated from control or inhibitor-treated N2a cells were shown.

(C) QRT-PCR analysis showed the levels of LGTV in N2a cells at 72 h p.i. Uninfected N2a cells were treated with 5 μM inhibitor. For LGTV-infection, N2a cells were first treated for 4 h with an inhibitor then followed by infection (Inhibitor/I) or cells were first infected for 4 h with LGTV and then treated with inhibitor (I/inhibitor). LGTV (6 MOI) was used to infect 1 x 10^5 N2a cells in the presence (5 μM) or absence of inhibitor. LGTV transcript levels were normalized to mouse *beta-actin*.

(D) Plaque assays performed with different dilutions (1:10, 1:100, 1:1000) of exosomes fraction isolated from control DMSO-treated or inhibitor-treated N2a cells were shown.

(E) Quantitative assessment of the number of plaques from DMSO-treated or inhibitor-treated was shown. P values were determined by the Student's two-tail *t*-test is shown.

(F) The detection of E-protein of Laboratory virus stocks treated with either GW4869 inhibitor (5 and 10 μM) or DMSO as control was shown.

This figure was adapted from the published journal article (Zhou et al., 2018).

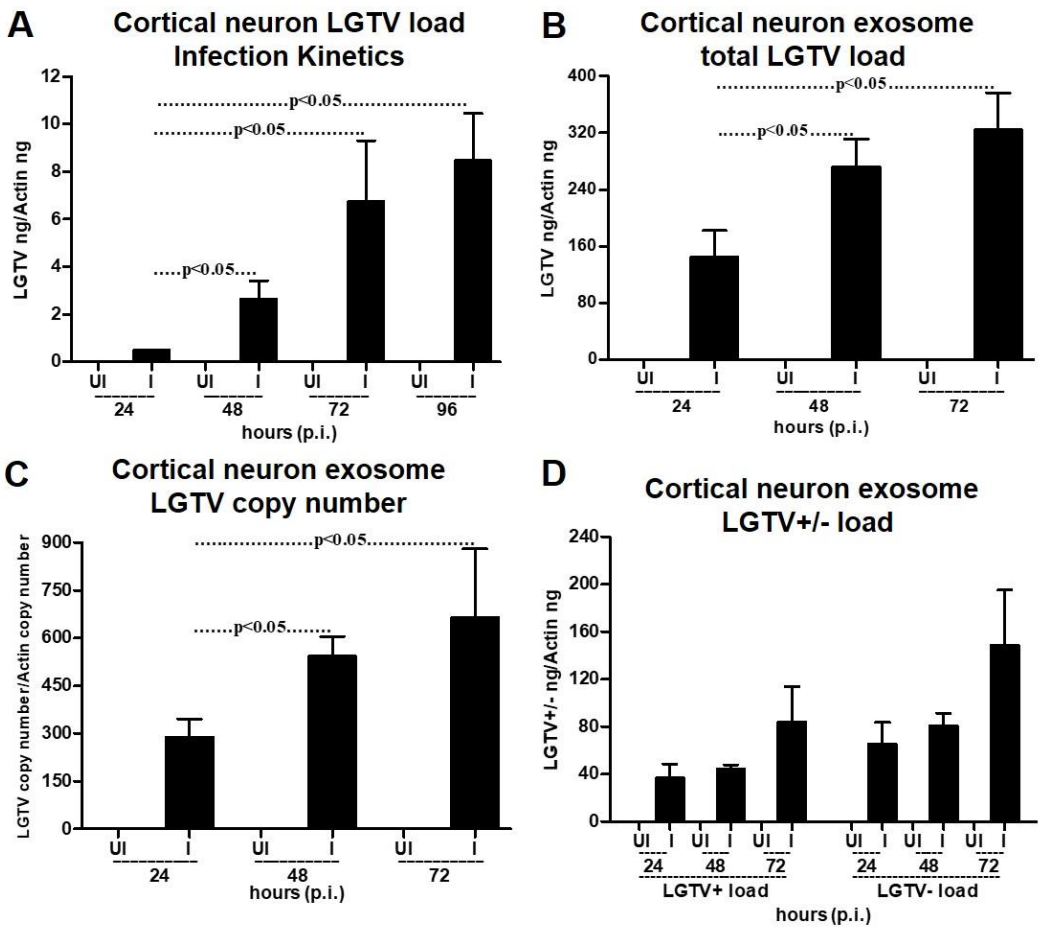

Figure 19. Detection of LGTV RNA in Exosomes of Mouse Cortical Neurons

(A) QRT-PCR analysis showed the LGTV infection kinetics in primary cultures of mouse cortical neurons at different time points (24, 48, 72, 96 h p.i.).

(B) QRT-PCR analysis showed the total LGTV loads in exosomes isolated from cortical neurons at different time points (24, 48, and 72 h p.i.).

(C) QRT-PCR analysis showed the LGTV copy number in exosomes isolated from cortical neurons at different time points (24, 48, and 72 h p.i.).

(D) QRT-PCR analysis showed the LGTV positive-sense and negative-sense strand in exosomes isolated from cortical neuronal cells at different time points (24, 48, and 72 h p.i.). LGTV (4 MOI) was used to infect 1 x 10^5 murine cortical neuronal cells. “UI” indicated uninfected and “I” indicated LGTV-infected. LGTV transcript levels were normalized to mouse *beta-actin*. P values were determined by the Student's two-tailed *t*-test. Representative data were shown from at least three independent experiments.

This figure was adapted from the published journal article (Zhou et al., 2018).

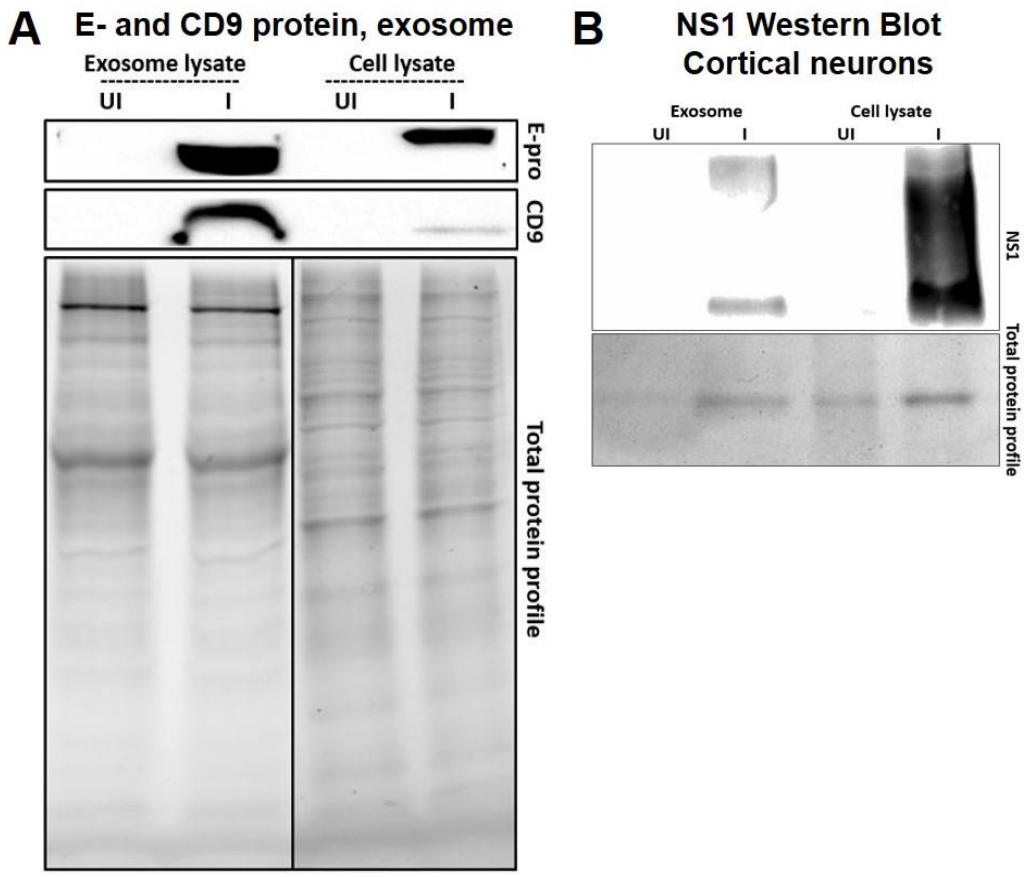

Figure 20. Detection of LGTV Proteins in Exosomes of Primary Cultures of Cortical Neurons

(A) Immunoblotting analysis showed the detection of LGTV E-protein and mammalian exosomal marker CD9 in exosome fraction and total lysates from whole cells prepared from uninfected (UI) or infected (I) cortical neuronal cells at 48 h p.i. The stain-free gel showed the total protein profile that served as the loading control.

(B) Immunoblotting analysis showed the NS1 levels in total neuronal lysates and exosomes derived from LGTV-infected (MOI 4; 72 h p.i.) cortical neurons. Uninfected (UI) cells and exosomes derived from these cells served as controls, in addition to total protein profiles. For immunoblotting assays, 2 x 10^7 cortical neuronal cells were infected with 4 MOI of LGTV.

This figure was adapted from the published journal article (Zhou et al., 2018).

Neuronal Exosomes Containing Viral RNA and Proteins are Infectious

Plaque assays verified that exosomes derived from cortical neurons could carry infectious and reproductive viral RNA, because of the significantly increased number of plaques, with the evidence upon infection with exosomes (in different dilutions; of 1:10, 1:100, 1:1000) in comparison to the infection with supernatant fractions (Figures 21A-21C). Similar data were previously obtained for N2a cells, suggesting that LGTV is concentrated in neuronal exosomes. Additionally, exosome fractions derived from LGTV-infected cortical neurons at several time points (of 24, 48, 72 h p.i.) were able to re-infect naive cortical neuronal primary cultures (Figure 21D). A magnificent higher viral burden was detected in the cortical neurons which are infected with exosome fractions (collected from 24, 48, 72 h p.i.) in comparison to the infection with the supernatant preparations generated from alternative time points (Figure 21D). These results suggested that exosomes from LGTV-infected cortical neurons are potential mediators of LGTV transmission among neurons.

Exosome Inhibitor GW4869 Treatment on Cortical Neuron Reduces Viral Infection

Furthermore, the presence of exosome-inhibitor at 10 or 20 μM significantly reduced viral infection in cortical neurons when compared to DMSO-treated controls (Figure 22A). However, no variation in the viral burden of cortical neurons were detected upon treatment with 1 μM exosome inhibitor in comparison to DMSO-treated control (Figure 22A). Exosomes isolated from 10 μM-treated cortical neurons showed significantly depressed re-infecting viral loads of naive cortical neurons in comparison to the infections performed with exosomes derived from DMSO-treated control (Figure 22B). Plaque assays revealed that LGTV-containing exosomes derived from DMSO-treated neurons enclosed notable and increased LGTV loads, comparing to exosomes derived from 10 μM exosome inhibitor-treated group (Figures 22C and 22D). Overall, these results suggest that LGTV and maybe TBEV, use exosomes as novel modes of transmission among neuronal cells.

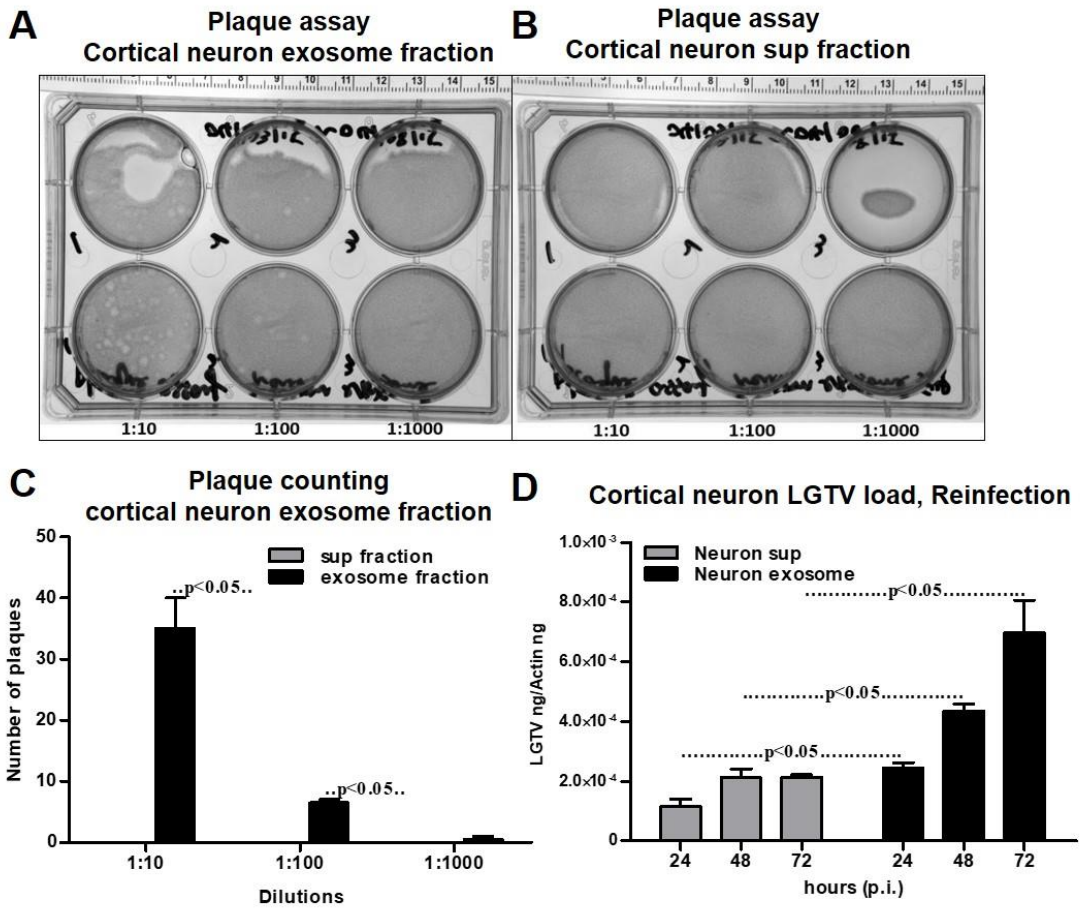

Figure 21. Exosomes Containing LGTV RNA and Proteins that Derived from Cortical Neurons are Infectious

(A-B) Plaque assays performed with different dilutions (1:10, 1:100, 1:1000) of exosome pellet or corresponding different volumes (600, 60, 6 µl) of supernatant fractions prepared from LGTV-infected cortical neuronal cells were shown. The rulers at the top were determined the scale for the plaque assay from the representative images. Representative images from two independent experiments were shown.

(C) Quantitative assessment of the number of plaques from exosomal and supernatant fractions was shown.

(D) QRT-PCR analysis of viral loads in 1x 10^5 naïve cortical neuronal cells at 24 h p.i., infected through treatment with exosomes (20 µl) or supernatant fractions (400 µl) prepared from 24, 48 and 72 h p.i., LGTV-infected neurons showed the presences of LGTV. LGTV transcript levels were normalized to mouse *beta-actin*. P values were determined by the Student's two-tailed *t*-test is shown. Representative data were shown from at least three independent experiments.

This figure was adapted from the published journal article (Zhou et al., 2018).

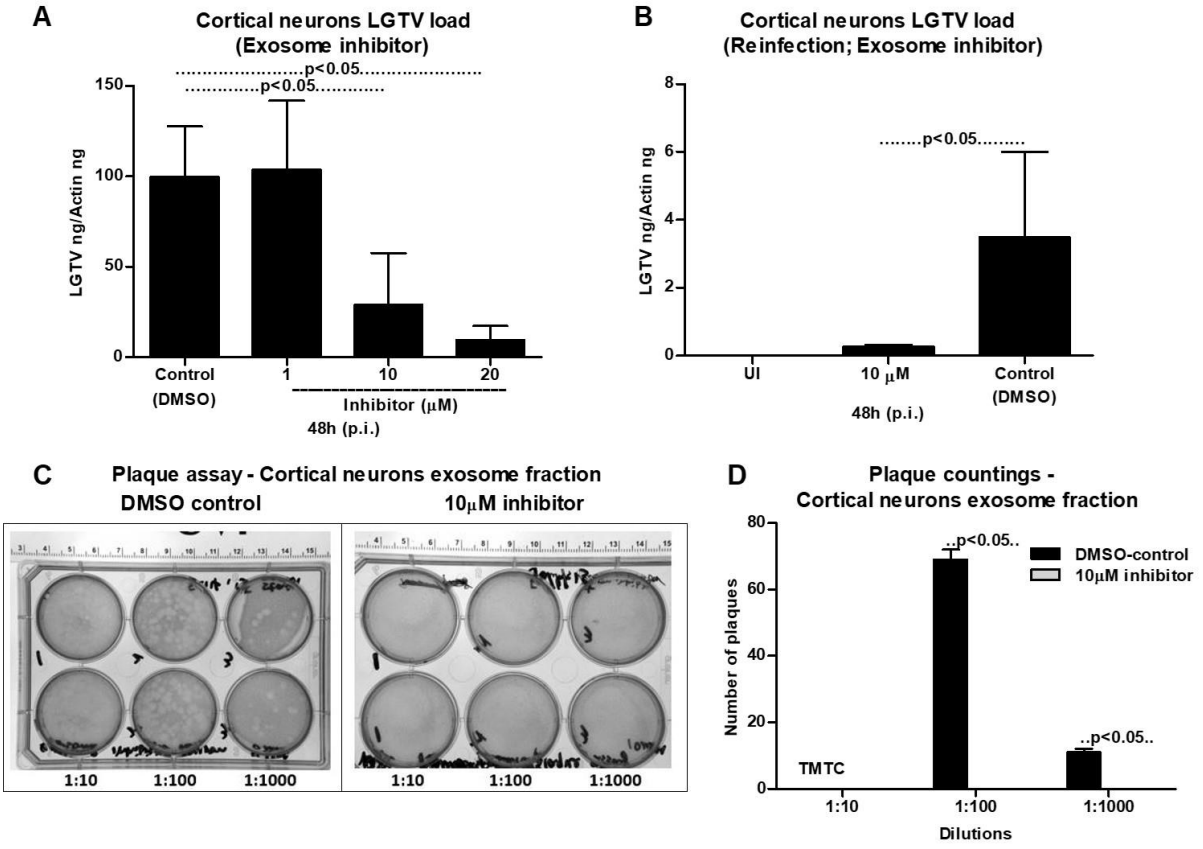

Figure 22. Treatment of Cortical Neurons with Exosome Inhibitor Affects LGTV Infection

(A) QRT-PCR analysis showed the levels of LGTV in exosomes isolated from cortical neuronal cells at 48 h p.i. in the presence of exosome inhibitor at different concentrations (1, 10, 20 μM). Cortical neuronal cells were pre-treated with exosomes inhibitor for 4 h followed by infection with LGTV. Exosomes isolated from cortical neuronal cells treated with DMSO served as a control.

(B) QRT-PCR analysis showed the levels of LGTV in fresh cortical neuronal cells at 48 h p.i., infected by treatment with exosomes (20 μl) isolated from control or inhibitor-treated mouse cortical neuronal cells. “UI” indicated uninfected cells that served as control. LGTV transcript levels were normalized to mouse *beta-actin*.

(C) Plaque assays performed with different dilutions (1:10, 1:100, 1:1000) of exosomes fractions isolated from control DMSO-treated or inhibitor-treated cortical neuronal cells were shown. The rulers at the top determined the scale for the plaque assay. Representative images were shown from two independent experiments.

(D) Quantitative assessment of the number of plaques was shown. TMTC indicates “too many to count”. P values were determined by the Student's *t*-test is shown. Representative data were shown from three independent experiments.

This figure was adapted from the published journal article (Zhou et al., 2018).

2.3 DISCUSSION

Exosomes contribute to the transmission and communication of intracellular materials among cells and from one tissue to the other as well (Fevrier and Raposo, 2004; Thery, 2011; Bang and Thum, 2012). Several biological presumptions and medical requirements have been affixed with the exosomes as potential mediators of messages transmission and communication between cells and tissues (Thery et al., 2002; Johnstone, 2006; Keller et al., 2006; Van Niel et al., 2006). For the first time our appealing data show that exosomes are considered as novel mediators for transmission of arthropod-borne *flaviviruses* such as LGTV, WNV, and TBEV that infect a wide variety of vertebrate hosts, as well as humans. It has been found that tick cells secrete exosomes that are carriers of the tick-borne virus, LGTV, (Figures 6, 7, 9, and 10) suggest that other tick-borne *flaviviruses* such as TBEV and POWV might also use this mode of transmission from arthropods to humans. Cryo-EM data elucidated that exosomes derived from either arthropod or neuronal cell are of different sizes and were in the ranges of 30 to 250 nm (Figures 6A and 13A). Exosomes derived from both arthropod and neuronal cells had many of the exosome sizes between 50 to 100 nm and fewer vesicles from sizes of 200 to 250 nm in both uninfected and infected groups (Figures 6C, 6D, 13C and 13D), suggesting purity in isolation methods. Increased number of exosomes in LGTV infected in comparison to the uninfected groups (Figures 6B and 13B), suggested higher production and release of exosomes. To generate virus preparations for structural investigations, concentrated supernatants, perhaps titers with 10^9 to 10^{12} PFU/ml and centrifugal forces of 200,000g are performed (Fragnoud et al., 2015), which are not similar in exosomal isolation methods. Whereas, with the purpose to minimize the viruses and large protein aggregates that co-sediments during ultracentrifugation, the buoyant density of exosomes was adopted for purification purposes. Continuous or discontinuous sucrose density gradient centrifugation has been performed thoroughly to purify exosomes. However, this approach does not permit division of exosomes from viruses, macro vesicles and large micro-vesicles with comparable sedimentation velocities (Tauro et al., 2012). Substituting sucrose with iodixanol (OptiPrep) in the velocity gradients using 5 to 40% density gradients has been

shown to conquer the restrictions and end up with purified exosomal fractions (Tauro et al., 2012). Detection of tick HSP70 in exosomal fractions (Figure 9A), suggesting that it could be a novel arthropod marker that may be transmitted in exosomes from saliva and facilitate tick feeding on vertebrate host. Recently, it is reported that arthropod HSP70 may aid in the host fibrinogenlysis at the tick bite site (Vora et al., 2017). Detection of CD9 in all uninfected preparations and the enrichment in fractions 4 and 5 suggested that these fractions are exosomes. The visible shift in enrichment of CD9 in LGTV-infected fraction 3 and 4, and no detection in fractions 1 and 6, suggested the presence and enrichment of other proteins or cargo (including viral E-protein in fraction 4) in those preparations. Our findings demonstrated the enrichment of both arthropod and neuronal E-protein in exosomal fractions 4 and 5 supported the presence of viral E-protein in exosomes (Figures 6E and 13E). It can be proposed that due to space limitation and narrowly regulated cargo sorting mechanisms, exosomes are undoubtedly filled with viral RNA and proteins that are trafficked to extracellular fate and later recycled back via merging with plasma membranes. If entire viral particles are perhaps exported through exosomes, it could be anticipated enclosure (or packaging) of few LGTV viruses of 40 to 60 nm size in ~150 to 200 nm diameter of arthropod/neuronal cell-derived exosomes. No detection of any viral particles or fully assembled virions inside of the exosomes, in several of the preparations processed for cryo-electron microscopy. However, it doesn't exclude the possibility of viral particles' presence in the exosomes. Based on these findings, it is believed that if viral RNA (both positive- and negative-sense strands) and proteins are loaded into exosomes, they can be exported and consequently transmitted to the neighboring cells and far distant tissues for pathogenesis in short times. The matured virions of positive-sense RNA strand exit cells through membrane budding. However, the replicative which is the negative-sense viral RNA genome is cytosolic (Mukhopadhyay et al., 2005; Li et al., 2008; Apte-Sengupta et al., 2014; Kuhn et al., 2015). Observations of both positive and negative-sense RNA strands in tick/neuronal cell-derived exosomes indicates that exosomes facilitate the transmission of both negative- and positive-sense strands RNA genomes. The higher loads of negative-strand RNA in the exosomes derived from neuronal cells implied that LGTV negative-strand RNA might simply get trafficked during endocytosis/uptake by these cells. The

negative strand of RNA generally exists as dsRNA with positive-sense strand. Thus, it seems that dsRNA may be present inside exosomes, instead of single-stranded positive or negative strand of LGTV. Furthermore, entry of more viral RNA and proteins into cells through receptor-mediated endocytosis mechanism may simply force the replicative viral RNA to exit the host cell and look for other neighboring cells via the exosome-mediated transmission. The study shows that exosome-mediated viral transmission is clathrin dependent process (Figure 17D) further suggest a significant function for exosomes as viral RNA and protein transporters.

Up-regulation of some proteins in LGTV-infected tick exosomal lysates, comparing to the uninfected controls indicates the importance of these proteins in assisting the transmission of tick-borne *flaviviruses* from exosomes derived from tick cells (Figure 9A). This research branch, in the future, should concentrate on the identification and characterization of these remarkable cargo proteins on arthropod exosomes that could be selected for the development of a novel transmission-blocking vaccine (Neelakanta and Sultana, 2015). The presence of LGTV RNA (of RNase A treatment studies) and E- protein inside exosomes but not outside in suspensions of exosomal fractions, suggest that exosomes not only securely carry and protect the viral RNA (both positive and negative strands), but also transport the essential viral E-protein into host endosomal membranes, then to release viral content inside cells. It has been noted that exosome-mediated viral transmission is clathrin-dependent suggests a possibility that receptor-mediated endocytosis may uptake of infectious exosomes into naive cells. The trans-well assays data performed with tick cell-derived exosomes and human keratinocytes, HaCaT cells, (Figure 10D) suggest that tick spit/secreted saliva containing exosomes (loaded with LGTV viral RNA and proteins), could assist the transmission of this virus from the tick bite site to the vertebrate host skin side. No differences, or flat kinetics of LGTV infection in human keratinocytes, suggested that these cells may not keep persistent infection but prefer to transmit viruses to dendritic/ other migratory immune cells in the skin at their earliest. It is assumed as well that keratinocytes are probably highly immune tolerant and may keep viral infections at a low level. Plenty of infectious LGTV RNA and proteins inside exosomes also indicates that exosomes may rapidly facilitate the dissemination of these viral factors within the tick

body (for instance, upon entry, from hemolymph to salivary glands, then midgut during transmission) or transmission through saliva to the vertebrate host upon infected arthropod bite or blood-feeding. Infection of vascular endothelial cells with tick cell-derived exosomes containing LGTV infectious RNA and proteins suggest that upon tick blood-feeding, arthropod exosomes facilitate infection of the blood endothelium in the vertebrate host. It is noteworthy that the GW4869 inhibitor significantly lowered LGTV in exosomes derived from tick, bEnd.3, N2a and neuronal cells (Figures 10D, 11F, 18A and 22A). These results demonstrate a common pathway shared in the formation and release of exosomes on both arthropods' and vertebrates' sides. Taken together, these data revealed a novel mode of *flavivirus* transmission from the arthropod vector to the vertebrate host via exosomes that could be considered as transmission-blocking strategies.

Most of the *flaviviruses* can infect and replicate in the vertebrate brain microvascular endothelial cells that line and guard the BBB. Infected endothelial cells prefer the *flaviviruses* to come inside cells membrane and cause neuro-invasion of the CNS (Sultana et al., 2009; Sultana et al., 2012; Neal, 2014; Suen et al., 2014). It has been emphasized that initial entry of few infected exosomes isolated from endothelial cells, lining the BBB, may lead to the transmission of virus into the CNS. Infection of neuronal cells and secretion of large amount loads of infectious exosomes by neuronal cells may induce the breaching of the BBB, thus, allowing entry of more significant peripheral viral loads, as well as the trafficking of immune cells from the periphery. Based on the results (Figures 11C-11F), the assumption that the initial batch of infected-brain microvascular endothelial (bEnd.3) cell-derived exosomes containing more loads of infectious LGTV RNA and proteins might enter into the CNS at an early time point (24 h p.i. of endothelial cells). The higher viral loads in exosomes that derived from brain endothelial cells from early time points (24 h p.i.) in comparison to less loads in exosomes at later time points more distantly suggest that earlier transmission of viral RNA via exosomes that infect neighboring neuronal cells. It was also addressed that bEnd.3 cells (in infection kinetics assays) showed stronger resistant to LGTV infection without severe cytopathological effects in comparison to neuronal cells. It can be assumed that the brain endothelial cells may not tolerant the higher rate of viral

replication or persistent infection for longer time. This could end up with higher packaging of LGTV viral RNA and perhaps proteins in bEnd.3 cell-derived exosomes that would cause the dissemination of *flaviviruses* to neuronal cells at earlier times. The trans-well assay (Figure 11F) could imitate viral transmission in *in vivo* scenario, where infected bEnd.3 cells derived exosomes might transmigrate across astrocyte foot layer and infect neurons in the CNS. This result could be directly connected to the *in vivo* circumstance that proposes virus transmission from infected-brain microvascular endothelial cells (lining the BBB) to the interior of the CNS. Overall, these studies suggest that infected-brain endothelial cells may not delight *flavivirus* replication for longer times and thus, transmit this viral RNA and proteins to their neuronal counterparts via exosomes at the earliest.

This study also demonstrates that neuronal exosomes are likely able to manipulate transmission of tick-borne *flavivirus* RNA and proteins from one neuron to the others. Higher loads of E-protein (2 to 4 folds more) in exosomes derived from murine cortical neurons when compared to the *in vitro* cultures of N2a cell-derived exosomes indicate higher packaging of viral RNA and proteins in cortical neurons (Figure 20A). It is considered that the observation of lower mass for LGTV E-protein in both N2a cells and cortical neurons is because of the possible de-glycosylation of E-protein. The de-glycosylated E-protein in laboratory viral stocks indicated a mixture of virions with exosomes in those frozen supernatants. Whereas, this effect showed no evidence in arthropod cell-derived exosomes, addressing that E-protein in arthropod exosomes may not undergo protein modification. Glycosylated form of LGTV E- protein in arthropod cells is maintained chances to speed up exosome fusion process and viral infection of host cells immediately respond to host-seeking and tick blood-feeding on the vertebrate host. It has also been seen that in mosquitoes, WNV E-protein is heavily glycosylated and is essential for pathogen transmission to the vertebrate host (Moudy et al., 2009). The assumption is that the presence of a de-glycosylated form of viral E-protein in neuronal and other mammalian cell-derived exosomes may allow viral E-protein to keep its stability in these small vesicles through the transmission from one cell to its neighbors. In addition, it can be assumed that more viral E-protein packing in vertebrate neuronal exosomes may be reasonable only if E-protein exists in the de-

glycosylated form with less molecular mass when compared to the glycosylated form. Furthermore, arthropod and vertebrate host may prefer different conformations of E-protein that would assist when substances inside exosomes are delivered to the host cytosol. The de-glycosylation of E protein in neuronal exosomes may also increase the infectious ability to form matured virions in a new hostile micro-environment. Higher loads of CD9 in exosomes derived from neurons prove that cortical neuronal cells might have a greater yield of exosomes, comparing to the *in vitro* cultured N2a cell line (Figures 14D and 20A). It is practical to consider that neurons have complex approaches of cell communication, including synaptic transmission and neurotransmitter release that might require a greater yield of exosomes in the CNS. Low total protein content was shown in the N2a and cortical neuronal exosomes in comparison to the protein content in the whole cells, suggesting that only a small portion of proteins could be essential and imported as cargo in LGTV-infected exosomes derived from cortical neurons. Total protein profiles in N2a cells showed a lack of some exosomal proteins upon LGTV infection, hinting that these proteins may affect or inhibit viral proteins in exosomes derived from N2a cells. Future studies in identifying these reduced exosomal proteins upon LGTV infection would assist in discovering novel therapeutic targets against transmission. The detection of E-protein at higher molecular mass (<250kDa) in native-PAGE gels, indicated that exosomes might contain a higher order structures of E-protein as oligomers. The presence of NS1 in same samples at similar molecular mass further indicated that exosomal preparations might enclose polyprotein (Figure 15C). The presence of highly infectious LGTV RNA and proteins in exosomes from neuronal cells suggested that these cells upon infection, mediate viral dissemination in the CNS. Also, detected WNV in neurons derived exosomes, further addresses that exosomes as a novel transmission mode for both tick- and mosquito-borne *flaviviruses* in neuronal cells. The assumption is that exosomes may keep the viability of this viral RNA and proteins that may favor persistent pathogenesis.

GW4869 (dihydrochloride hydrate) is a cell-permeable but selective inhibitor for neutral sphingomyelinase (an essential enzyme required for exosomes formation and release). The effect of this inhibitor on both arthropod and mammalian cells used in this study indicates neutral sphingomyelinase do present in these cells. Treatment with

GW4869 affected LGTV replication, loads and transmigration from one cell type to others supporting that LGTV or other tick-borne *flaviviruses* may use neutral sphingomyelinase for packaging into exosomes; furthermore, studies would interpret the role of neutral sphingomyelinase on LGTV and other *flaviviruses* packaging in arthropod or mammalian exosomes. In N2a cells, 1 μM of inhibitor was sufficient to decrease the loads of LGTV (as proved by infection, reinfection and plaque assay) in contrast to higher doses (10 and 20 μM) of GW4869 that was required for inhibition of viral loads in primary cortical neuronal cells (Figure 22A). The clear sensitivity of N2a cells upon GW4869 treatment could be elucidated by the possibility of a low number of exosomes or less neutral sphingomyelinase in these cells when compared to cortical neurons. The role of GW4869 on LGTV infection in N2a cells indicated that inhibition of exosomes either before or after infection would affect LGTV loads and transmission (Figure 18C). The results from this study suggested that inhibition of exosomes reduced LGTV loads in both arthropod and mammalian cells, furthermore, infection with tick-borne *flaviviruses* was affected when exosome formation and release were hampered with GW4869 treatment. The observation of no effects of GW4869 on laboratory viral stocks suggested that it is specific for blocking the release of exosomes and has no direct effect on viral particles. It would be intriguing to determine if GW4869 or other novel exosome inhibitor(s) could serve as potential therapeutic approaches for treating flaviviral infections. The model (Figure 23) clarified the role of exosomes in the transmission of tick-borne *flavivirus* RNA and proteins from the arthropod to human cells and disseminated these infectious exosomes within the vertebrate host. Overall, this study indicated that exosomes play magnificent roles: a) In the transmission of tick/mosquito-borne *flaviviruses* from infected arthropod to the vertebrate host cells. b) In the infection of the human skin keratinocytes (HaCaT) and vascular endothelial cells (HUVEC) during tick bite/blood feeding. c) In mediating brains, infectious exosomes invade microvascular endothelial cells and cause neuro-invasion. d) In the infection of neuronal cells resulting in a higher yield of exosomes containing infectious viral RNA and proteins, essential for the dissemination and infection of naive neuronal cells in the CNS that causes neuropathogenesis and severe neuronal loss.

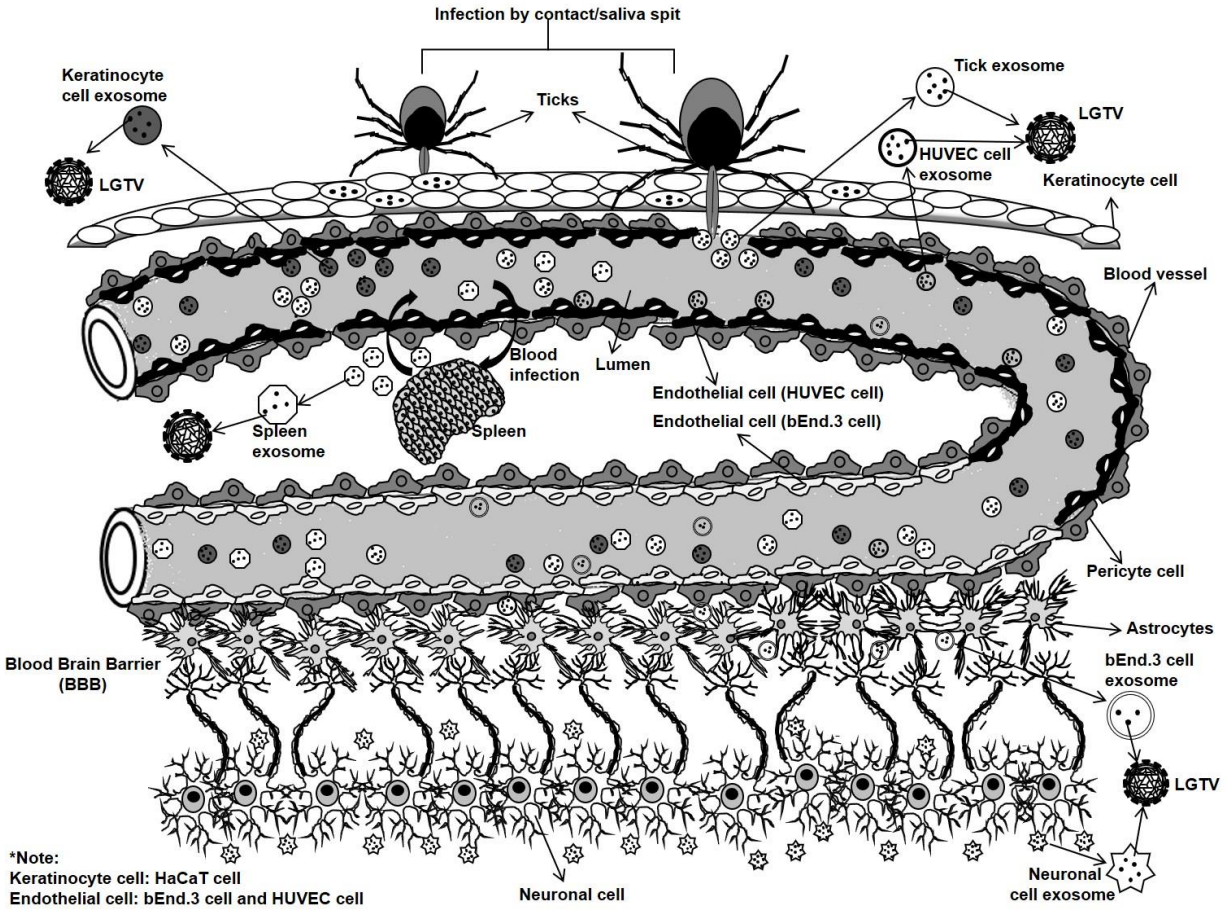

Figure 23. Proposed Model Shows Arthropod-Borne *Flaviviruses* Transmission to Human Host via Arthropod Exosomes

Tick bite or injection/spit of saliva from infected ticks' deposits exosomes containing viral infectious RNA or proteins securely to humans. Exosomes derived from tick cells/saliva infect human skin (keratinocytes) or may directly deposit saliva enriched with exosome containing tick-borne viruses into the blood capillaries/vessels. Exosomes derived from vascular endothelial cells containing *flaviviruses* infect neighboring endothelial cells leading into infection of the peripheral system. Higher viral loads in peripheral tissues increase viremia in blood and eventually allow entry and replication of these arthropod-borne viruses in brain microvascular endothelial cells that line the BBB. Early production and higher loads of *flaviviruses* in brain endothelial cells would allow these viruses to cross BBB and infect neurons. Infected neurons produce high numbers of exosomes containing infectious RNA and proteins that fuse with cell membranes of naïve neuronal cells thereby infecting neighboring neurons and leading to the spread of infection and severe neuronal loss. This figure was reproduced from the published journal article (Zhou et al., 2018).

2.4 EXPERIMENTAL PROCEDURE

Cell Culture and Infection of *in vitro* Cell Lines

Ixodes scapularis ISE6 tick cell line was obtained from Dr. Ulrike Munderloh, University of Minnesota. ISE6 cells were cultured as per the culture methods provided by Dr. Munderloh (Oliver et al., 2015). Human keratinocytes (HaCaT cells) or Human Umbilical Vein Endothelial Cells (HUVEC) were obtained from Drs. Loree Heller and John Catravas laboratories, respectively. Vero (African Green Monkey kidney), mouse brain endothelial (bEnd.3 cells) and mouse neuroblastoma Neuro-2a or N2a cells were purchased from ATCC and were grown according to Company guidelines. Briefly, HaCaT, Vero, bEnd.3 and N2a cells were grown in complete DMEM medium containing 5 to 10% heat-inactivated FBS (Invitrogen/ ThermoScientific). HUVEC cells were grown in human lung MVEC medium (M199 medium containing 150 mg ECGF Exosomes bovine brain extract and 20% FBS) kindly provided by Dr. Catravas laboratory. To determine the infection kinetics, 1 x 10^5 cells were seeded in a 12-well plate, infected with various multiplication of infections (MOI 1; tick cells), (MOI 6: Vero, HaCaT, HUVEC, bEnd.3 and N2a cells) of LGTV. Wild type LGTV (LGT-TP21) strain used in this study was obtained from Dr. Alexander G. Pletnev, NIAID, NIH. Cells were collected at different time points (24, 48, and 72 or 96 and 120 h post-infection, p.i.) and processed for RNA or protein extractions. Details for infection studies corresponding to the data shown in different figures are mentioned in their respective Figure legends. Briefly, for infection experiments (or re-infection studies) with exosome fractions containing infectious LGTV RNA and proteins, 1 x 10^5 HaCaT/HUVEC cells or N2a cells were infected with 20 µl (from 150 µl) of tick (6.6 x 10^4 pfu/ml) or bEnd.3/N2a cells (3.5 x 10^3 pfu/ml) derived exosomal fractions, respectively. The same ratio of supernatant fractions (collected from the step before PBS wash during exosome isolation) from tick or bEnd.3/ N2a cells were used. Titers were determined after plaque counting and calculations. For studies with exosomes and exosome-free supernatant fractions, infected cells (infected with exosomes or supernatant fractions collected at different time points) were either collected at 24 or 48 or 72 h p.i. and processed for RNA extractions. For infection of mouse N2a cells with WNV, CT2741 wild-type strain (MOI 5) had been

used and cells had been analyzed for WNV loads in cells and exosomes at different time points (24, 48 and 72 h p.i.).

Cryo-Electron Microscopy

Exosomes were vitrified as previously described (Sherman et al., 2006; Sherman et al., 2009) on carbon holey film grids (R2x2 Quantifoil; Micro Tools GmbH, Jena, Germany; or C-flat, Protochips, Raleigh, North Carolina). Briefly, purified concentrated suspensions of exosomes in PBS were applied to the holey films in a volume of ca. 3 µl, blotted with filter paper, and plunged into liquid ethane cooled in a liquid Nitrogen bath. Computerized Vitrobot plunger (FEI, Hillsboro, OR) was used for freezing. Frozen grids were stored under liquid Nitrogen and transferred to a cryo-specimen holder (70 deg. 626, Gatan, Inc., Pleasanton, CA, or 2550 cryo-tomography holder, E.A. Fischione Instruments, Inc., Export, PA) under liquid Nitrogen before loading into a JEOL 2200FS, or a JEOL 2100 electron microscopes (JEOL Ltd., 3-1-2 Musashino, Akishima, Tokyo 196 to 8558, Japan). JEOL 2200FS was equipped with an in-column energy filter (omega type) and a field emission gun (FEG); JEOL 2100 had a LaB6 filament; both were operating at 200 keV. Grids were maintained at near-liquid Nitrogen temperature (-172 to -180°C) during imaging. Preliminary screening and imaging of exosomes was done using a 4k x 4k Gatan US4000 CCD camera (Gatan, Inc., Pleasanton, CA), and final imaging was done at indicated 40,000x magnification with a 5k x 4k Direct Electron Detector camera (DE-20, Direct Electron, Inc., San Diego, CA) using a low-dose imaging procedure. An in-column omega electron energy filter was used during imaging with a zero-loss electron energy peak selected with a 20 eV slit. Images were acquired with a ca. 20 electrons/A2 dose; the pixel size corresponded to 1.5 A on the specimen scale. A 2.0 to 2.3 µm defocus range was used for imaging. Overall, individual exosome images were acquired from two-three independent batches of exosomes from tick and N2a cells. For quantitation of exosomes size ranges, the sizes were manually analyzed by using scale bar from cryo-EM images and counted exosomes per image in each group. Three independent estimations and counting were performed without any bias. Percentages (for size determination) were calculated based on the total number of

exosomes in each size range. In addition, the total number of exosomes/cryo-EM images were counted and analyzed.

OptiPrep Density Gradient Exosome (DG-Exo) Isolation from Concentrated Culture Medium

Tick cells (1.2 x 10^7 cells cultured in 12 of Nunc tubes; ThermoScientific) or N2a neuronal cells (8 x 10^7 cells cultured in 8 different T75 flask; Greiner) were infected with either 1 MOI (tick cells; six of each tube) or 5 MOI (five of each flask with N2a cells) of LGTV. Remaining tubes (6) or flasks (4) were maintained as uninfected controls. The detailed protocol is shown (Figure 24). Supernatants (20-50ml) from uninfected/infected cells of respective cell types were collected and centrifuged at 4°C (480g for 10 min followed by 2000g for 10min to remove cell debris and dead cells). Cell culture supernatants were either filtered first (using 0.1 µm filtering devices; VACUCAP filter for conical tubes; Pall Laboratory/VWR) and concentrated to 2 to 2.5ml using the Corning Spin-X UF concentrators or centrifugal filter device with a 5 k nominal molecular weight limit (NMWL). The concentrated culture medium was processed for OptiPrep (DG-Exos) isolation as described (Tauro et al., 2012). In the case of OptiPrep (DG-iso) on laboratory virus stocks (7.4 x 10^6 pfu/ml), concentrated stocks of 1.5 ml supernatants were added directly to the gradient cushion. Briefly, discontinuous gradient of 40% (w/v), 20% (w/v), 10% (w/v) and 5% (w/v) solutions of iodixanol was prepared from the stock solution of OptiPrep 60% (w/v) of aqueous iodixanol (Axis-Shield PoC, Norway) with 0.25M Sucrose/10mM Tris, pH 7.5. The polycarbonate bottles with cap (Beckman Coulter) and maximum volume capacity of 26.3 ml were used to load the discontinuous gradient of iodixanol (4ml each of 40% (w/v), 20% (w/v), 10% (w/v) and 3 ml of 5% (w/v) from bottom to top). The cell culture supernatants (2 to 2.5ml) was overlaid onto the top of the gradient, and centrifuged at 100,000g for 18 h at 4°C. Six individual uninfected or infected fractions of ~3ml were collected (from top to bottom) manually (with increasing density) and diluted with 5ml of sterile PBS. Fractions were centrifuged at 100,000g for 3 h at 4°C, and followed by one more wash with 5ml of PBS and resuspended in 80 µl PBS. DG-Exos were stored at -80°C and used for analysis.

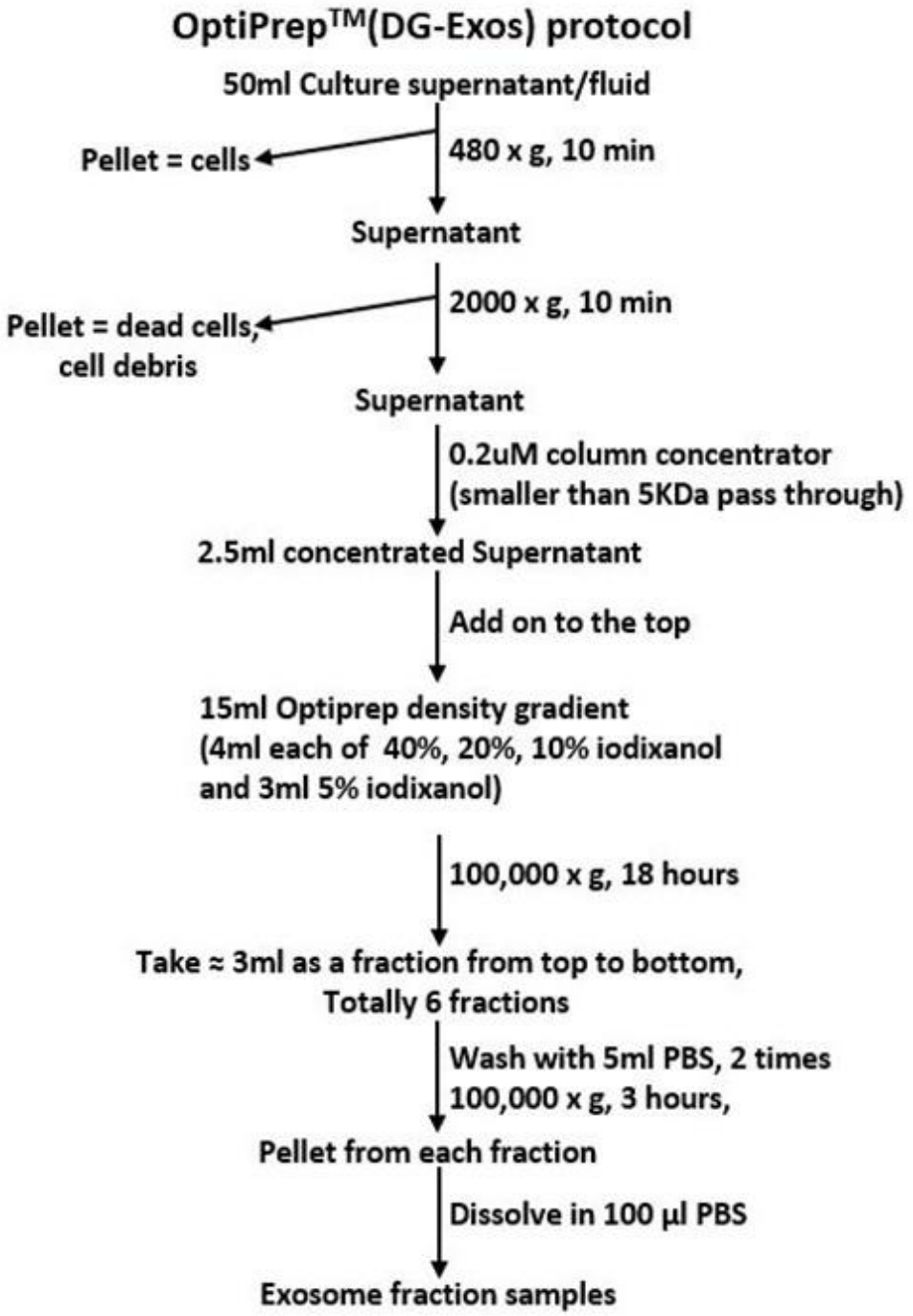

Figure 24. OptiPrep (DG-iso) Exosome Isolation Protocol

The schematic showed the entire procedure of isolating exosomes from different cell lines using the OptiPrep (DG-iso) gradient. After spinning, six fractions were generated and were ready for next experimental procedure. This figure was adapted from the published journal article (Zhou et al., 2018).

Isolation of Exosomes from Cell Culture Supernatant

Exosomes were isolated and purified by either DG-Exo gradient method as described before or differential ultracentrifugation method as described by (Théry et al., 2006). Details for exosome isolation procedure and modifications (used in this study) are also schematically shown and discussed in Figs 8 and 24 and in corresponding figure legends. Briefly, cells were seeded for exosomal- RNA (5 x 10^6 tick cells; 1 x 10^5 of either bEnd3.1 or N2a or murine cortical neurons) or protein (1 x 10^6 tick cells, 2 x 10^6 N2a cells or 2 x 10^7 cortical neurons) extractions in either 12/6-well or 10cm^2 plates in complete L15, DMEM or Neurobasal medium with FBS for overnight, respectively. The next day, cells were changed to the respective medium containing bovine exosome free FBS (Systems Biosciences Inc; SBI). Tick cells plated in commercially available exosome free FBS medium showed severe loss of cells, but infectious loads were not affected. After 4 to 6 hours of medium replacement, cells were infected with LGTV (tick cells MOI 1; bEnd3.1 and N2a cells MOI 6; and cortical neurons MOI 4). Tick cells were susceptible to 2 or 3 MOI of infection and showed massive death; hence 1 MOI dose was used for tick cell infection studies. Cell culture supernatants were spun at 300 x g, for 10 min, cells pellet was discarded, and the supernatant was spun again at 2000 x g for 10min. The pellet containing dead cells was discarded and the supernatant was spun again at 10,000 x g for 30 min to remove cell debris. Increased centrifugation times and rotor types were shown to improve exosome yield and purity (Cvjetkovic et al., 2014) and, hence these modifications for isolation of exosomes from tick cells were used. Either supernatants were spun at 100,000 x g, for 70 min (for bEnd.3, N2a and cortical neurons) or for 155 min (for ISE6 tick cells). Supernatants collected after this spin step served as supernatant fractions and were used as controls in our study (indicated in Figure 8). For plaque assays performed in this study 600, 60 and 6 µl and for infection studies 400 µl of supernatant fractions were used for all except HUVEC cells (300 µl). The pellets containing exosomes and any contaminants were washed one- time with ice-cold PBS and spun again at 100,000 x g, for either 70 min (for bEnd.3, N2a, cortical neuronal cells) or 155 min (for tick cells), respectively. Resulting exosomes pellets are referred to as exosome fractions in this study. Freshly prepared exosome pellets were collected in PBS (and stored frozen at -80°C for re-infection

studies performed on uninfected cells or for plaque assays or other tested evaluations) or resuspended in RNA lysis buffer for total RNA extractions, or in modified RIPA buffer (G-Biosciences, Bio Express) for total protein extractions. Exosomes from N2a cells were isolated using the total exosome isolation reagent and extracted total RNA and proteins with total exosome RNA and Protein Isolation Kit (Invitrogen/ThermoScientific) as per the manufacturer's instruction.

RNA Extraction, cDNA Synthesis and QRT-PCR Analysis

Total RNA from ISE6 tick cells, HaCaT, Vero, HUVEC, bEnd.3, N2a cells or murine cortical neurons infected with various MOI of LGTV or WNV or uninfected controls were extracted using Aurum Total RNA Mini Kit (BioRad) following manufacturer's instruction. By using the BioRad iScript cDNA synthesis kit, 1 µg RNA was converted to cDNA and the generated cDNA was used as a template for the amplification and determination of the viral burden.

For the determination of positive- or negative-sense strands of LGTV, the iTaq Universal SYBR Green One-Step Kit (BioRad) was used and followed the manufacturer's instructions. For the detection of positive- and negative-sense strands of LGTV RNA, published forward and reversed primers for Langat prM-E (Mitzel et al., 2007) were used. For WNV detection, published primers for *E* gene were used (Sultana et al., 2012). To normalize the amounts of templates, either tick or mouse or human *beta actin* amplicons were quantified with published primers (Sultana et al., 2010; Sultana et al., 2012). Equal amounts of tick/mouse/human cDNA samples were used in parallel for *beta actin* and Langat *prM-E*. The ratio of Langat *prM-E* gene copy/*beta actin* gene copy was used as an index to determine the rate of infection in each analyzed sample. QRT-PCR was performed using iQ-SYBR Green Supermix (BioRad, USA). Standard curves were prepared using 10-fold serial dilutions starting from standard 1 to 6 of known quantities of *actin* or Langat *prM-E* gene fragments and QRT-PCR reactions were performed as described (Sultana et al., 2009; Sultana et al., 2010; Sultana et al., 2012). To determine the copy number of viral RNA in exosomes, the LGTV RNA values with standards and converted to copy numbers were used using the formula: Number of copies (molecules) = (amount of amplicon) ng x 1023 molecules per

mole/ (length of dsDNA amplicon _ 660g per mole)² _1 x 10^9 ng per g. Alternatively, the online calculator was also used to convert viral loads to LGTV copy numbers (http://scienceprimer.com/copy-numbercalculator-for-realtime-pcr). For RNase A treatment, fresh exosomes from either uninfected or LGTV-infected N2a cells (2 x 10^7) were isolated, distributed the infected exosomes as treated (5 µg/ml RNase A, 37°C for 15 min) or untreated groups. Exosomes were also treated with Triton X-100 (0.1%, for 45 min at RT) and then followed by treatment with RNase A as before. N2a cells (2 x 10^5) were infected (72 h p.i.) with these treated, or untreated LGTV-infected exosomal samples were processed for RNA extractions and QRT-PCR. Untreated exosomal samples from uninfected group served as internal controls.

Immunoblotting

Western blotting was performed as described (Sultana et al., 2009; Sultana et al., 2012). For DG-Exos samples, equal volume (20 µl) of each fraction from 1 to 6 or 20 µg of total protein lysates from uninfected and infected cells or 10 µl of each fraction from virus stock samples were loaded onto 12% SDS-PAGE, followed by immunoblotting and labeling with highly cross-reactive 4G2 monoclonal antibody to detect LGTV E-protein or exosomal specific markers such as HSP70 (rabbit polyclonal; Cell Signaling Technologies, Inc) or CD9 (mouse monoclonal; Invitrogen/ThermoScientific) and respective secondary antibodies (Santa Cruz Biotechnologies, Inc). For immunoblotting using cell lysate and exosome lysates, briefly, 5 x 10^6 ISE6 tick cells, or 2 x 10^6 N2a cells or 2 x 10^7 cortical neurons were seeded in 10 cm^2 plates and allowed to settle/adhere for overnight. The next day, the media on N2a cells and neurons was changed to DMEM or Neurobasal medium, respectively containing bovine exosome free FBS (Systems BioSciences, Inc; SBI). ISE6 cells were retained with complete L-15 media containing 5% regular FBS (to avoid massive cell death and loss observed when processed for exosome isolation using commercially available exosome-free FBS; SBI). After 4 to 6 hours of media replacement, cells were infected with LGTV (tick cells, MOI 1; N2a cells, MOI 6 and cortical neurons, MOI 4). After 72 h (tick cells) or 24, 48, 72 h p.i. (N2a cells and neurons), cell culture supernatants were collected and processed for exosome isolation by ultracentrifugation (Figure 8). The exosome fractions collected

after PBS wash and the adherent cells collected from the same plates (washed twice with 1 x PBS), were resuspended in modified RIPA buffer. Total protein amounts were estimated using the BCA kit (Pierce/ThermoScientific). 25 µg (tick cells) or 30 to 35 µg (N2a and cortical neurons) of total cell lysates or total exosomal proteins were loaded and separated them on either 12% (Laboratory casted) or pre-casted 4 to 20% SDS-PAGE gradient stain-free gels (NuSep; BioExpress). Followed by gel electrophoresis, blots were blocked in buffers and probed with either highly cross-reactive 4G2 (obtained from Dr. Michel Ledizet, L2 Diagnostics; under non-reducing conditions) or CD9 (Invitrogen/ThermoScientific; under non-reducing conditions) or monoclonal anti-Langat virus NS1 (Clone 6E11; BEI Resources) antibodies, followed by mouse monoclonal HRP-conjugated secondary antibodies (Santa Cruz Technologies, Inc). Total protein profiles (images obtained from stain-free gels after running or imaged from Coomassie-stained gels) serve as loading controls. For protease-resistance assay using proteinase K (that generally digest proteins in biological samples), typical working concentrations of 50 to 100 µg/ ml (for tick cells; 50 µg/ml) or much above the concentrations (for N2a cells; 100 µg/µl)were used. Briefly, fresh exosomes (ultracentrifugation methods) from tick (2 x 10^6) or N2a cells (2 x 10^7) were isolated and treated with Proteinase K for 15 min at 37°C. Samples were then heat-inactivated at 60°C for 10 min and loaded on SDS-PAGE gels and processed for immunoblotting with 4G2 antibody followed by relevant secondary antibody. Antibody binding was detected with the WesternBright ECL kit (Advansta, BioExpress). Blots were imaged using Chemidoc MP imaging system and processed using Image Lab software from the manufacturer (BioRad).

Native-PAGE Analysis

For the native-PAGE analysis, ISE6 tick cells (2 x 10^6) were seeded in regular L15 medium for overnight and infected with LGTV (MOI 1). For N2a cells (5 x 10^6), they were plated in regular complete DMEM medium and allowed them to adhere for overnight, cells were then replaced with exosome-free FBS medium. After 4 h of media change, N2a cells were infected with LGTV (6 MOI). Post 72 h of infection, tick/N2a cell culture supernatants were processed for isolation of exosomes. Exosomes collected from uninfected or LGTV-infected tick/N2a cells were resuspended in PBS and

distributed into three groups (from the same preparations), that were either held as untreated group on ice, treated with Triton-X-100 (0.03%; 30 min, RT), or processed for three cycles of freezing at -80°C (for each freezing cycle samples were incubated for 1 h). After treatment and processing, protein lysates were prepared in a non-reducing and non-denaturizing sample buffer (62.5 mM Tris-HCL, pH 6.8, 25% Glycerol and 1% Bromophenol blue), that maintained the proteins secondary structure and native charge density. Gels were pre-run for 60 min in gel running buffer (25 mM Tris and 192 mM Glycine). Uninfected or LGTV-infected exosomal preparations with different treatment or untreated samples were separated on 12% native-PAGE gels. Gels were transferred on to nitrocellulose membranes followed by immunoblotting using 4G2 or NS1 monoclonal antibodies followed by mouse monoclonal HRP-conjugated secondary antibodies (Santa Cruz Technologies, Inc). Total protein profiles (Coomassie-blue stained gel) serve as loading controls. Antibody binding was detected with WesternBright ECL Kit (Advansta, BioExpress). Blots were scanned using Chemidoc MP imaging system and instructions from the manufacturer (BioRad).

ELISA

N2a cell-derived exosomes from 5 x 10^6 uninfected or LGTV-infected (MOI 6; 72 h p.i.) cells were collected and resuspended in PBS (250 µl/sample). Exosomal fractions were grouped as untreated or treated with 0.1% of Triton-X-100 for 30 min. Nunc grade ELISA plates were coated with 50 µl of untreated or Triton-X-100 treated- uninfected or infected samples for overnight and incubated at 4°C. Samples were incubated with 4G2 antibody for 1 h, followed by HRP-conjugated mouse monoclonal secondary antibody for another 1h as described (Sultana et al., 2009). SureBlue TMB Microwell Peroxidase substrate and Stop solution (KPL) were used and followed the manufacturer's instructions. After stopping the reactions with TMB Stop solution, optical density was measured from triplicate samples at an absorbance of 450nm using a Multimode infinite M200 Pro Microplate reader (Tecan).

E-Protein-Antibody-Beads Binding Assays

LGTV-infected tick or N2a cell-derived exosomes (from 72 h p.i.) were freshly isolated from 2 x 10^6 tick cells (infected with MOI 1) or 5 x 10^5 N2a cells (infected with 6 MOI). Exosomes from GW4869 inhibitor (5 µM) treated tick or N2a cells were isolated. For inhibitor treatment, cells were seeded in plates for overnight, changed to exosome-free FBS medium (in case of N2a cells) and after 4 h, treated with exosome release GW4869 inhibitor for 4h, followed by infection with LGTV for 72 h p.i. The exosomes collected from untreated or inhibitor treated cells were resuspended in PBS and grouped into three categories for both inhibitors treated or untreated samples as; untreated, treated with 4G2 antibody (that recognizes LGTV E-protein) or relevant isotype control antibody (R & D Systems) groups. Exosomal fractions were incubated for 1 h (RT) with respective antibodies followed by incubation (4°C) with protein A/G agarose beads (Pierce/ThermoScientific) for another 30 min. The antibody-beads complexes were spun (13,000 rpm) at 4°C for 30 min and supernatants were collected and lysed in RNA lysis buffer, processed for RNA extractions, followed by cDNA synthesis and QRT-PCR to detect LGTV loads.

Trans-Well Assays

Assays were performed to analyze the trans-migration of infectious exosomes from infected cells (seeded in inserts; upper chamber) to uninfected cells seeded in 12-well plates (lower chamber). Sterile, polycarbonate tissue culture-treated trans-well inserts (12mm insert size) with 0.4 µm microporous membrane pore size were used in our assays (Corning). 1 x 10^5 ISE6 tick or bEnd.3 cells in inserts (upper chamber) were plated and 1 x 10^5 HaCaT or N2a cells were seeded in 12-well plates (lower chamber). Inserts with tick or bEnd.3 cells were first kept in a separate 12-well plate containing 0.5 ml (in order to keep microporous membranes moist/ wet) of L-15 (tick cells) or DMEM complete medium (bEnd.3 cells), respectively. Inhibitor treated group in trans-well assays was treated with 5 µM of GW4869 inhibitor, and at 24 h post-treatment, tick cells or bEnd.3 cells were either infected with exosomes containing LGTV (25 µl of the exosome fraction collected from infected tick or bEnd.3 cells) or with LGTV from laboratory viral stocks (MOI 1 for tick cells or MOI 6 for bEnd.3 cells) prepared from

infected Vero cell culture supernatants. Four hours post-infection inserts with tick or bEnd.3 cells (with the change of new media) were moved to 12-well plates containing HaCaT or N2a cells, respectively. Exosomes containing viral RNA and proteins produced from tick or bEnd.3 cells could transmigrate and infect HaCaT or N2a cells (that were kept uninfected). After, 48 h post incubation with inserts (containing either infected tick or bEnd.3 cells in inserts or upper chambers), HaCaT or N2a cells from lower chamber were washed with ice-cold PBS (3x) and collected for RNA extractions, cDNA synthesis and QRT-PCR to determine viral loads from cells.

Plaque Assays

Plaque assays were performed as described (Sultana et al., 2009). To determine infectious and replicative viruses after incubation with exosome and exosome-free supernatant fractions, Vero cells were seeded in 6-well plates at densities of 1 x 10^6 cells per well, allowed them to adhere and grow as monolayers to reach 65 to 85% confluency (for ~24 h). Exosome fractions containing unknown PFU (plaque forming units) of LGTV viral genomes were collected from tick cells (5 x 10^6 cells) or N2a cells or murine cortical neurons (1 x 10^5 cells) and resuspended in 250 µl of PBS, 30 µl of this suspension (exosome fraction) was used for plaque assays. Exosome free supernatants (600 µl) that corresponds to the same ratio of exosome fractions were used as controls. Serial dilutions (1:10, 1:100 and 1:1000) of the exosomes or supernatant fractions were prepared in duplicate (shown are the representative plate images from two-three independent experiments). Monolayers of Vero cells were infected with exosomes or supernatant fractions or with exosomes from 1 µM or 10 µM(LGTV-infected N2a cells or mouse cortical neurons) of GW4869 inhibitor-treated or DMSO-treated controls. Four hours post-infection, medium was removed and warm 2% Seaplaque agarose (Lonza) overlay with complete DMEM media (1:1 ratio) containing antibiotic and antimycotics solution (1% each; Sigma) was added. Plates were incubated for 6 to 7 days, at 37°C, 5% CO2. After incubation period, plaques were stained with 0.03% of Neutral Red (Sigma) for 4 h, and the stain was removed to either count plaques on the same day or otherwise plates were incubated (inverted and

covered in foil) for overnight, and then plaques were counted next day to determine the viral titers from LGTV-infected exosomal fractions from tick/neuronal cells.

Isolation and Infection of Murine Cortical Neurons

Gestation period (day 13) wild-type female C57BL/6 (Charles River Laboratories) mice were purchased and allowed to reacclimatize. All animal experiments were done in accordance with the University Animal Care and Use Committee regulations. Primary cortical neurons were isolated from embryonic day-16 (E16) brains (Sultana et al., 2009; Sultana et al., 2012). Murine cortical neurons (1×10^5) were seeded in a 12-well plate coated with poly-L-Lysine and cultures were established in neurobasal complete medium with FBS. After 24h of plating, half of the medium was replaced with FBS free neurobasal media, to slow growth of glial cells. For infection kinetics, cortical neurons were infected with LGTV (MOI 4) (after 48 h of post-seeding), neurons were collected at different time points (24, 48, 72 and 96 h p.i.) and processed for RNA extractions. For infection with neuronal cell-derived exosomes or supernatant fractions, 1×10^5 murine cortical neurons were infected with 20 µl of neuronal exosomes (2.2×10^3 pfu/ml) or 400 µl of exosome free supernatant fractions (collected from the step before PBS wash during exosome isolation, See Figure 8). Cells were harvested at 48 h p.i. and processed for RNA extraction. Protein extractions were collected from uninfected or LGTV-infected cortical neurons (seeded at 1×10^7 cells) or from exosomes isolated from these cell culture supernatants.

Inhibitor Treatments

For exosome inhibition studies, GW4869, a cell-permeable, a selective inhibitor for Neutral Sphingomyelinase (N-SMase) (Santa Cruz Biotechnologies, Inc) was used and DMSO worked as controls. Cells did not show any toxicity at tested doses. For both trans-well assays, inhibitor-treated group was treated with 5 µM exosome inhibitor. N2a cells or murine cortical neurons were seeded at 1×10^5 cells in a 12-well plate. Next day, before treatment with inhibitor, cells were replaced with bovine exosome free-FBS (Systems BioSciences, Inc.) containing DMEM (N2a cells) or neurobasal medium (neurons). Cells were treated with either 1, 5 or 10 µM (N2a cells) or with 1, 10 or 20 µM

(neurons) of inhibitor for 4 h, followed by infection with LGTV (N2a cells, MOI 6; cortical neurons MOI 4). Plaque assays were performed with 30 µl of exosome fractions derived from N2a cells or cortical neurons to determine the unknown titers for both DMSO control and inhibitor treated groups, respectively. N2a cells were either pre- or post-treated with inhibitor, where cells were first treated with inhibitor (5 µM) for 4 h followed by infection for 72 h or vice versa, respectively. Supernatants collected from uninfected controls and cells infected with LGTV (laboratory virus stocks with known titers) (48 h p.i.) were processed for exosome isolation. Purified exosomes were resuspended in PBS and processed for either RNA extraction or used for infection of new cells to determine re-infection kinetics or used to determine viral titers by plaque assays. For GW4869 treatment on laboratory virus stocks, the viral supernatants (collected from Vero cells) were treated with known titers (7.4×10^6 pfu/ml). 30 µl of the virus stocks were used and treated with either DMSO or inhibitor (5 and 10 µM for 4 h at 37°C) followed by immunoblotting with 4G2 antibody. For 4G2 functional blocking antibody studies, N2a cells (2×10^5) were plated, treated with 5 µg of antibody for 4 h and infected cells with freshly isolated exosomes from LGTV-infected (72 h p.i.) N2a cells. N2a cells were infected through infectious exosomes for 72 h p.i. and collected for RNA extractions and QRT-PCR analysis. Untreated samples serve as a control. For Pitstop-2 inhibitor treatment, N2a cells (2×10^5) were treated with 30 µMPitstop-2 (dissolved in DMSO) for 15 min followed by infection through freshly isolated exosomes from LGTV-infected (72 h p.i.) N2a cells. Cells were collected for RNA extractions after 72 h p.i. and further processed for QRT-PCR. DMSO treated cells served as controls.

Statistics

The statistical difference observed in data sets was analyzed using GraphPad Prism6 software and Microsoft Excel. The non-paired, two-tail Student *t*-test was performed (for data to compare two means) for the entire analysis. Error bars represent mean (+SD) values, P-values of <0.05 were considered significant in all analysis. Statistical test and P-values are indicated for significance.

Ethics Statement

All animal work in this study was carried out in strict accordance with the recommendations in the Guide for the Care and Use of Laboratory Animals of the National Institute of Health. The approved protocol from the Institutional Animal Care and Use Committee (Animal Welfare Assurance Number: A3172-01) (permit number: 16-017) and the approved IBC protocol (number 12-014) were used in this study.

CHAPTER 3

EXOSOMES MEDIATE ZIKV TRANSMISSION THROUGH SMPD3 NEUTRAL SPHINGOMYELINASE IN CORTICAL NEURONS

3.1 INTRODUCTION

Mosquito-borne Zika virus (ZIKV) is a positive-sense single-stranded RNA virus that belongs to the family *Flaviviridae* and *flavivirus* genus (Wang et al., 2017b). ZIKV has been highlighted due to its recent epidemic outbreak in Brazil and disseminates in several parts of the Western Hemisphere including the United States of America (Russo and Beltrao-Braga, 2017; Wang et al., 2017b). ZIKV refers to the Spondweni serocomplex and is firmly conserved with dengue (DENV) and the West Nile virus (WNV) (Wang et al., 2017b). Mostly, infections with ZIKV are asymptomatic (~80%) with flu-like symptoms and affiliate with the clinical phenomenon. The transmission of ZIKV by sexual approaches, with reproductive viral particles that be detected in semen for at least two months, pose a significant global threat and a pathogen of high priority concern to the public health (Maxian et al., 2017; Moreira et al., 2017). Typically, *Aedes aegypti*, a mosquito species, transmits the majority of ZIKV infections to humans. However, ZIKV can also be disseminated through sexual contacts and transfusions of human blood by the clinical actions. In humans, the greatest concern is the vertical transmission of ZIKV from mother to neonates and this has drawn humans' attention due to the associated neurological manifestations (Faizan et al., 2016; Russo and Beltrao-Braga, 2017; van den Pol et al., 2017b; Wang et al., 2017b). ZIKV infection has been shown to affect both the Central Nervous system (CNS) and the Peripheral Nervous System (PNS). It also causes severe neurological complications such as

Guillain-Barré syndrome (GBS with muscle weakness and paralysis) and the conscientious manifestation of microcephaly (Faizan et al., 2016; Lagunas-Rangel et al., 2017; Russo and Beltrao-Braga, 2017; van den Pol et al., 2017b; Wang et al., 2017b). Microcephaly, a less studied neurodevelopmental disorder is a magnificent reduction in brain size and intellectual disability with deficient cell proliferation and severe death of cortical progenitor cells and their neuronal progeny (Olagnier et al., 2016; Lagunas-Rangel et al., 2017; Wen et al., 2017).

Although the emergence of ZIKV-associated congenital microcephaly and neuropathogenesis is being studied extensively, this line of research is currently very limited. Recently, significant and stunning progress has been made in developing stem cell-based cellular and animal models (Olagnier et al., 2016). Besides the identification of hidden molecular mechanisms and development of therapeutic strategies and vaccines, the engagement of human tissues samples has led to a better perception of ZIKV infections (Olagnier et al., 2016; Russo and Beltrao-Braga, 2017; van den Pol et al., 2017b). In a developmental ZIKV infected mouse model, it has been shown that astrocytes were targeted throughout the brain after ZIKV entered the CNS after peripheral inoculations (Van den Pol et al., 2017b). ZIKV has been shown to significantly infect and replicate in mouse neural stem cells (mNSCs), mouse astroglial cells, and different regions of brain including neocortex and hippocampal regions (CA1 and CA3), thereby raising several concerns related to long-term memory issues (Olagnier et al., 2016; Van den Pol et al., 2017b). ZIKV RNA has been detected in neural tissues, human neural progenitors, matured neurons and has been interacted with an increase in the apoptosis-related genes in those neuronal cells (Li et al., 2016; Oh et al., 2017a; Van den Pol et al., 2017b). The cerebral cortex, a four-layered structure that mediates the higher cognitive functions, including learning and memory has been severely affected in microcephalic patients (Faizan et al., 2016). Two independent studies have also shown that ZIKV infection can significantly reduce the growth of neural stem cells and brain organoids that can be directly connected to the ZIKV-associated congenital microcephaly (Ming et al., 2017; Qian et al., 2017; Wen et al., 2017). A comparative analysis approach in the developing neocortex has identified ZIKV specific alterations and preferential infection of neural stem cells (Brault et al.,

2016). However, this study does not elucidate the critical steps of how ZIKV arrives the brain. Also, the transmission dynamics of ZIKV in and between neurons or their stem cells is broadly unexplored.

Exosomes have been shown to perform both neuroprotective and toxic roles in the CNS (Chivet et al., 2012). Several reports have indicated neuronal exosomes serve as novel therapeutic targets for neurological disorders such as Alzheimer's disease (Chivet et al., 2012; Janas et al., 2016; Kanninen and Malm, 2016). In this current study, the assumption that ZIKV uses exosomes to transmit to other neurons and spread infection through neuronal connectivity in establishing embryonic fetal and neonatal brains was evaluated. This study shows that exosomes derived from mouse cortical neurons carry ZIKV infectious RNA and proteins that mediate viral transmission to other neurons, thus assisting in viral dissemination throughout the CNS. Also, this work suggests that neutral Sphingomyelinase SMPD3 (nSMase2), an enzyme sphingomyelin phosphodiesterase, is engaged in ZIKV infection, replication, and mediates viral materials transmission via neurons derived exosomes. SMPD3 hydrolyzes sphingomyelin to phosphocholine and ceramide and is predominantly expressed in the neurons of the CNS to control postnatal growth and development (Stoffel et al., 2005; Stoffel et al., 2016; Menck et al., 2017). Furthermore, SMPD3 has been shown to inhabit in the Golgi apparatus and is ubiquitously expressed, thereby suggesting its significant role in ZIKV replication (Stoffel et al., 2005; Stoffel et al., 2016). Taken together, this study not only provides a model in understanding the importance of exosomes but can also explore some new strategies on the development of exosomal-based drugs or therapeutics and/or vaccines to interrupt the ZIKV infections in neonatal brains.

3.2 RESULTS

ZIKV Infect Mouse Cortical Neurons in a Time and Dose-Dependent Manner

Smaller head circumference, intellectual ability and seizures that characterize microcephaly, has been strongly associated with ZIKA virus (ZIKV) infections (Faizan et al., 2016; Olagnier et al., 2016; Wen et al., 2017). Also, an interaction between ZIKV and diminished neuronal differentiation or expended cell death in neuronal cells has been shown (Faizan et al., 2016; Russo and Beltrao-Braga, 2017; van den Pol et al., 2017a). In spite of determine the right time of neuronal differentiation and to analyze if cells in primary cultures are perhaps not in progenitor state during ZIKV infection, Neuronal cultures for either 72 or 120 h (post-plating) were plated followed by infection with ZIKV (for another 72 h p.i., 5 MOI; Multiplication of Infection). Freshly dissected primary murine cortical neurons culture from embryonic (E16) developing mouse brains were infected. Primary cultures were stained for both neuronal marker MAP-2 (Microtubule Associated Protein-2) and GFAP (Glial Fibrillary Acidic Protein), a transitional filament protein used as astrocyte marker (Figure 25). At both post-plating time points of 72 and 120 h, it had been found that progenitor cells were fully differentiated as neurons as revealed by the staining for MAP-2 (green) followed by detection with Alexa Fluor 488 (Figure 25). No astrocytes or other glial cells or neuronal precursor cells (NPCs) (for GFAP positive staining, and detection with Alexa Fluor 594) had been found in the primary cultures of murine cortical neurons at 72 or 120 h of post-plating, followed by infection with ZIKV (for another 72 h) (Figure 25). Also, the bright field (BF) images, predominantly showed neuronal cells in the primary cultures at both 72 and 120 h post-plating of cells (Figure 25). Infection of primary cultures of cortical neurons at/after 72 or 120 h post-plating had no differences upon ZIKV infection. Some of the DAPI-positive but weak MAP-2 stained cells were found to have strong staining for ZIKV Envelope (E) protein (detected by 4G2 monoclonal antibody, followed by Alexa Fluor 594 secondary antibody) (Figure 26). It was presumed that neuronal cells perhaps had revoked their neurites due to severe ZIKV infection, thus leading to neuronal death in those weak MAP-2 stained cells. It was also observed that ZIKV rapidly infected (5 MOI) murine cortical neurons with increased cell death at 96 h post-infection (p.i.) when

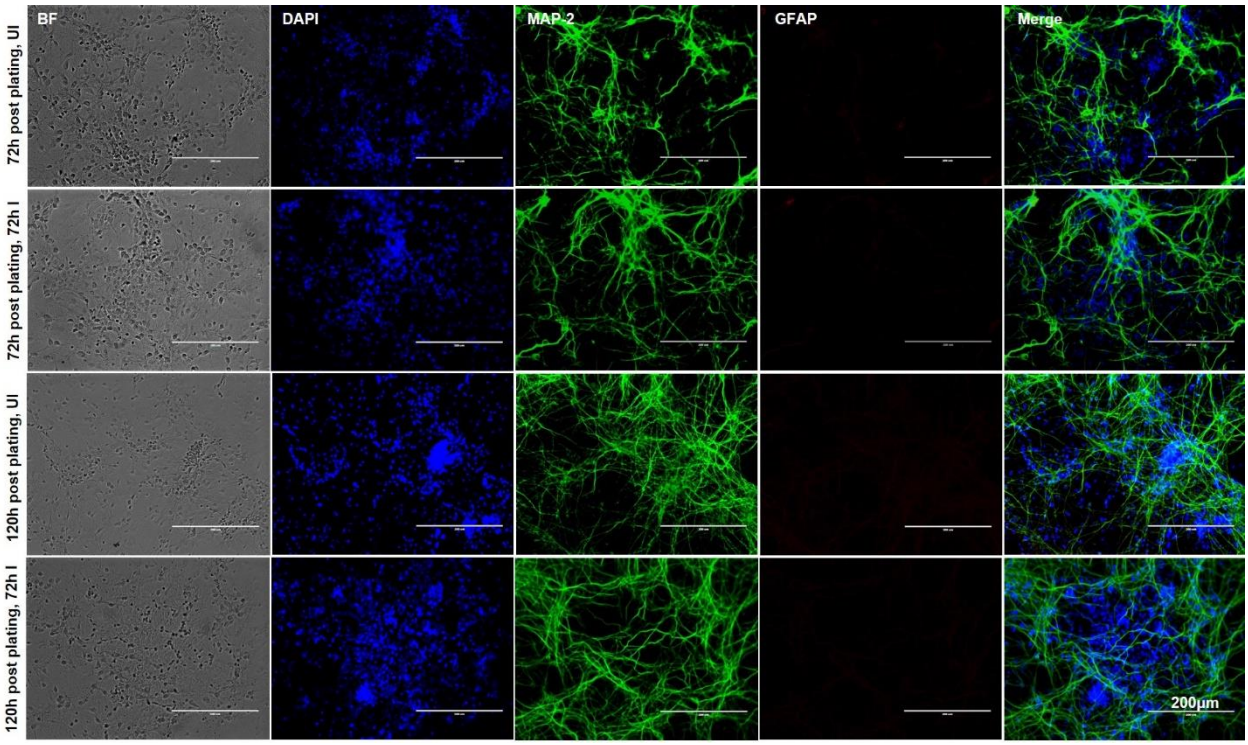

Figure 25. Murine Cortical Neurons in Primary Cultures are Differentiated as Neurons from Progenitor Cells

Phase-contrast and fluorescent microscopic images showed the primary cultures of cortical neurons from uninfected (UI) or ZIKV (I) infected (MOI 5; 72 h p.i.) groups at two different time points (72 and 120 h post-plating). Cortical neurons were stained for a neuronal marker (MAP-2) or astrocyte marker (GFAP) to show the presence of neurons and the absence of glial cells. DAPI staining for nuclei served as an internal control. Uninfected neurons served as a control. Representative images obtained from the EVOS FL system were shown. Scale bar indicated 200 μm in all panels. This figure was reproduced from the published journal article (Zhou et al., 2019).

compared to the uninfected control (Figure 27A). Furthermore, cortical neurons' death with ZIKV infection was harsh at 120 h p.i., comparing to the infection at early time points, suggesting longer incubation times leading to severe damage and neuronal death, perhaps contributing to tissue loss (Figure 27A). Several neuronal connections were eliminated, and severe damage was shown due to massive cell deaths in murine cortical neurons at 120 h p.i., (Figure 27A). No morphological changes or cell loss at earlier tested time points (24, 48 and 72 h p.i.) of ZIKV infection (Figure 27A) were

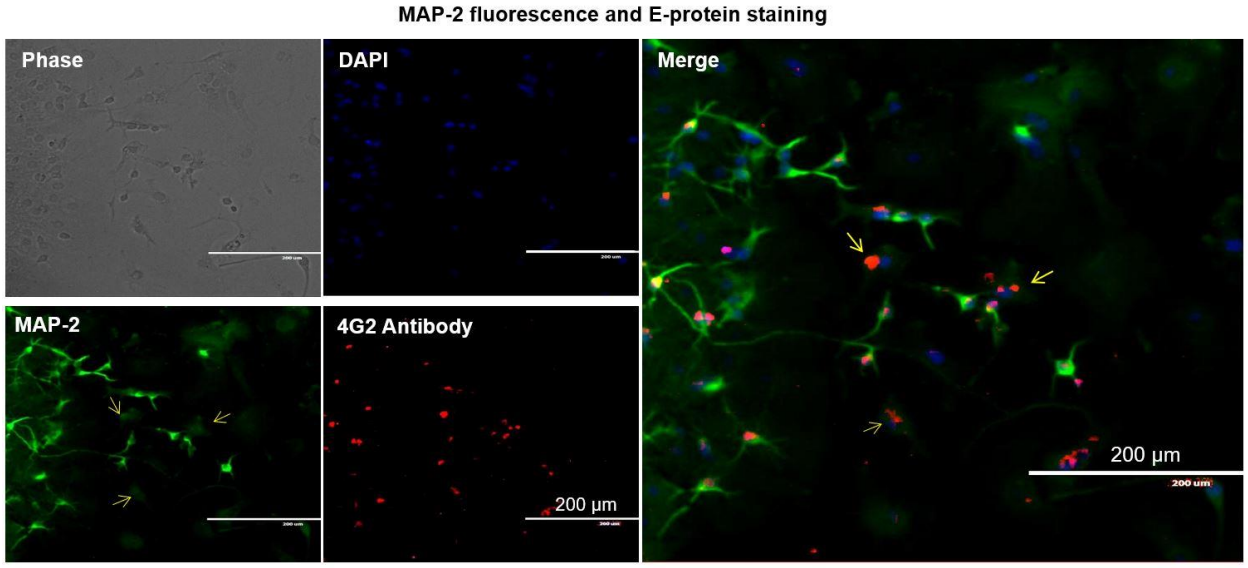

Figure 26. Cortical Neurons Showed Diminished MAP-2 Signals Upon ZIKV Infection

Primary cultures of cortical neurons showed the enhanced ZIKV E-protein staining (as detected by the 4G2 monoclonal antibody, followed by Alexa Fluor 594) and the reduced MAP-2 fluorescence (as detected by MAP-2 monoclonal antibody followed by Alexa Fluor 488) in cells. Bright-field and DAPI images were shown as controls. Neurons were infected with ZIKV (5 MOI; 72 h p.i.) viral stocks and representative images obtained from the EVOS FL system were shown. Scale bar indicated 200 µm in all images. This figure was reproduced from the published journal article (Zhou et al., 2019).

found. The quantitative analysis for measuring cell viability of primary cultures of cortical neurons by MTT assay showed the decreasing of viable cells at later time points (72, 96 and 120 h) of ZIKV infection (Figure 27B).

To measure the neuronal cell loss, is due to longer incubations with ZIKV infection, an independent experiment with different doses (MOI 1, 2.5 and 5) of ZIKV was performed. At 72 h p.i., not many considerable morphological changes were found in ZIKV infected cortical neurons at tested doses (of MOI 1, 2.5 and 5) (Figure 28A). Whereas, the quantitative analysis provided by MTT assay indicated some reduction in cell viability at 72 h post-ZIKV infection with 5 MOI (Figure 28B). These results suggest that neuronal cell death at 96 h p.i., and onwards is mostly due to the consequences of protracted infection of neurons with ZIKV and the neuronal stress related to infection. QRT-PCR analysis performed on the neuronal samples collected at different time points proved that ZIKV loads (both E-gene and *NS5* mRNA transcripts) were magnificently (P

< 0.05) enhanced at 72 h p.i., in comparison to the other time points (of 24, 48 and 96 h p.i.,) (Figures 29A and B). The lower loads of ZIKV at 96 h p.i. was perhaps because of the severe neuronal cell death observed at this time point (Figures 29A and 29B). Immunoblotting analysis (using a highly cross-reactive 4G2 monoclonal antibody that recognizes the viral Envelope (E)-protein) showed similar results with increased ZIKV E-protein at 72 h p.i., in comparison to the loads at other time points (Figure 29C). It was also shown that HSP70 (heat-shock protein 70, an enriched marker in mammalian exosomes) loads were boosted upon ZIKV infection at 48, 72 and 96 h p.i., when compared to their corresponding uninfected controls (Figure 29C). HSP70 levels were rarely detected at 24 h p.i. in the tested conditions (Figure 29C). Furthermore, a dose-dependent enhancement in ZIKV loads was evidence both at the RNA (E-gene and *NS5* mRNA transcripts) and protein levels when cortical neurons were infected with 1, 2.5 or 5 MOI at 72 h p.i. (Figures 29D-29F). In both time and dose-response tested groups (Figures 29A, 29B, 29D and 29E), *NS5* mRNA amplification was found to be higher in comparison to the E-gene amplification; hence *NS5* detection was used in our further analysis. Total protein profile gel images served as loading controls in the immunoblotting analysis (Figures 29C and 29F). Densitometry analysis from total cell lysates showed the quantitative differences in E-protein (from both the time point and dose-response samples) and HSP70 levels obtained between the ZIKV infected (MOI 5) and uninfected controls (Figures 30A-30C). Overall, these results suggested time- and dose-dependent infection kinetics of ZIKV in mouse cortical neurons.

Detection of Exosomes Derived from Mouse Cortical Neurons by Cryo-EM and Western Blot

Regardless of the importance of ZIKV infection and its cause of severe neurological complications such as GBS and the more attentive manifestation of microcephaly in neonates, the transmission modes of ZIKV within the neonatal and adult brain cells were known little. Increased HSP70 levels in neuronal cells upon infection (Figure 29C) suggested that ZIKV perhaps uses neuronal exosomes for transmission and spread of infection in the brain. It has been shown that cortical neurons release exosomes in culture that contained enriched exosomal markers

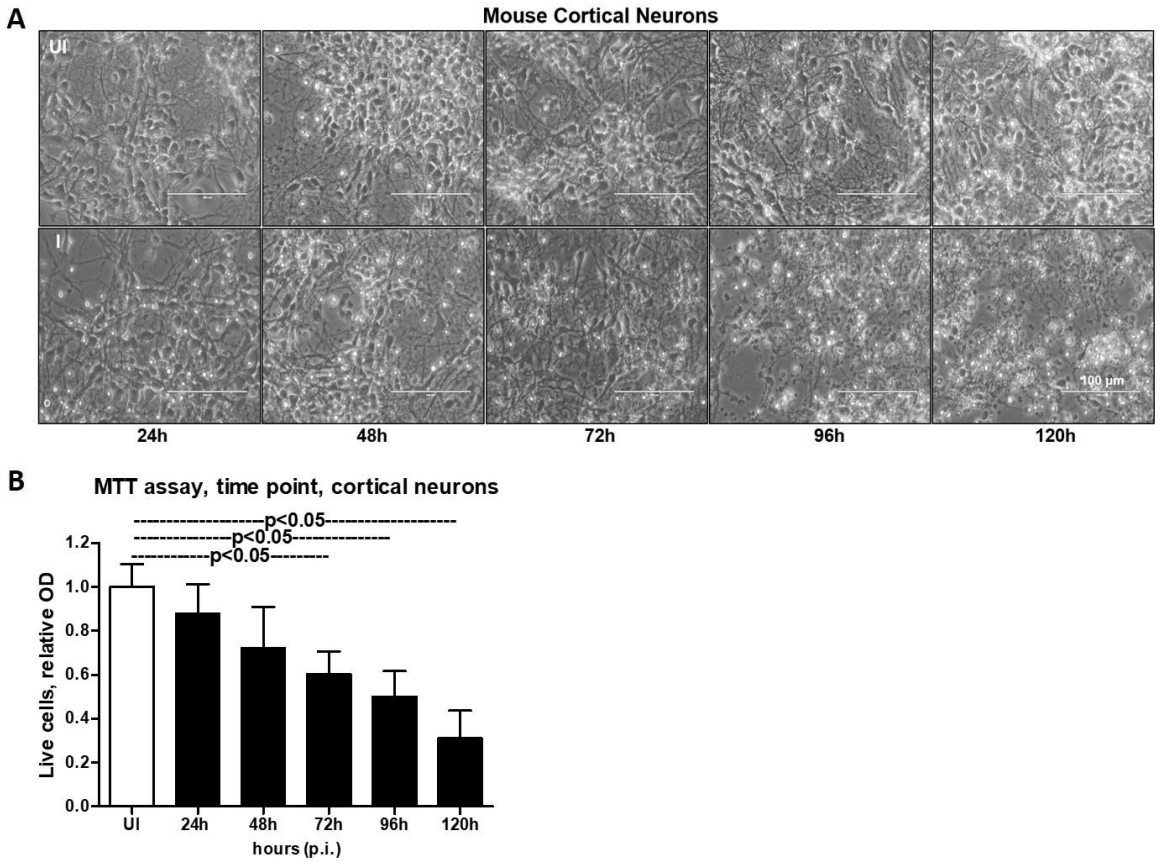

Figure 27. Murine Cortical Neurons in Primary Cultures are Susceptible to ZIKV Infection at Longer Incubation Time

(A) Phase-contrast images showed primary cultures of cortical neurons from uninfected (UI) and ZIKV (I) infected (MOI 5) groups at different time points (of 24, 48, 72, 96, and 120 h p.i.). Uninfected neurons served as a control. Representative images obtained from the EVOS FL system were shown. Scale bar indicated 100 µm in all panels.

(B) MTT assay showed cell viability of mouse cortical neurons at different time points (of 24, 48, 72, 96, and 120 h p.i.) upon ZIKV infection (5 MOI). Relative optical density showed live cells in culture. Uninfected controls kept for 120 h were considered as controls.

This figure was reproduced from the published journal article (Zhou et al., 2019).

(Olagnier et al., 2016; Zhou et al., 2018b). Due to increased viral loads at 72 h p.i., this time point was considered for the isolation of exosomes from cortical neuronal cultures. Using either density gradient centrifugation technique; OptiPrep™ (DG-Exo isolation), or by differential ultracentrifugation, exosomes from murine cortical neurons were isolated (Tauro et al., 2012; Olagnier et al., 2016). Detailed protocols and descriptions are

published in the recent work on neuronal exosomes (Olagnier et al., 2016; Zhou et al., 2019). Cryo-Electron Microscopy (EM) performed on neuronal cell-derived exosomes showed their sizes in the ranges of 30-200 nm in diameter (Figure 30A) that are similar to exosomes isolated from other mammalian cells. Quantitative analysis of the heterogeneous populations of neuronal exosomes was performed to determine any differences between ZIKV-infected and uninfected cell-derived exosomes (Figures 30B and 30C). The highest percentage of exosomes size was between 50-100 nm and 100-150 nm (in diameter) in both uninfected and ZIKV-infected groups (Figures 30B and 30C). However, ZIKV infected neuronal cell-derived exosomes had increased percentages in 0-50 nm but decreased percentages in 100-150 nm and 150-200 nm sizes in comparison to the uninfected group (Figures 30B and 30C). Also, higher percentages of larger exosomes or Extracellular Vesicles (EVs) of sizes 200-500 nm were observed upon ZIKV infection in comparison to the uninfected group (Figures 30B and 30C). In addition, the higher number of exosomes in cryo-EM images collected from ZIKV-infected (n = 25) group was noted in comparison to the uninfected (n = 13) group (Figure 30D). These data suggest increased production and or release of neuronal exosomes upon ZIKV infection.

To find whether ZIKV proteins are evident in neuronal exosomes, six different fractions from samples collected at 72 h p.i. were collected, following the Opti- Prep™ (DG-Exo) isolation method as described in (Tauro et al., 2012; Zhou et al., 2018b). Neuronal HSP70 was detected in 20 µl of the infected exosomes from three to five fractions. Barely detectable levels of HSP70 were noted in fractions one, two and six but enhanced levels were noted in fractions three to five (Figure 30E). HSP70 loads were also detected in exosomal fractions three-five obtained from uninfected cortical neuronal cells, but with higher levels in fractions five (Figure 30E). Additionally, for detailed characterization of exosomes, the presence of other exosomal markers such as CD63 and CD9 were detected in fractions from both ZIKV-infected and uninfected groups (Figure 30E). CD63 loads were enriched in fractions three-six in ZIKV infected and fractions four-six in uninfected controls. Barely detectable loads were observed in one and two fractions in both infected and uninfected groups (Figure 30E). CD9 was also enriched in fractions four and five in both ZIKV-infected and uninfected controls, and

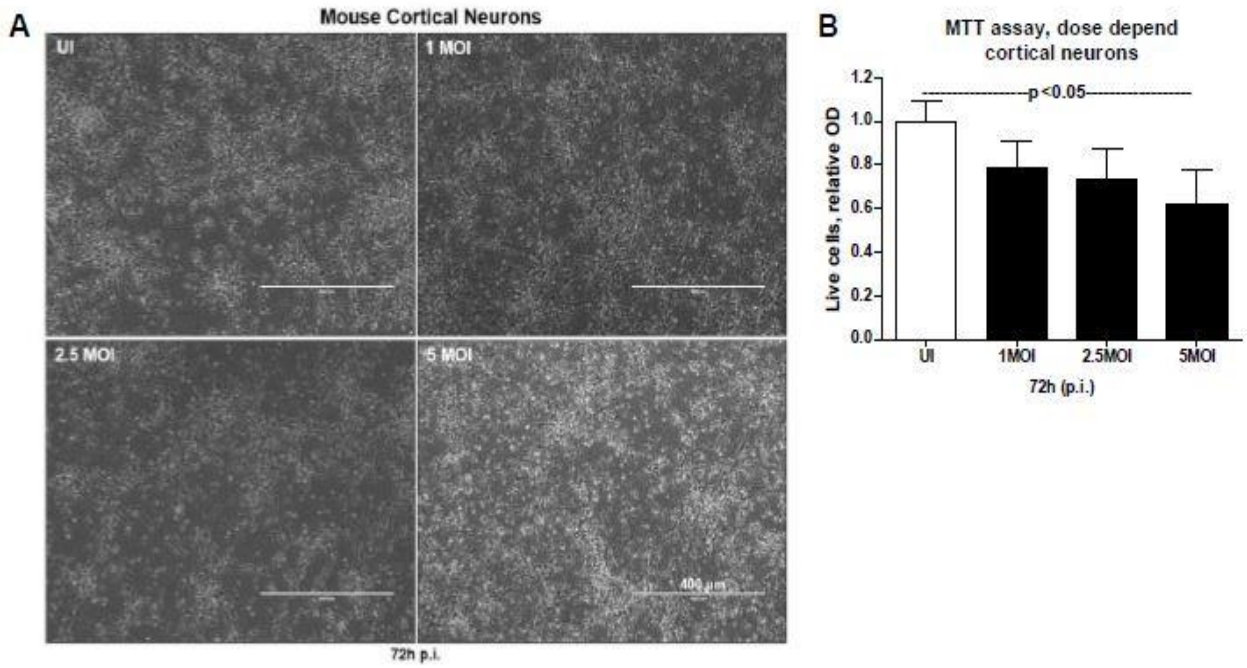

Figure 28. Murine Cortical Neurons in Primary Cultures are not Affected with 1 and 2.5 MOI Doses of ZIKV at 72 p.i.

(A) Phase-contrast images showed primary cultures of cortical neurons from uninfected (UI) or ZIKV-infected (72 h p.i.) groups and at different doses of infection (MOI 1, 2.5 and 5) were shown. Uninfected neurons served as a control. Representative images obtained from the EVOS FL system were shown. Scale bar indicated 400 µm in all panels.

(B) MTT assay showed the cell viability of mouse cortical neurons at different doses (1, 2.5, and 5 MOI) of ZIKV infection (72 h p.i.). Relative optical density showed live cells in culture. Uninfected controls kept for 120 h were considered as controls.

This figure was reproduced from the published journal article (Zhou et al., 2019).

detectable levels were found in fractions two and three of the infected group (Figure 30E). In other fractions (one and six), CD9 loads (Figure 30E) could not be detected. It was found that ZIKV E-protein levels were enhanced in infected exosomal fraction four, however, other fractions (two, three and five) also showed a weak signal for E-protein (Figure 30E). As expected, ZIKV E-protein was not detected in any uninfected fractions (Figure 30E).

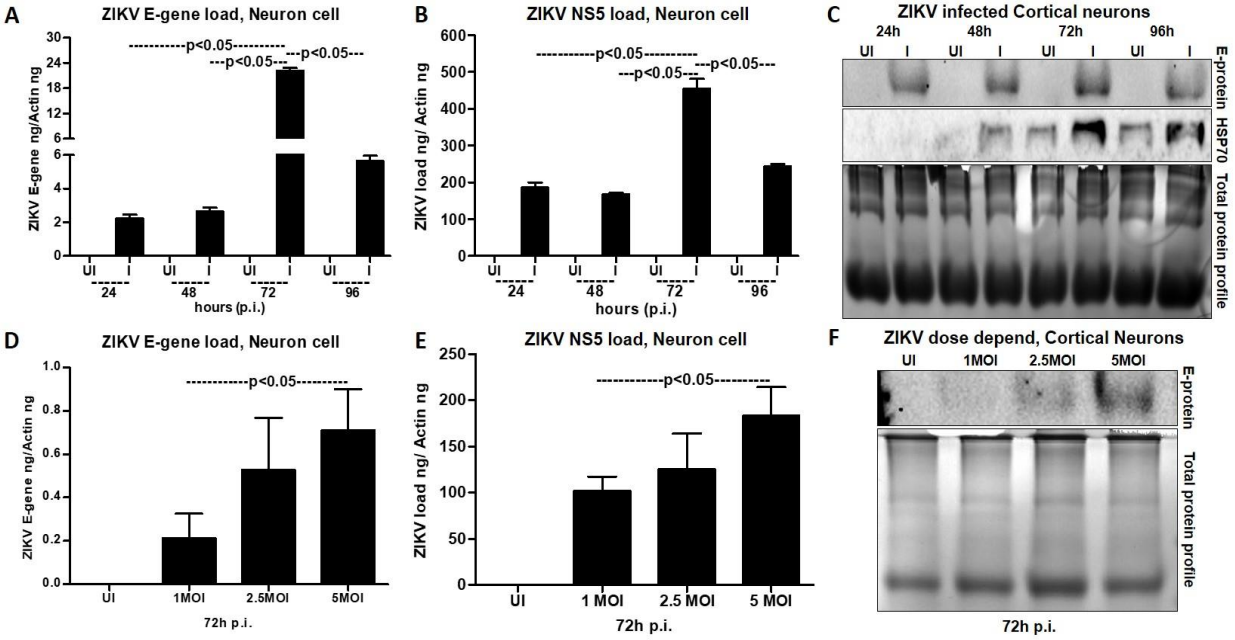

Figure 29. ZIKV Infects Primary Cultures of Cortical Neurons in a Time- and Dose-Dependent Manner

(A-B) QRT-PCR analysis showed the ZIKV loads (MOI 5) determined by either E-gene or *NS5* mRNA transcripts in neuronal cells at different time points (of 24, 48, 72, and 96 h p.i.). Uninfected cells (UI) at indicated time points served as controls.

(C) Immunoblotting analysis showed the ZIKV E-protein levels at different time points (24, 48, 72, and 96 h p.i., MOI 5). HSP70 loads served as an internal control.

(D-E) The ZIKV loads at different MOI of infection (1, 2.5, 5 MOI) determined by either E-gene or *NS5* mRNA transcripts were shown from 72 h p.i.

(F) Immunoblotting analysis showed the viral E-protein loads in cortical neurons upon infection with various doses (1, 2.5, 5 MOI). Uninfected cells were used as control in all panels.

The total protein profiles shown by Coomassie-stained gels served as loading controls. All gene transcript levels were normalized to mouse *beta-actin*. P values were determined by the Student's two-tail *t*-test.

This figure was reproduced from the published journal article (Zhou et al., 2019).

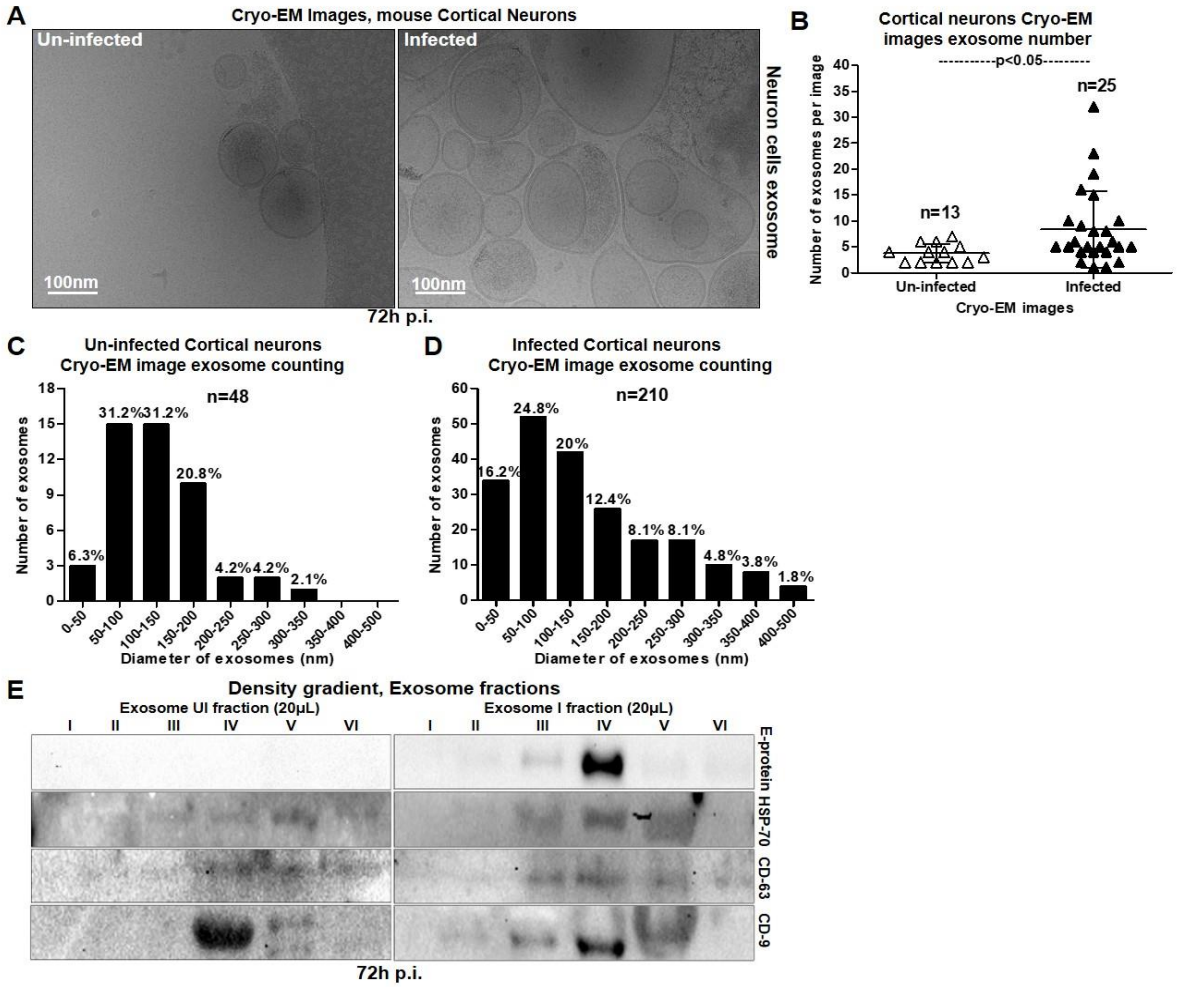

Figure 30. Exosomes Derived from Murine Cortical Neurons are in Heterogenous Populations

(A) Cryo-EM representative images showed the exosomes isolated from uninfected (UI) or ZIKV-infected (I) (MOI 5; 72 h p.i.) cortical neuronal cells. Scale bar indicated 100 nm.

(B) The size distribution of exosomes isolated from uninfected or ZIKV-infected neuronal cells was shown. The Y-axis represented the exosome number and X-axis indicated the exosome size in diameter (e.g., 0-50 nm).

(C-D) Percentages were calculated based on the total number of exosomes in each size range. Exosome numbers counted from uninfected and ZIKV-infected groups were shown. The Y-axis represented the exosome number and X-axis indicated the samples analyzed. P values were determined by the Student's two-tail *t*-test.

(E) Immunoblotting images from OptiPrep density gradient exosomes preparation (DG-Exo-isolation) showed the enhanced ZIKV-E (MOI 5, 72 h p.i.) protein loads and presence of HSP70, CD63 and CD9 (exosomal markers) in different exosome fractions. Exosomes derived from uninfected cells served as controls. Roman numerical indicated the fraction numbers.

This figure was adapted from the published journal article (Zhou et al., 2019).

Cortical Neurons Derived Exosomes Contain ZIKV RNA and proteins

Since, in most of the cases, ZIKV-E protein was detected in fraction 4 (the fraction with enhanced levels of all exosomal markers), this fraction was assumed as more viral RNA/proteins presented and their coincidence to increased infectivity on the naïve recipient cells. It was found that naïve primary murine cortical neurons cultures were infected via incubations (for 72 h) with infectious exosomes from different preparations (derived from ZIKV-infected cortical neurons, at 72 h p.i., and 5 MOI) showed the highest infectivity with fraction 4 (Figure 31A). Exosomes from lower fractions 5 and 6, also suggested enhanced infectivity in comparison to the upper (1-3) fractions (Figure 31A). Next, loads of ZIKV in exosomes derived from cortical neurons infected at different time points (of 24, 48, 72, and 96 h p.i., 5 MOI) were measured. Like viral loads obtained in cortical neuronal cells, ZIKV RNA loads were magnificently ($P < 0.05$) higher at 72 h p.i., when compared to the other time points (of 24, 48 and 96 h p.i.) (Figure 31B). The lower loads of ZIKV at 96 h p.i., is perhaps because of the neuronal cell death observed at this time point (Figure 27A). It was presumed that a smaller number of exosomes were released upon the massive death of neurons at 96 h p.i., (Figure 31B). Immunoblotting with 4G2 antibody showed increased ZIKV E-protein loads at 72 h p.i., in a time-dependent manner, comparing to the viral loads at 24 and 48 h p.i., (Figure 31D). The reduced loads of ZIKV RNA and E-protein at 96 h p.i., matches with the severe neuronal loss at this time point (Figures 31B and 31D). HSP70 in exosomes derived from neuronal cells was detected further indicated the presence of the exosomal marker in both uninfected and infected exosomal lysates (Figure 31D). Furthermore, increased ZIKV RNA and E-protein loads were shown in neurons derived exosomes with a raise in viral doses from 1, 2.5 and 5 MOI at 72 h p.i., (Figures 31C and 31E). Total protein profiles were considered as loading controls in the immunoblotting analysis (Figures 31D and 31E). These results suggested that cortical neuronal cell-derived exosomes enclosed ZIKV RNA and E-protein with enhanced loads.

ZIKV RNA and Proteins Securely Contained inside Exosomes are Infectious during Transmission

RNase A-treatment assays were performed, to test the probability that ZIKV RNA is not perhaps outside the exosomes, and thus taken up by the recipient cells. ZIKV-infected neuronal cells derived exosomes (from 72 h p.i., 5 MOI) were freshly isolated (resuspended in PBS) and co-incubated with RNase A (5 µg/ml, for 15 min, at 37°C). No differences were found in ZIKV *NS5* transcript loads between infected-treated and untreated groups (Figure 32A). The uninfected group treated with RNase A treated as an internal control (Figure 32A). The laboratory viral stocks (5 MOI) with known titers (Vero cell culture supernatants, 14 days post-infection) were treated with RNase A, aiming not to ignore the effect of RNase A on viruses. No differences were detected in viral loads determined from naïve cortical neuronal cells upon incubation with laboratory viral stocks generated from RNase A-treated or untreated groups (Figure 32A). As the previous results with DENV2 (Vora et al., 2018), it was the assumption that the flavivirus RNA genome is secured inside exosomes/virions and is not capable of RNase A-mediated degradation. Next, it was tested if the exosome-mediated viral transmission is relying on ZIKV E-protein in naïve cortical neuronal cells. Infectious exosomes (enclose viral RNA and proteins) or laboratory-generated viral stocks (high infectious dose of MOI 8 or low dose of MOI 0.8) were treated with antibodies (3 µg of each) ZV-2, ZV-16 or with highly affinity neutralizing antibodies ZV-54, ZV-67 (Zhao et al., 2016) for 4 h at 37°C followed by ZIKV infection (for 72 h). No differences in ZIKV loads were detected in neuronal cells re-infected with infectious exosomes that were treated with either ZV-2 or ZV-16 or with ZV-54 or ZV-67 neutralizing antibodies when compared with their corresponding untreated controls (Figure 32B). Antibody treatments of exosomes derived from uninfected cells were used as internal controls for the infectious exosome group (Figure 32B). A magnificent reduction was detected in ZIKV loads in neuronal cells that incubated with ZV-2, ZV-16 or ZV-54, ZV-67 antibodies, treated with high (8 MOI) or low (0.8 MOI) doses of laboratory viral stocks in comparison to their corresponding untreated controls (Figure 32B). Furthermore, ZV-54 and ZV-67 antibodies treatments with high (8 MOI) or low (0.8 MOI) doses of laboratory viral stocks showed significantly ($P < 0.05$) stronger neutralization effects in comparison to ZV-2 or

ZV-16 antibodies, in both the high and low viral doses groups (Figure 32B). In addition, immunofluorescence assays (IFA) were tested on neuronal cells (using 4G2 monoclonal antibody). Similar results were shown from infectivity assays suggesting no differences in ZIKV E-protein staining of neurons that were incubated with infectious exosomes that were either maintained untreated or treated with ZV-2, ZV-16 or highly affinity ZV-54 or ZV-67 neutralizing antibodies (Figure 35). Regarding to neuronal cells incubation with high (8 MOI) or low (0.8 MOI) viral doses of ZIKV (pre-treated with either ZV-2, ZV-16 or ZV- 54, ZV-67 antibodies), neutralization effects matching to less detection of viral E-protein/staining and less fluorescently labeled cells was the evidence when compared with their corresponding untreated controls (Figures 36 and 37). It was also assumed that when compared with ZV-2 and ZV-16, the extremely affinity ZV-54 or ZV-67 antibodies had higher neutralization effects with dramatically depressed E-protein stained positive cells. Next, cortical neurons were treated with 5 µg of 4G2 antibody (that neutralizes ZIKV poorly), followed by infection via exosomes derived from ZIKV-infected neuronal cells (72 h p.i., 5 MOI), to investigate if treatment with 4G2 antibody influences or impedes viral transmission (Figure 32C). No differences in viral loads were detected in antibody-treated or untreated groups of neuronal cells, considering the incubation of infectious exosomes derived from ZIKV-infected neurons (Figure 32C). The inclusion of ZIKV laboratory stocks with known titers (MOI 5) suggested reduced viral loads in cortical neurons served with 4G2 antibody when compared with the untreated controls (Figure 32C). These data suggest that E-protein is securely enclosed the exosomes. Whereas, E-protein on the surface of the virions is reachable to ZV-2, ZV-16, ZV-54 or ZV-67 or 4G2 antibodies and treatments with these antibodies suggested differential neutralizing effects due to the use of laboratory viral stocks. These results further indicated that E-protein is perhaps not on the surface of exosomes and may not be required for manipulating viral RNA and protein transmission via exosomes. To determine if the exosomes-mediated viral transmission is clathrin-dependent, cortical neuronal cells were co-incubate with clathrin specific inhibitor (Pitstop-2; 30 µM for 15 min) and infected these Pitstop-2 treated cells with infectious exosomes isolated from ZIKV-infected (5 MOI; 72 h p.i.) cortical neuronal cells. No differences were detected in ZIKV loads (at 72 h p.i. of naïve cortical neuronal cells) in

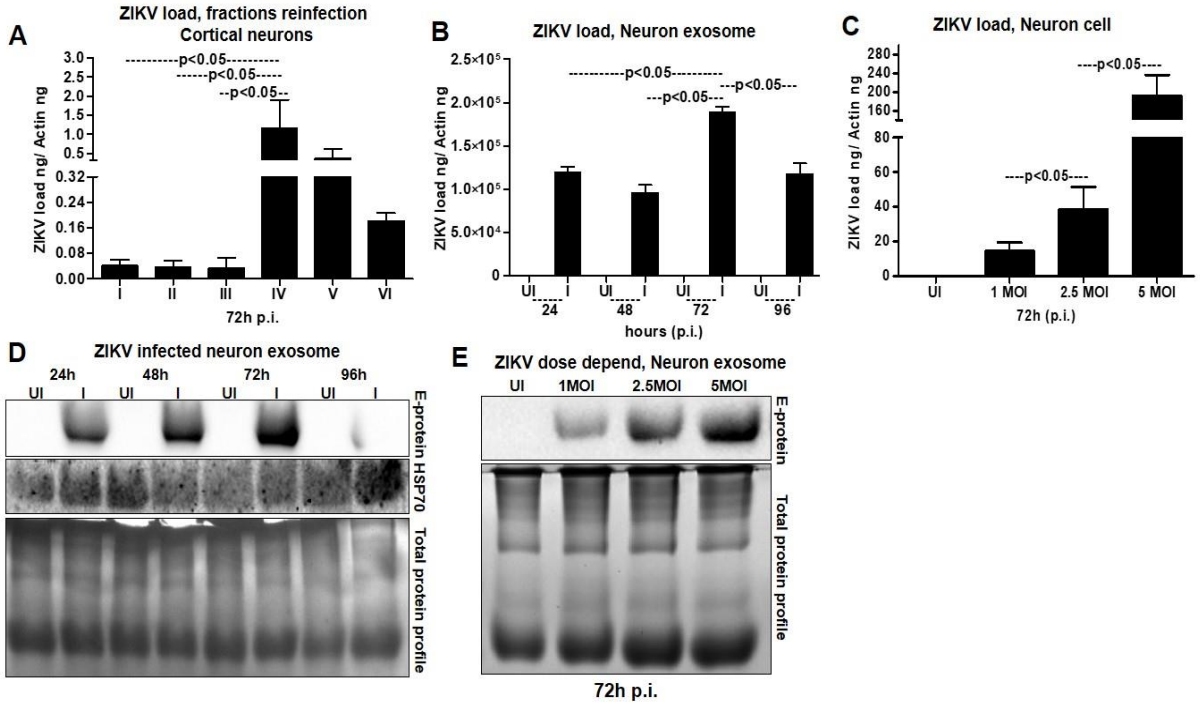

Figure 31. Exosomes Derived from Murine Cortical Neuronal Cells Contain Infectious ZIKV RNA and E-protein

(A) Infection (72 h p.i.) of naïve primary cultures of murine cortical neurons showed the increased infectivity and transmission from infectious exosomal fractions 4-6 in comparison to other lower fractions (1-3).

(B) QRT-PCR showed the ZIKV (I) RNA loads (MOI 5) from cortical neuronal cell-derived exosomes at different time points (24, 48, 72 and 96 h p.i.). Uninfected (UI) groups from each respective time point served as controls.

(C) ZIKV loads from neuronal cell-derived exosomes collected from cortical neurons infected with different doses (MOI 1, 2.5 and 5) at 72 h p.i., were shown.

(D) Immunoblotting showed the ZIKV-E protein loads (MOI 5) and HSP70 levels in neuronal cell-derived exosomes isolated at different time point samples (24, 48, 72, and 96 h p.i.). HSP70 loads showed the presence and enrichment of exosomal marker and served as an internal control.

(E) Immunoblotting showed the ZIKV-E protein loads at different doses (MOI 1, 2.5 and 5, at 72 h p.i.) of infection (I) in neuronal cell-derived exosomes collected from infected-cortical neurons. Uninfected (UI) cell-derived exosomes collected from uninfected cortical neurons served as a control.

Total protein profiles served as controls. The ZIKV *NS5* transcripts were normalized to mouse *beta-actin* transcripts. P values were determined by the Student's two-tail *t*-test. This figure was adapted from the published journal article (Zhou et al., 2019).

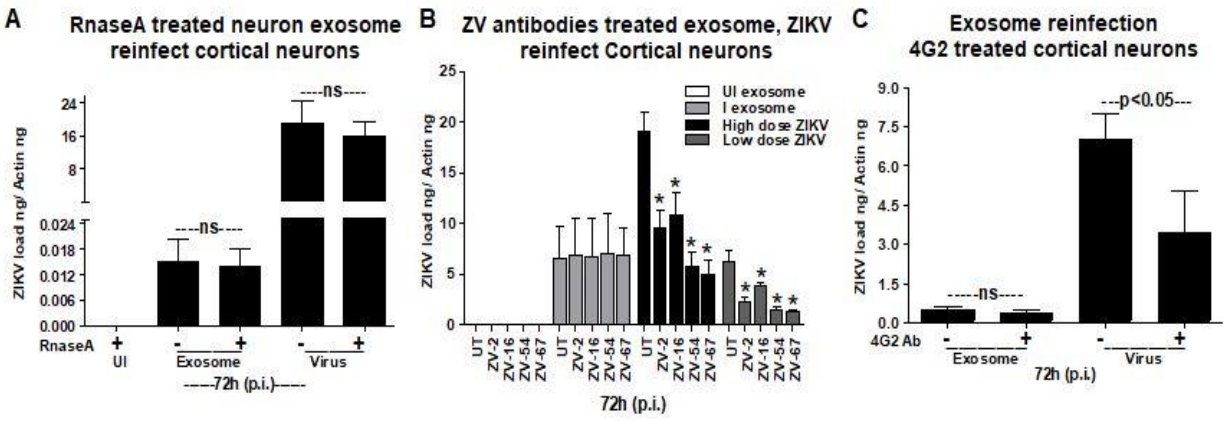

Figure 32. Exosomes from Primary Cultures of Cortical Neurons are Infectious and Transmit ZIKV to Naïve Neuronal Cells

(A) Infections via freshly prepared exosomes from ZIKV-infected (MOI 5, 72 h p.i.) cortical neuronal cells or laboratory ZIKV viral stocks treated with RNase A on naïve cortical neuronal cells (72 h p.i.) were shown. Untreated ZIKV-infected or RNase A-treated uninfected exosome or untreated-virus stock groups served as controls.

(B) ZIKV loads (72 h p.i.) in neuronal cells incubated with ZIKV-infectious exosomes or laboratory viral stocks (8 MOI as high dose or 0.8 MOI as low dose) treated with ZV-2, ZV-16 or ZV-54, ZV-67 antibodies were shown. Cells incubated with uninfected cell-derived exosomes served as a control. The untreated groups included in all panels, respectively, served as controls.

(C) QRT-PCR analysis showed the viral loads in cortical neurons treated with 4G2 antibody followed by infection with exosomes derived from ZIKV-infected (MOI 5; 72 h p.i.) cortical neurons or laboratory viral stocks. Untreated groups serve as controls. ns indicated no significance in all the groups.

This figure was adapted from the published journal article (Zhou et al., 2019).

Pitstop-2 treated group when compared with the DMSO (vehicle)-treated controls (Figure 38). These data indicated that the transmission to naïve neuronal cells mediated by exosome is clathrin-independent.

To test whether exosomal RNA was infectious to naïve cortical neurons, the viral titers were measured in exosomes by operating a virus dilution assay. Representative images from neuronal cells infected through incubations with exosomes or exosome-depleted supernatants are shown from the virus dilution assay (Figure 33). Increased fluorescent signal (as determined by immunostaining with 4G2 antibody) was obvious in neurons infected with infectious exosomes when compared with infection upon

incubation with the supernatant fraction (Figure 33). As an internal control, the viral dilution assay was also implemented on cortical neuronal cells by infecting with ZIKV virus stocks (5 MOI, 72 h p.i.). Exosome-mediated ZIKV-infected cells detected enhanced E-protein staining with a 4G2 antibody when compared with the supernatant preparation- treated cells (Figure 33). Phase-contrast images showed similar morphology of infected-neurons (Figure 33).

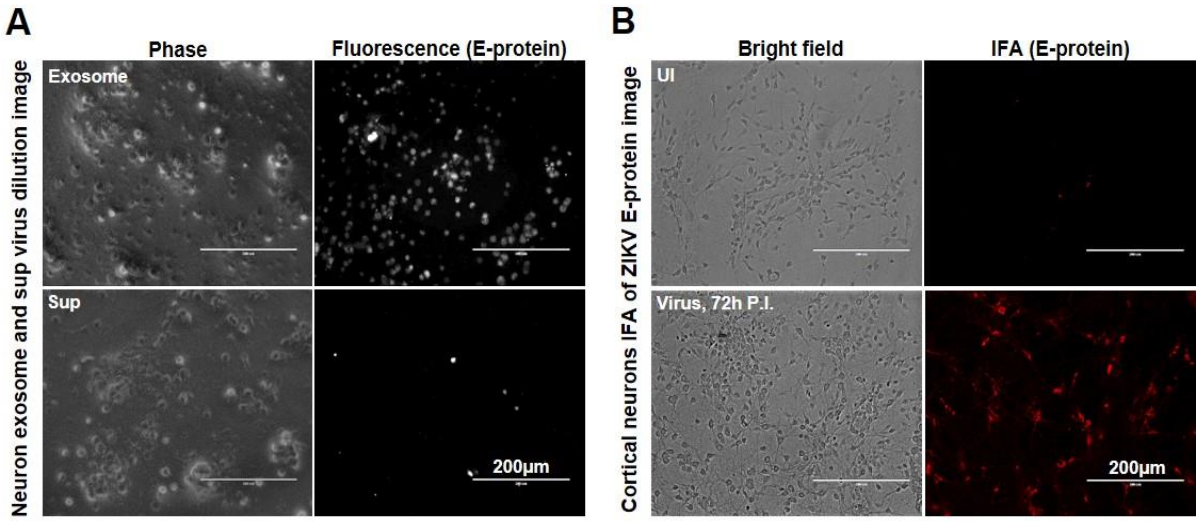

Figure 33. Fluorescent and IFA Images of E-protein Detection

(A,B) Representative fluorescent images showed the detection of E-protein in neuronal cells infected via exosomes (upper panel) derived from the ZIKV-infected (MOI 5; 72 h p.i.) cortical neurons or infected using ZIKV laboratory viral stocks (for 72 h p.i., lower panel). Neuronal cells treated with exosome-depleted supernatant (sup, in a similar ratio) served as a control for exosome group. Uninfected cells served as a control for ZIKV laboratory stock infected group. Scale bar indicated 200 μm in all panels. This figure was adapted from the published journal article (Zhou et al., 2019).

Quantification of fluorescent signals (determined by counting the percentages of fluorescently labeled infected cells staining the E-protein) in neuronal cells infected with exosome preparations when compared with the supernatant fraction (for 72 h p.i.) further supported the microscopic observation (Figure 34A). Dilution 6 was served for both microscopic and quantitative analysis of infected cells from each replicate. The

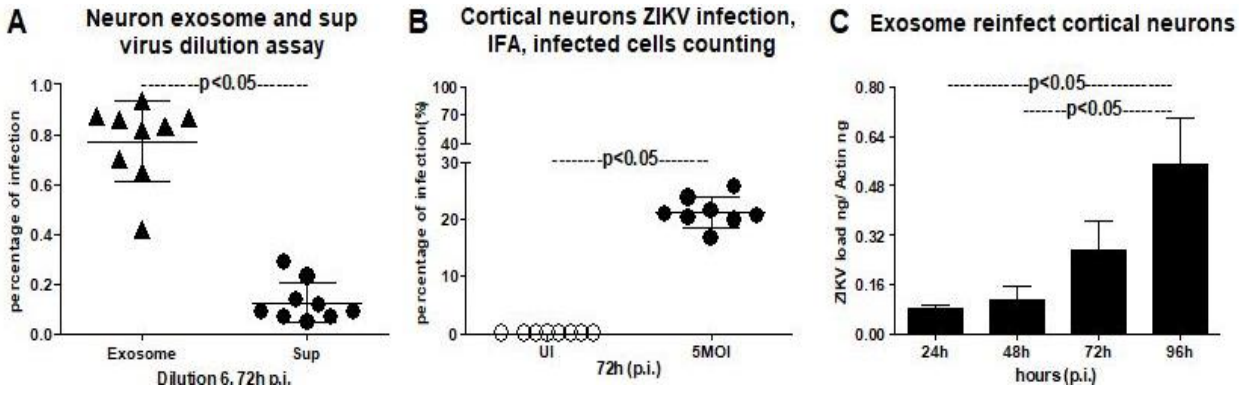

Figure 34. Quantitative Assessment of the Number of ZIKV-Infected Cortical Neurons

(A) Quantitative assessment of the number of ZIKV-infected (detected by the 4G2 antibody) (MOI 5; 72 h p.i.) neuronal cells treated with exosomes (in dilution 6) or supernatant fractions were shown.

(B) Quantitative assessment of the number of fluorescent neuronal cells, (detected by 4G2 antibody) infected (MOI 5; 72 h p.i.) with laboratory ZIKV viral stocks was shown.

(C) ZIKV loads in cortical neuronal cells (at different time points of 24, 48, 72, and 96 h p.i., and 5 MOI) infected via infectious exosomes were shown in naïve cortical neuronal cells for transmission and replication of viral RNA. The ZIKV loads were indicated based on *NS5* transcripts normalized to mouse *beta-actin* transcript levels. P values were determined by the Student's two-tail *t*-test.

This figure was adapted from the published journal article (Zhou et al., 2019).

quantification of fluorescent signals (determined by counting the percentages of fluorescently labeled infected cells showing the E-protein staining by 4G2 monoclonal antibody) in neuronal cells infected with ZIKV virus stocks (5 MOI, 72 h p.i.) suggested infectivity of the viral stocks (Figure 34B). Then, it was tested if exosomes derived from ZIKV infected neurons (from 72 h p.i., 5 MOI) are infectious and reproductive in uninfected/naïve cells. QRT-PCR analysis suggested that murine cortical neuronal cells treated with ZIKV-infected exosomes derived from neuronal cells (isolated from an independent batch of infected cells) rapidly transmitted infectious exosomal RNA to uninfected recipient neurons (Figure 34C). Also, it was indicated that infectious exosomal RNA replicated in the naïve/uninfected neuronal cells in a time-dependent manner at the measured time points of 24, 48, 72 and 96 h p.i. (Figure 34C). These results indicate that neuronal exosomal RNA is infectious, viable, and replicative in naïve recipient cortical neuronal cells of the CNS.

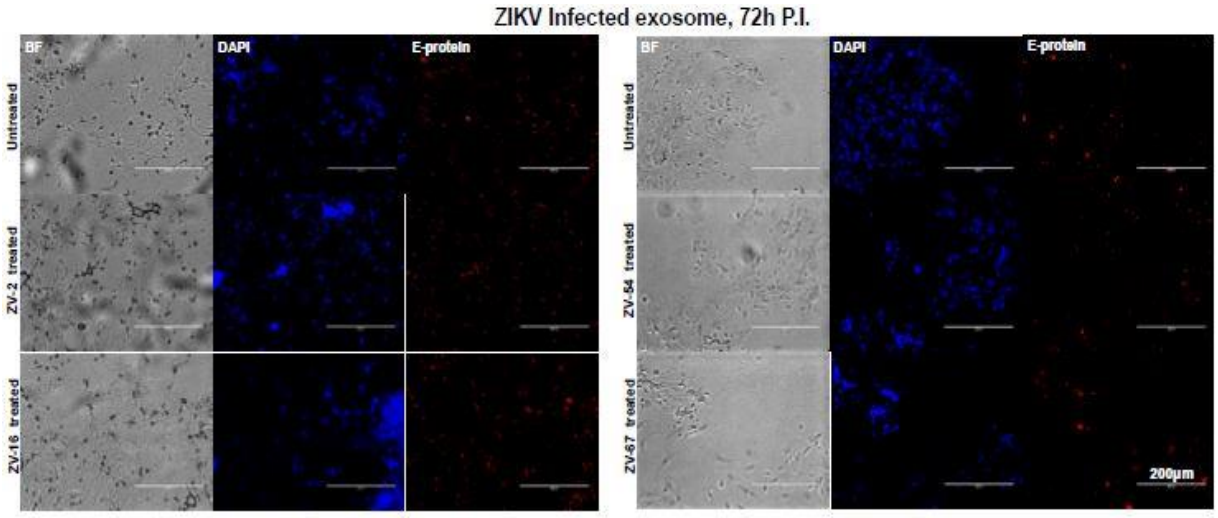

Figure 35. Murine Cortical Neurons Incubated with ZIKV Infectious Exosomes Pretreated with ZV-2, ZV-16, or ZV-54, ZV-67 Antibodies Had no Neutralizing Effects

Infectious exosomes (20 μl of PBS suspension collected from ZIKV-infected (MOI 5; 72 h p.i.) cells) treated (4 h, 37 ° C) with antibodies ZV-2, ZV-16, or ZV-54, ZV-67 followed by incubations on primary cultures of mouse cortical neuronal cells (for 72 h) showed no neutralizing effects. The respective untreated groups served as controls for antibody treatments. Neurons were fixed, permeabilized, and stained for ZIKV E-protein (using the 4G2 monoclonal antibody, followed by Alexa Fluor 594 for detection) that showed no differences in infectivity when cultures were incubated with infectious exosomes pretreated with respective neutralizing antibodies. Images obtained from Bright Field (BF) and DAPI staining were shown as controls. Representative images obtained from the EVOS FL system were shown. Scale bar indicated 200 μm in all images. This figure was adapted from the published journal article (Zhou et al., 2019).

Neutral Sphingomyelinase SMPD3 (nSMase2) Facilitates ZIKV Infection and Transmission via Exosomes

It has been shown that the membrane-associated enzyme SMPD3 (nSMase2; 71 kDa) is one of the most investigated neutral Sphingomyelinase that is triggered by anionic phospholipids such as phosphatidylserine (PS) and phosphatidic acid (PA) (Clarke and Hannun, 2006; Menck et al., 2017). Activation of SMPD3 in cells plays a significant role in cellular responses (Stoffel et al., 2005; Clarke and Hannun, 2006; Menck et al., 2017). The stimulation of nSMase upon ZIKV infection was obtained in both neuronal cells and exosomes resuspended in PBS. At both measured time points

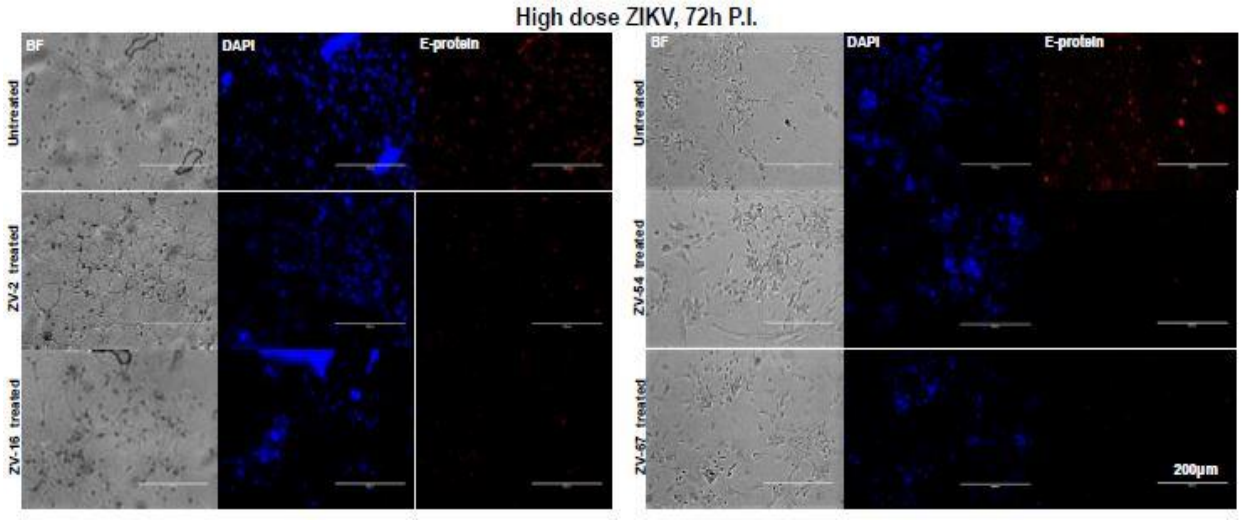

Figure 36. Murine Cortical Neurons Incubated with High Dose of ZIKV Pre-treated with ZV-54, ZV-67 Antibodies Had Strong Neutralizing Effects

Neuronal cultures incubated with a high dose of ZIKV (MOI 8) laboratory stocks pretreated with ZV-54, ZV-67 3 antibodies showed strong neutralizing effects in comparison to the ZV-2, ZV-16 antibodies-treated or untreated controls. Neurons were stained for ZIKV E-protein (using the 4G2 monoclonal antibody, followed by Alexa Fluor 594) that showed reduced infectivity (as indicated by reduced signal or intensity) in groups treated with antibodies. The untreated group served as a control for respective antibody treatments. Images obtained from Bright Field (BF) and DAPI staining were shown as controls. Representative images obtained from the EVOS FL system were shown. Scale bar indicated 200 µm in all images. This figure was adapted from the published journal article (Zhou et al., 2019).

(24 and 72 h p.i.), neutral Sphingomyelinase activity (measured as milliunits) was magnificently ($P < 0.05$) enhanced in ZIKV-infected cortical neurons and in exosomes isolated from these neurons (Figures 39A and 39B). To address if the increasing in Sphingomyelinase activity is dependent on the cell number and the formation/release of exosomes, murine cortical neurons at different cell concentrations were plated and collected cells and derived exosomes at 72 h p.i., from ZIKV infected (5 MOI) or uninfected controls. No significant differences were detected in Sphingomyelinase activity from cells plated at different densities, perhaps the growing cells had kept the same fold of SMPD3 activity (Figure 39C). An increase in Sphingomyelinase activity was tested in exosomes derived from different number of cells plated in increasing

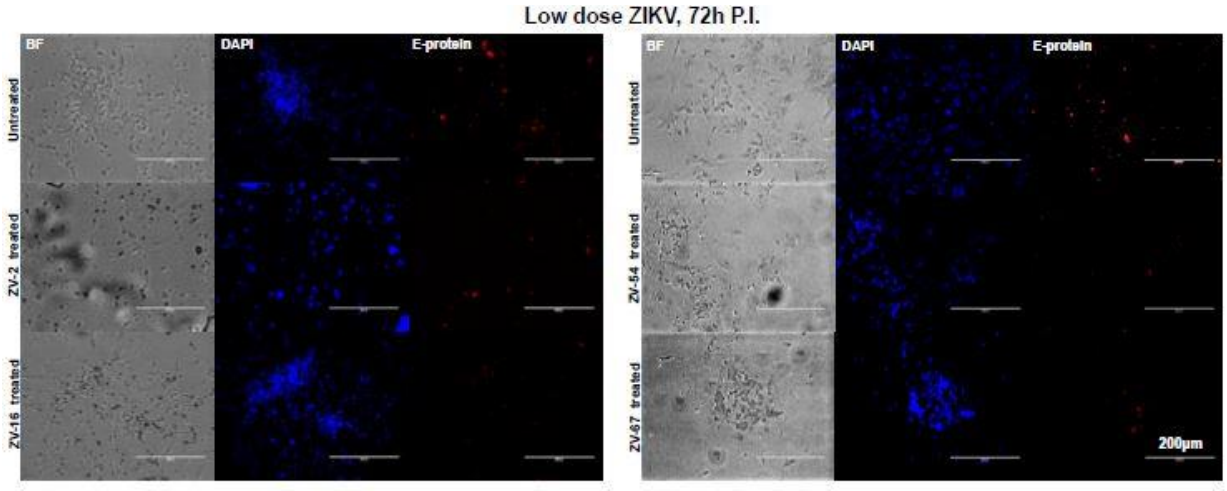

Figure 37. Murine Cortical Neurons Incubated with Low Dose of ZIKV Pre-treated with ZV-54, ZV-67 Antibodies Had Strong Neutralizing Effects

Neuronal cultures incubated with a low dose of ZIKV (MOI 0.8) laboratory stocks pretreated with ZV-54, ZV-67 antibodies showed strong neutralizing effects in comparison to the ZV-2, ZV-16 antibodies-treated or untreated controls. Neurons were stained for ZIKV E-protein (using the 4G2 monoclonal antibody, followed by Alexa Fluor 594) that showed the reduced signal or intensity in groups treated with antibodies. The untreated group served as a control for antibody treatments. Images obtained from Bright Field (BF) and DAPI staining's were shown as controls. Representative images obtained from the EVOS FL system were shown. Scale bar indicated 200 µm in all images. This figure was adapted from the published journal article (Zhou et al., 2019).

densities and this also reflected a rise in ZIKV infected cells derived exosomes (Figure 39D). This result also corresponds with the increasing amounts of total proteins extracted from either cells or exosomes isolated from ZIKV-infected (5 MOI) or uninfected controls (Figures 40A-40F). No significant ($P < 0.05$) differences were detected in total protein amounts extracted from ZIKV-infected or uninfected cells and neither from total proteins collected from ZIKV-infected or uninfected exosomal lysates (Figures 40B, 40C, 40E and 40F). It was also known that ZIKV infection, significantly ($P < 0.05$) upregulated *smpd3* transcripts levels in neuronal cells at both 72 and 96 h p.i. (Figure 41A). No differences in *smpd3* transcript levels were found in exosomal preparations isolated from ZIKV-infected group in comparison to the uninfected controls (Figure 41B). As exosomal *smpd3* transcripts were normalized to actin (Figure 41B), it

was further confirmed that this is not because of the lower actin transcripts in exosomes. QRT-PCR analysis for *gapdh* loads and normalization to the *smpd3* transcripts with either of the housekeeping genes performed no significant ($P < 0.05$) differences (Figure 40G). Like the *smpd3* transcripts levels, the SMPD3 protein loads were upregulated at both 72 and 96 h p.i., in ZIKV-infected neuronal cell lysates when compared with the uninfected controls (Figure 41C). Total protein profile gel image was considered as loading control (Figure 41C). Densitometry analysis from total cell lysates showed the quantitative differences in SMPD3 protein levels (from different time points) observed between the ZIKV infected (MOI 5) and uninfected controls (Figure 40H). Silencing of *smpd3* expression by siRNA treatment showed significantly ($P < 0.05$) lower loads of smpd3 transcript levels at 72 h ZIKV p.i., when compared with the untreated or control (scrambled) siRNA-treated groups (Figure 41D). Significantly ($P < 0.05$) reduced ZIKV loads were obtained in *smpd3*-siRNA- treated cells when compared with untreated or controlled-siRNA-treated control groups (Figure 41E). These results indicate that SMPD3 facilitates ZIKV infection in murine cortical neurons.

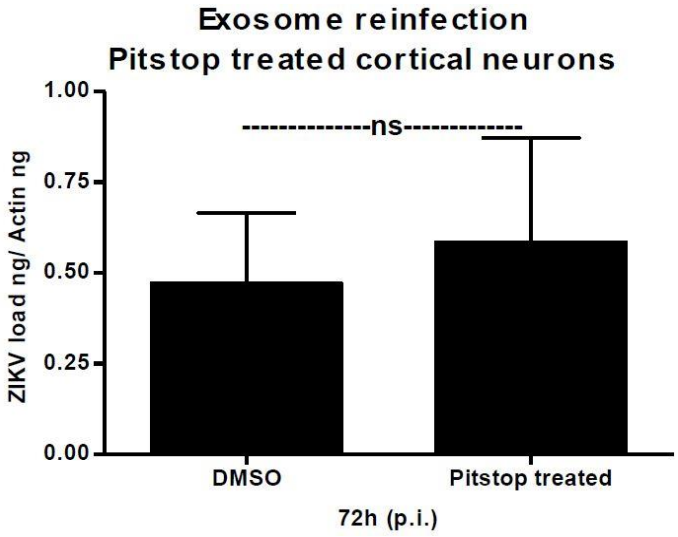

Figure 38. Exosome-Mediated Viral Transmission is not Dependent on Clathrin

QRT-PCR analysis showed the ZIKV loads (5 MOI, 72 h p.i.) from mouse cortical neurons either treated with clathrin specific inhibitor (Pitstop-2) or with DMSO control. The ZIKV *NS5* gene transcript levels were normalized to mouse *beta-actin*. P value was determined by the Student's two-tail *t*-test. This figure was reproduced from the published journal article (Zhou et al., 2019).

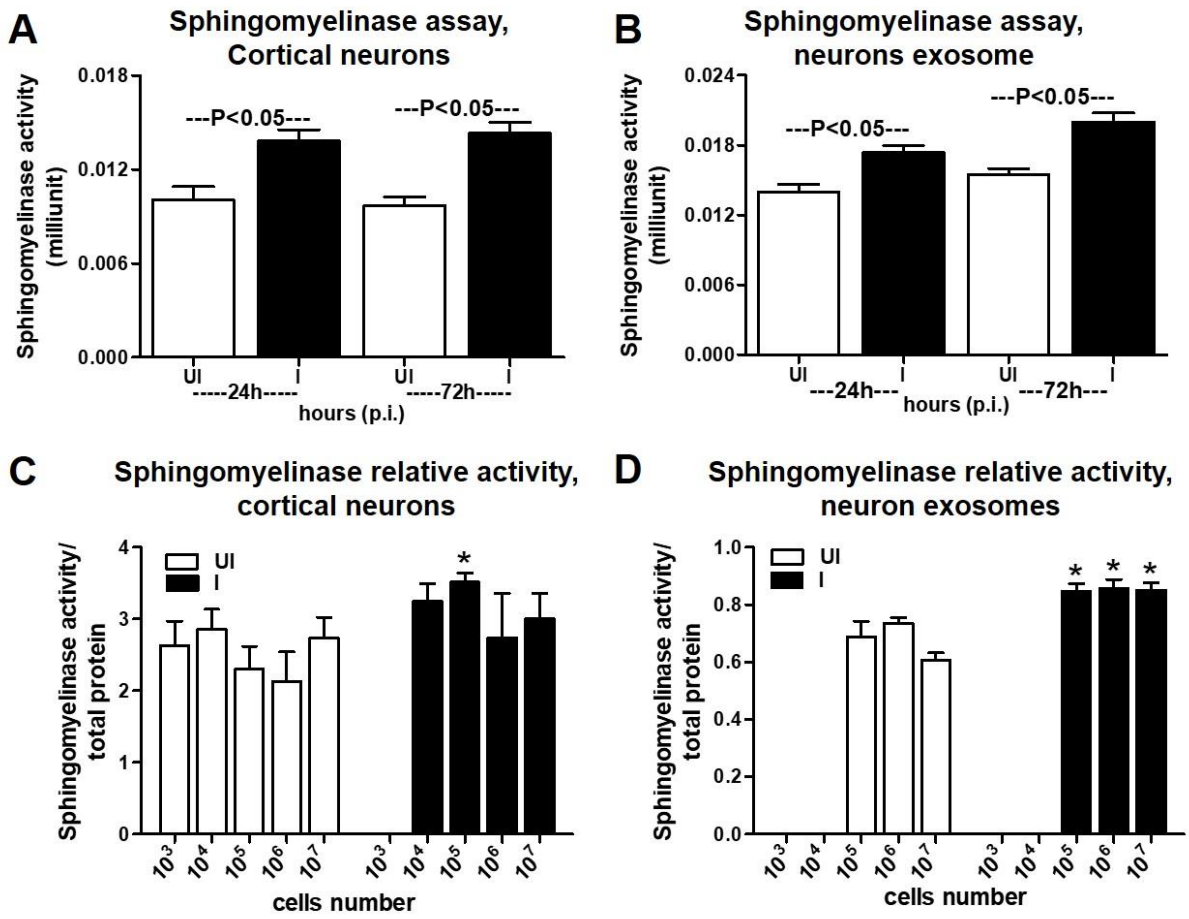

Figure 39. ZIKV Induces Expression of SMPD3, a Neutral Sphingomyelinase Critical for Exosome Production and Release

(A-B) Neutral sphingomyelinase activity assays performed on cell lysates or exosomal lysates were shown. Neuronal cell and exosomal lysates derived from ZIKV-infected (MOI 5) was used from 24 and 72 h p.i. Lysates from uninfected neurons or exosomes served as controls. The Y-axis represented the activity of neutral sphingomyelinases (shown in milliunits) and X-axis indicated the hours in each panel.

(C-D) SMPD3 activity (measured over the amount of total proteins) in neuronal cells or in neuronal cell-derived exosomes determined from different numbers/densities of plated cells were shown. The white bar indicated uninfected and the black bar denoted infected groups. The asterisk indicated significance.

This figure was adapted from the published journal article (Zhou et al., 2019).

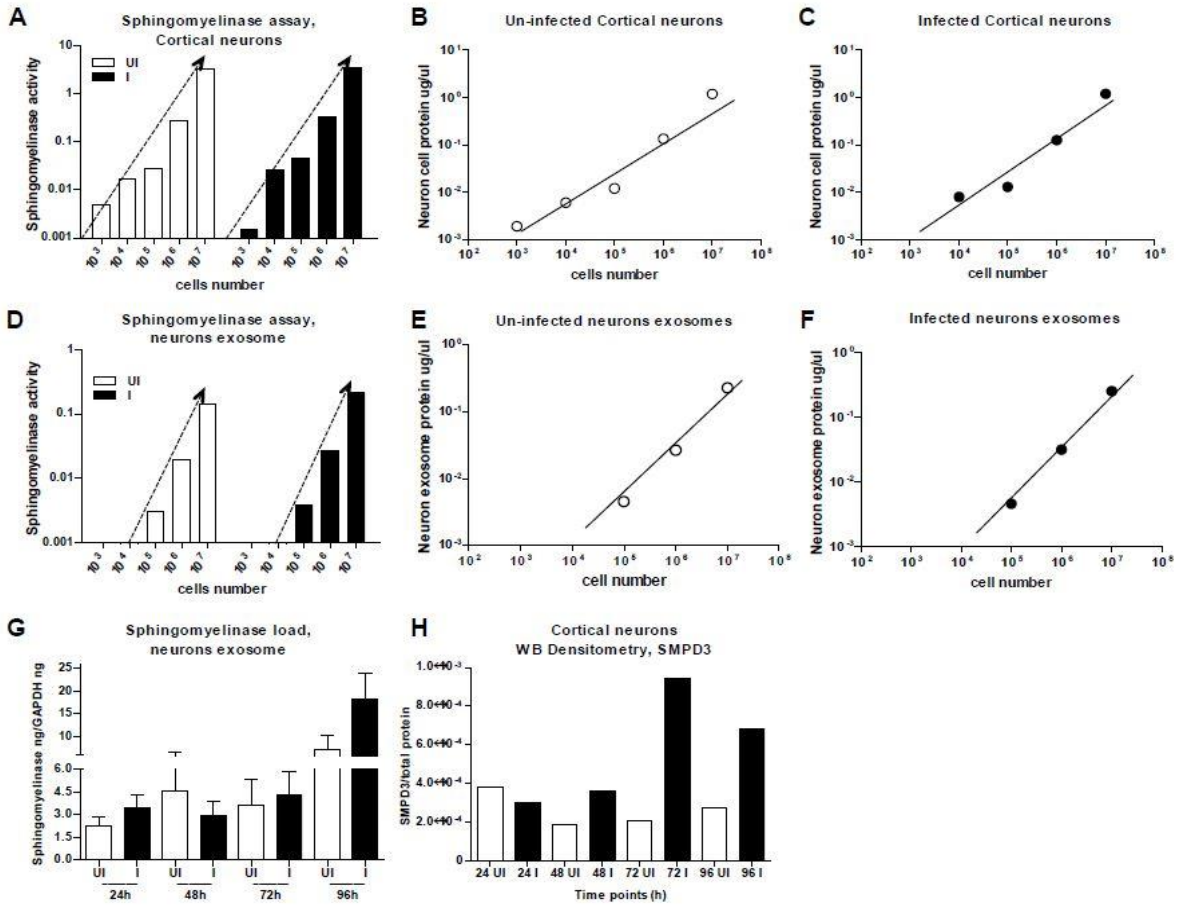

Figure 40. SMPD3 Activity, Total Protein Amounts, Evaluation of SMPD3 Loads Normalized to *gapdh* and Densitometry of SMPD3 Immunoblot

(A) SMPD3 activity from uninfected or infected cells, measured using cell lysates was shown.

(B-C) Total protein loads determined from uninfected or infected cells were shown.

(D) SMPD3 activity measured from uninfected or infected groups were shown.

(E-F) Total protein loads determined from uninfected or infected exosomes were shown. Cells were plated at different densities (10^3, 10^4, 10^5, 10^6, 10^7), and exosomes were derived from these varying cell densities. The X-axis indicated the total protein loads determined from these cells or exosomes and the Y-axis showed different densities (10^3, 10^4, 10^5, 10^6, 10^7) of cells plated or exosomes derived from the varying numbers of cells. The dotted arrow represented a linear increase in SMPD3 activity.

(G) QRT-PCR analysis showed the expression of *smpd3* mRNA transcripts in uninfected (UI) or ZIKV-infected (I) (MOI 5) cortical neuronal cell-derived exosomes isolated at different time points (24, 48 72 and 96 h p.i.) of infection. The *smpd3* gene transcript levels were normalized to mouse *gapdh* levels. P value was determined by the Student's two-tail *t*-test.

(H) Densitometry analysis for the immunoblotting image in Figure 41A showed the SMPD3 levels at different time points (24, 48, 72, and 96, h p.i.) in total cell lysates from uninfected (UI) or infected (MOI 5) (I) groups. This figure was reproduced from the published journal article (Zhou et al., 2019).

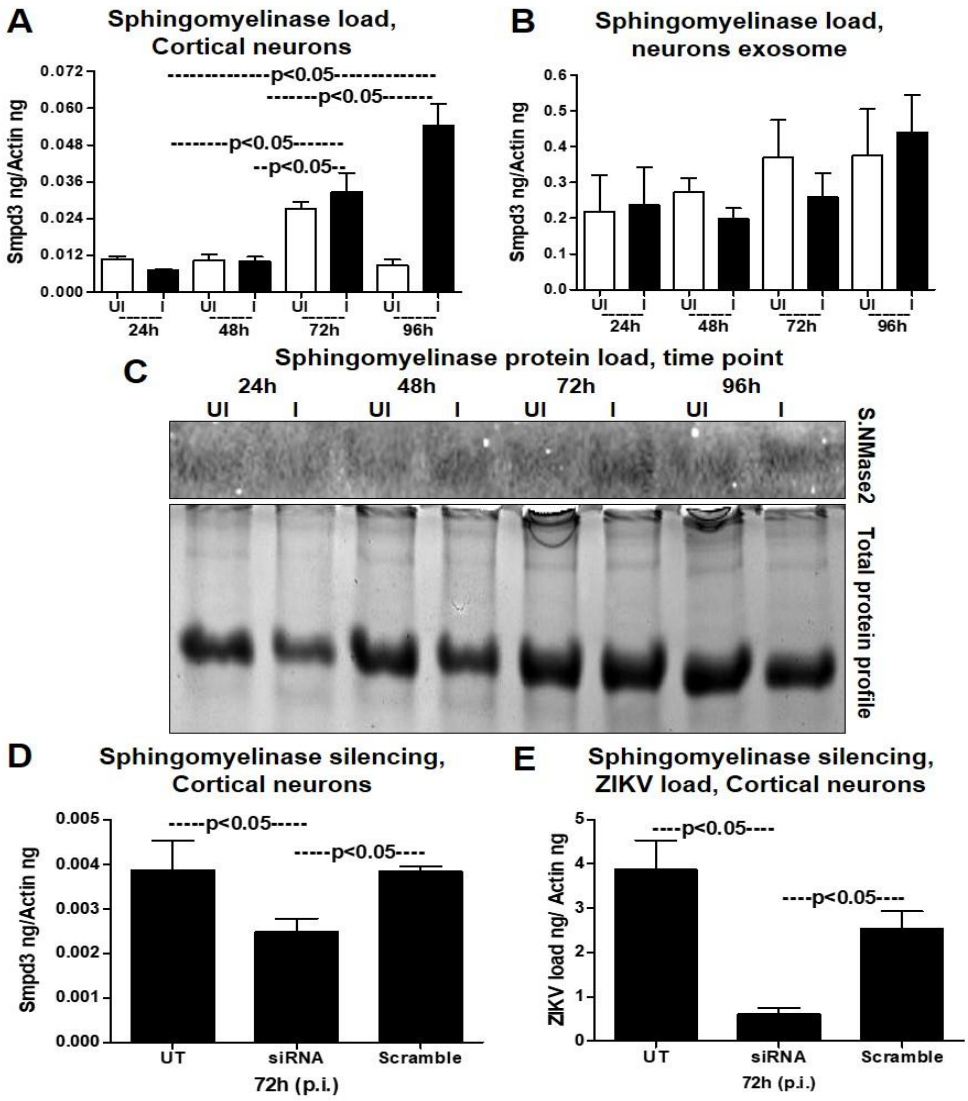

Figure 41. SMPD3 Gene and Protein Levels of Cortical Neurons and Derived Exosomes

(A-B) QRT-PCR analysis showed the expression of *smpd3* mRNA transcripts in uninfected (UI) or ZIKV-infected (I) (MOI 5) cortical neuronal cells or in cortical neuronal cell-derived exosomes isolated at different time points (24, 48 72, and 96 h p.i.).

(C) Immunoblotting analysis showed the SMPD3 protein levels in uninfected (UI) or ZIKV-infected (I) cortical neuronal cells at 24, 48 72, and 96 h p.i. The total protein profile image from Coomassie-stained gel served as a control.

(D-E) QRT-PCR analysis showed the expression of *smpd3* or ZIKV *NS5* mRNA transcript loads (I), to reveal silencing efficiency or viral burden in untreated (UT) or *smpd3* specific siRNA or scrambled siRNA-treated ZIKV-infected (MOI 5; 72 h p.i.) murine cortical neuronal cells. Untreated cells were used as controls. The *smpd3* or ZIKV *NS5* gene transcript levels were normalized to mouse *beta-actin* levels. P values were determined by the Student's two-tail *t*-test. This figure was adapted from the published journal article (Zhou et al., 2019).

Exosome Inhibitor GW4869 Reduced ZIKV Loads and Transmission through SMPD3

It has been announced by literature that inhibition of nSMases with exosome inhibitor GW4869 or by siRNA silencing amend the metabolite composition of cells and Extracellular Vesicles (EVs), therefore, blocking exosomes release (Menck et al., 2017). The inhibition effects of GW4869 inhibitor on exosome budding and release upon ZIKV infection in murine cortical neuronal cells were performed. GW4869 inhibitor treatment (20 μM) gained significantly ($P < 0.05$) reduced loads of ZIKV in infected cortical neurons (5 MOI, and at different time points of 24, 48 and 72 h p.i.) (Figures 42A-42C). No differences in ZIKV loads were obtained when neuronal cells were treated with lower doses (5 and 10 μM) of GW4869 inhibitor. Furthermore, it was suggested that the reduction in ZIKV loads in murine cortical neuronal cells was in a dose- and time-dependent manner, a dramatic reduction in viral loads showed up at 72 h p.i. GW4869 treatments at 20 μM concentration in comparison to the mock (vehicle; DMSO) groups (Figures 42A-42C). Immunoblotting with 4G2 antibody showed reduced ZIKV E-protein loads upon GW4869 treatment at 20 μM concentration when compared with the other doses of 5 and 10 μM and corresponding time points (24, 48 and 72 h p.i.,) and DMSO controls (Figure 42D). At 72 h p.i., treatment with GW4869 at 20 μM concentration, showed larger reduction in ZIKV E-protein loads when compared with the early tested time points of 24 and 48 h p.i., (Figure 42D). Total protein profile gel images from corresponding time points (24, 48 and 72 h p.i.) of ZIKV- infected neurons are considered as loading control (Figure 42D). Besides the murine cortical neuronal cells, the potential roles of GW4869 inhibitor on exosome release from ZIKV-infected cortical neurons were measured. QRT-PCR analysis suggested that exosomes isolated from cortical neurons treated with GW4869 inhibitor (at all tested doses of 5, 10 and 20 μM; and time points of 24, 48 and 72 h p.i.) had magnificently ($P < 0.05$) reduced ZIKV RNA loads when compared with the DMSO control (Figures 43A-43C). This reduction in ZIKV loads was more essential in exosomes in comparison to the reduction showed in cortical neurons that released these exosomes (Figures 42A-42C and Figures 43A-43C). As reduced ZIKV RNA, it was noted that ZIKV E-protein loads were significantly

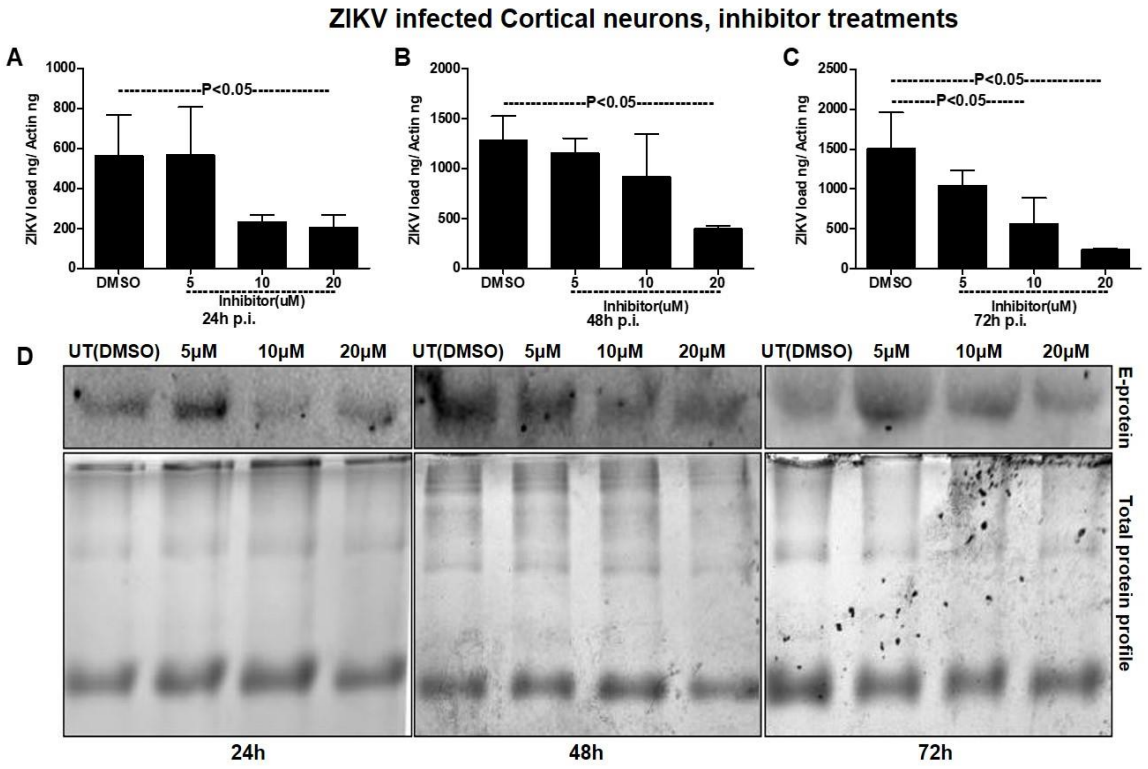

Figure 42. ZIKV Infected Cortical Neurons Inhibitor Treatments

(A-C) QRT-PCR analysis showed the expression of *NS5* mRNA transcripts to reveal viral burden in cortical neuronal cells infected with ZIKV (MOI 5) at different time points of 24, 48, and 72 h p.i. ZIKV *NS5* gene transcript levels were normalized to mouse *beta-actin* levels. P values were determined by the Student's two-tail *t*-test.

(D) Immunoblotting analysis showed the levels of viral E-protein in ZIKV-infected (MOI 5) cortical neuronal cell lysates from different time points (24, 48, and 72 h p.i.) of infection. GW4869 inhibitor was treated for four hours at tested doses of 5, 10, or 20 μM and at indicated time points of 24, 48, and 72 h p.i. Lysates prepared from DMSO-treated cells served as a mock control. The total protein profile images from Coomassie-stained gels served as controls.

This figure was reproduced from the published journal article (Zhou et al., 2019).

reduced as well in cortical neurons-derived exosomes at all the tested doses (5, 10, and 20 μM) and time points (24, 48 and 72 h p.i.) when compared with their corresponding DMSO controls (Figure 43D). Total protein profile gel images from all time points (24, 48 and 72 h p.i.) of ZIKV infected neurons-derived exosomes considered as loading control (Figure 43D). Densitometry analysis from total cell (for

data shown in Figure 42D) and exosomal (for data shown in Figure 43D) lysates indicated the quantitative differences in E protein loads (from the GW4869 time points and dose-response immunoblot analysis) obtained between the ZIKV infected (MOI 5) and uninfected controls (Figures 44A-44C; for immunoblots shown in Figure 42D and Figures 44D-44F; for immunoblots shown in Figure 43D).

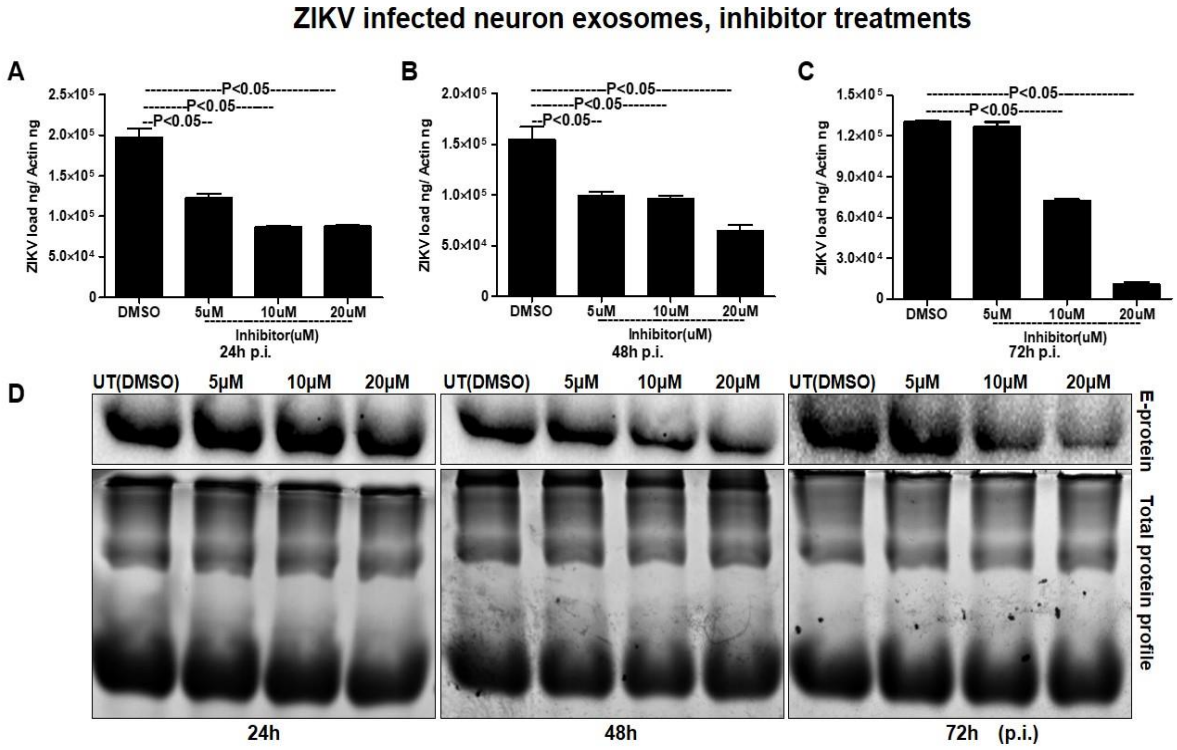

Figure 43. ZIKV Infected Neuronal Exosomes Inhibitor Treatments

(A-C) QRT-PCR analysis showed the expression of *NS5* transcripts to reveal viral burden in ZIKV-infected (MOI 5) cortical neuronal cell-derived exosomes collected at different time points of 24, 48, and 72 h p.i. ZIKV *NS5* gene transcript levels were normalized to mouse *beta-actin* levels. P values were determined by the Student's two-tail *t*-test.

(D) Immunoblotting analysis showed the levels of viral E-protein in ZIKV infected (MOI 5) cortical neuronal cell-derived exosomal lysates at different time points (24, 48, and 72 h p.i.) of infection. GW4869 inhibitor was tested at 5, 10, or 20 μM concentrations and at indicated time points. Lysates prepared from DMSO-treated cells served as mock controls. Total protein profile images from Coomassie-stained gels served as controls.

This figure was reproduced from the published journal article (Zhou et al., 2019).

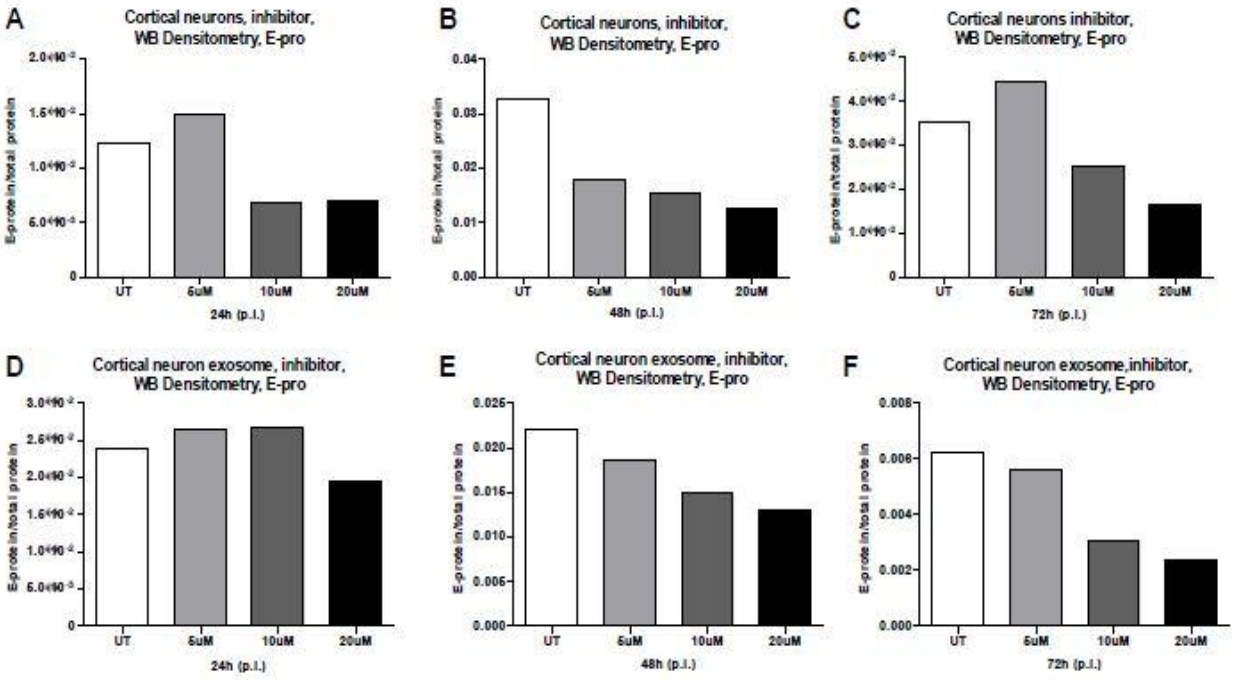

Figure 44. Densitometry Analysis for ZIKV E-protein Immunoblots Showed Differences in GW4869 Inhibitor Treated Samples

(A-C) Densitometry analysis for the immunoblotting images in Figure 42D for viral E-protein at different viral doses (5, 10, and 20 μM) in total cell lysates generated at different time points (24, 48, and 72 h p.i.) from uninfected (UI) or ZIKV-infected (MOI 5) (I) groups were shown.

(D-F) Densitometry analysis for E-protein levels in Figure 43D generated from total exosomal lysates at different doses (5, 10, and 20 μM) and at different time points (24, 48, and 72 h p.i.) from uninfected (UI) or ZIKV-infected (MOI 5) (I) groups were shown.

This figure was reproduced from the published journal article (Zhou et al., 2019).

Furthermore, it was found that upon treatment with GW4869 inhibitor, *smpd3* transcript levels in both cortical neurons (Figures 45A-45C) and neuronal exosomes (Figures 45D-45F) were crucially ($P < 0.05$) reduced (at 20 μM dose in cortical neurons and all tested doses of 5, 10 and 20 μM in neurons-derived exosomes at time points of 24, 48 and 72 h p.i.) when compared with their corresponding DMSO-treated controls (Figure 45). Like ZIKV loads, *smpd3* transcript levels were also less in exosomes in comparison to the infected-cortical neurons (Figure 45). These results elucidate that exosome

release inhibitor GW4869, blocks SMPD3-mediated ZIKV transmission and infection in cortical neurons.

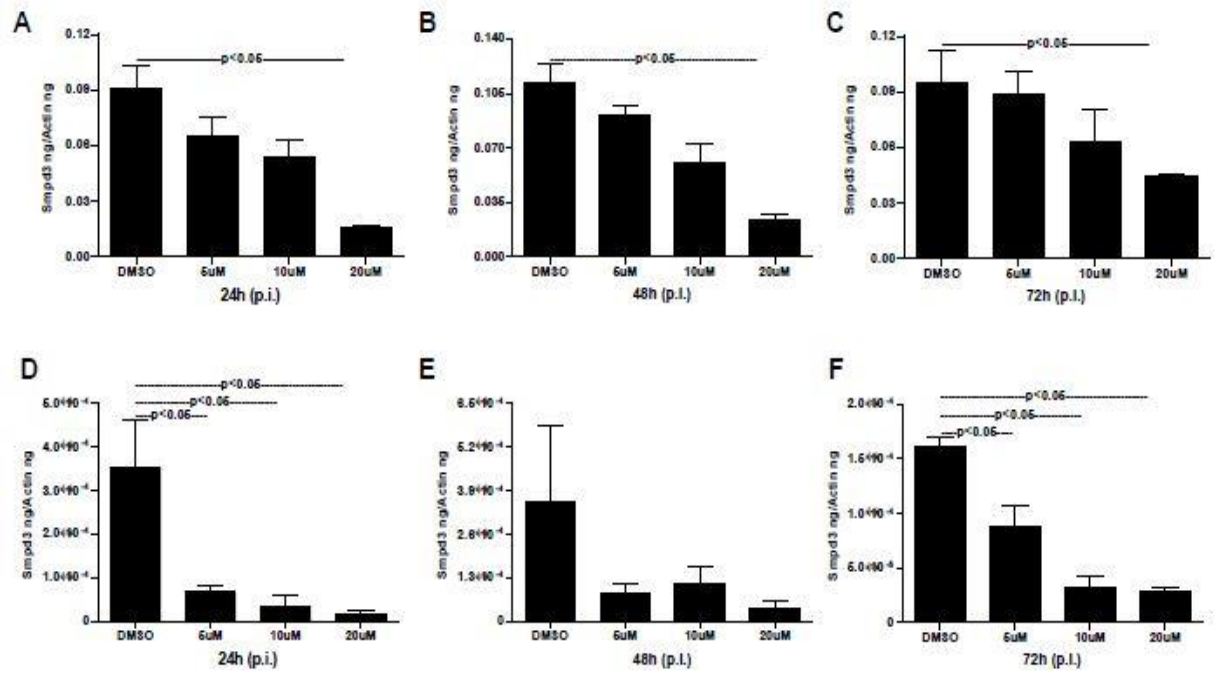

Figure 45. Treatment with GW4869 Affects *smpd3* Loads in Murine Cortical Neurons and Neuronal Cell-Derived Exosomes

(A-C) QRT-PCR analysis showed the expression of *smpd3* mRNA transcripts in ZIKV-infected (MOI 5) cortical neurons collected at different time points of 24, 48, and 72 h p.i. The GW4869 inhibitor was tested at 5, 10, or 20 μM at all indicated time points.

(D-F) QRT-PCR analysis showed the expression of *smpd3* mRNA transcripts in ZIKV-infected (MOI 5) neuronal cell-derived exosomes collected at different time points of 24, 48, and 72 h p.i. The GW4869 inhibitor was tested at 5, 10, or 20 μM at all indicated time points. DMSO groups served as mock controls. The *smpd3* gene transcript levels were normalized to mouse *beta-actin*. P values were determined by the Student's two-tail *t*-test.

This figure was reproduced from the published journal article (Zhou et al., 2019).

3.3 DISCUSSION

Neurotransmission, also known as synaptic transmission, is a procedure by which neuronal cells communicate with one another and send electrical impulses and signaling molecules/chemicals, including neurotransmitters (Di Maio, 2008). Axonal terminals of the mailing (presynaptic) neuron releases the neurotransmitters, including other cargo that binds to and activates the receptors or channels on the dendrites of a neuronal recipient (postsynaptic). With this firmly regulated neurotransmission process from sending neurons to the receiving neuron, the discharge of exosomes from sending neuronal cells and the entry of exosomes into neighboring receiving neuronal cells occurs on a continuous basis. Within a neural presynaptic terminal, two types of small membrane nanovesicles such as synaptic vesicles (SVs; that are ~35-55 nm in diameter) and exosomes (inside Multivesicular Bodies (MVBs); that are 50-200 nm in diameter) are discharged (Chivet et al., 2012; Budnik et al., 2016). Exosomes have been proved to represent a variety of intercellular exchange of effector molecules in order to perform presynaptic neurons to modify gene and protein expression in postsynaptic neurons (Chivet et al., 2012; Budnik et al., 2016). Neuronal exosomes have suggested transferring both membrane and cytoplasmic proteins, functional lipids (involved in signal transduction) or RNA (Chivet et al., 2012; Budnik et al., 2016). In receiving neurons, exosomal mRNA will be translated and the small RNA, including miRNA that mediates gene silencing is stimulated to bind specific genes for depression (Chivet et al., 2012; Budnik et al., 2016). Recent studies of functional RNA, miRNA and proteins in the exosomes have increased the consideration that has led to the emergence of numerous studies in identifying novel molecules present in neuronal exosomes (Anderson et al., 2016; Zhou et al., 2018b). Due to the existence of RNA in the exosomes, it was assumed if exosomes are also cargos of viral RNA from the latest emerging ZIKV. Exosomes have been considered as vehicles of transmission for a variety of microorganisms, and recent studies of Langat virus and WNV transmission through neurons-derived exosomes have provided new understanding into vector-borne flaviviral diseases drug development (Anderson et al., 2016; Zhou et al., 2018b). The recent publication has also proved that the entire dengue virus (Serotype 2; DENV2)

viral RNA genome is present and transmitted via mosquito cell-derived exosomes (Vora et al., 2018). In this study, it proved that ZIKV RNA and proteins are securely transported to the neurons through infectious exosomes. So far, no studies have demonstrated whether ZIKV-caused neurological phenomenon such as microcephaly, involve host neuronal exosomes.

The finding that neuronal cell-derived exosomes are the carriers of mosquito-borne *flavivirus* infectious materials indicate an innovative mode of ZIKV transmission. In this current study with ZIKV infections, the presence of MAP-2 (served as a neuronal marker) and GFAP (astrocyte glial marker) absence clearly indicated the complete differentiation from progenitor cells to cortical neurons in these studies with ZIKV infections. The result with weak or absence of MAP-2 staining, and positive DAPI staining showing enhanced ZIKV E- protein levels, suggested that perhaps there is neurite retraction due to stimulation of cell death in ZIKV infected neuronal cells. Increased neuronal death at 120 h p.i., when compared with the 72 h p.i., of murine cortical neurons infected with ZIKV (MOI 5) suggests that more incubation time and increasing infectious dose could be liable for the massive death of cortical neurons and their networks in developing brains. Additional, enhanced viral loads at 72 h p.i., (at both mRNA and protein levels) in neuronal cells and neuronal cell-derived exosomes indicated timing of peak induction in viral replication in neuronal cells and their transmission through exosomes. The result of high ZIKV loads in neurons suggests that viral materials could be easily transferred into exosomes via axonal transportation. Early diagnosis and detection of ZIKV infections in mothers could possibly block the transport and/or dissemination of infectious viral material that cause damage to the neonatal cells. It was assumed that cortical neuronal cells are critically damaged leading to death and neuronal networking loss, could perhaps result in small size of microcephalic brains. It has been proved that endoplasmic reticulum stress in embryonic brains *(in vivo*) results in unfolded protein feedback during ZIKV infection and associated microcephalic circumstances. Induction in HSP70 loads upon ZIKV-infection or in uninfected cells over the period of post incubations of cortical neurons elucidates a significant role for this chaperone to protect cortical neuronal cells from stress and toxic effects encountered during longer post incubations and viral infections. Detection of

increased HSP70 loads in neuronal exosomes may indicate a similar neuroprotective function as well. Multiple attempts with cryo-EM analysis obtained no detection of virions/viral particles in any performed images. No virion(s) or viral particles were observed neither inside nor outside exosomes. The cultures at 72 h p.i. was used as the selected time point for exosome isolation and cryo-imaging investigation. Usually for virus structure determination, concentrated supernatants generated from longer infection (7-14 days p.i.) with high viral titers ranging from 10^9 to 10^{12} PFU/ml and high centrifugal forces around 200,000 g are reported (Tauro et al., 2012; Vora et al., 2018; Zhou et al., 2018b). These conditions were not used in this neuronal exosomes preparation. In this analysis, exosomes were found to exist in heterogeneous populations varying from sizes of 30-200 nm. However, larger exosomes or EVs were also observed in a size range of 200-350 nm. ZIKV-infected neuronal cell-derived exosomes showed a higher percentage of smaller exosomes (0-200 nm in diameter) or larger vesicles called EVs (200-500 nm in diameter) indicating dense packaging or larger cargo transport through these exosomes, respectively. The presence of HSP70, along with CD63 and CD9 in fractions 3-5, demonstrated these fractions to be exosomes (perhaps containing exosomes 30-200 nm in size) due to the enriched presence of exosomal markers. Increased detection of ZIKV-E-protein in fraction 4 indicated that viral proteins are enriched in exosomes (of sizes 100-200 nm) that may correlate to fractions 3 and 4. The presence of the high amount of viral RNA and proteins in neurons derived exosomes in comparison to neuronal cells, suggest dense packaging of viral components in exosomes for transmission to neighboring neuronal cells. Infection of naïve recipient cortical neurons with infectious exosomal fraction 4 containing concentrated viral E-protein elucidated the presence of a higher amount of viral RNA and its correspondence to enhanced infectivity. Larger amounts of viral E-protein in exosomal fraction 4 directly correspond with the enhanced transmission. Additionally, these results address that an ample amount of viral material inside cells may randomly get transported into exosomes for transmission to neighboring neurons ending up with dissemination within the brains. The detection of no differences in viral loads or infectivity via exosomes treated with RNase A or antibodies (ZV-2, ZV-16 or ZV-54 or ZV-67), further indicates the presence of viral material secure inside

exosomes. An antibody binding to the exterior of virus particles brings out the neutralization of viral infectivity. The 4G2 monoclonal antibody has been proved as highly cross-reactive to several of the *flaviviruses*. However, a recent report has elucidated the 4G2 antibody as a poor neutralizing antibody for ZIKV (Haslwanter et al., 2017). The current study suggested that the neutralization effects with 4G2 were lower in comparison to the other antibodies, include ZV-2 or ZV-16. In addition, the use of ZV-54 or ZV- 67, the highly affinity neutralizing antibodies, indicated ZV-2 or ZV-16 antibodies are less potential when compared with the ZV-54 and ZV-67 antibodies. These results agree with the previous study that measured neutralization effects on different ZIKV strains (Zhao et al., 2016). However, similar data with no differences in viral loads or infection were obtained with infectious exosomes when any of these antibodies were used (ZV-2, ZV-16, ZV-54 or ZV-67 or 4G2), indicating that viral E-protein is located inside the lumen of these vesicles, but not exposed externally for binding to these neutralizing antibodies. Infections of naïve recipient cortical neurons via infectious neurons-derived exosomes further addressed exosomes as a novel mode for ZIKV transmission. It was assumed that exosome-mediated disseminated could be a rapid and efficient approach instead of matured virions-receptor manipulated transmission. In exosomes, large amount of viral material can be transmitted, and they can highly be infectious in recipient cells. Additionally, it is secure for the viral RNA and proteins to be protected and transported inside cargo toward to recipient cells via secured exosomes that can escape any immune checkpoints during transfer via longer journey such as periphery to the brain in the vertebrate host.

Neutral Sphingomyelinase 2 (SMPD3), or sphingomyelin phosphodiesterase is an enzyme that is liable for cleaving sphingomyelin (SM) to phosphocholine and ceramide, a second messenger involved in multiple cellular phenomenon including cellular stress (Clarke and Hannun, 2006; Menck et al., 2017). The cryo-EM images indicated increased formation and release of neurons-derived exosomes upon ZIKV infection. It was assumed that increased activation and levels of SMPD3, in neuronal cells perhaps was correlated with the stimulated release of exosomes upon ZIKV infection. Detection of *smpd3* mRNA levels suggested no crucial differences in neurons-derived exosomes; however, its larger enzymatic activity in both neuronal cells and

exosomes indicated that SMPD3 was critical for the release of neuronal exosomes during ZIKV infection. It was proposed that like increased SMPD3 protein levels detected in neurons, exosomes perhaps have higher protein loads. Silencing of *smpd3* in cortical neurons performed a magnificent deduction in viral loads thereby, suggesting a requirement for this neutral sphingomyelinase in mediating ZIKV infection. These results indicated that ZIKV-infection could increase the formation and/or release of exosomes from cortical neuronal cells by stimulating the protein and activity of SMPD3. The cell density-independent increase in SMPD3 activity in exosomes in comparison to cells (from which exosomes were derived) suggested a strong role for this enzyme in the production and release of exosomes. In cells, SMPD3 activity was principally kept as the growing cells maintained the same fold of activity that was unrelated to of the cell numbers plated. In human macrophage THP-1 cells, SMPD3 has been proved to contribute to the release of exosomes by prompting the budding of exosomes into MVBs (Li et al., 2013; Lang et al., 2016). Inhibition of SMPD3 either through shRNA or siRNA or GW4869 inhibitor treatment, has been indicated to hamper the secretion of exosomes (Essandoh et al., 2015; Lang et al., 2016). GW4869 is a pharmacological agent that influences neutral sphingomyelinase activity and blocks exosome formation and secretion (Essandoh et al., 2015). Very recently, it has been addressed that GW4869 can impede ZIKV infection by perhaps reducing the amount of neutral Spingomyelinase-2 in human fetal astrocytes, however, no insights into the sphingomyelin metabolism were addressed (Huang et al., 2018). GW4869 inhibitor has also been shown to inhibit the ceramide-mediated budding of MVBs and release of mature exosomes from MVBs (Li et al., 2013; Essandoh et al., 2015; Lang et al., 2016). The inhibition in viral loads upon treatment with GW4869 (in a dose- and time-dependent manner) addresses that GW4869 may be served as a candidate for the improvement of novel therapies to control ZIKV infection and transmission in and between cortical neurons. In both cortical neuronal cells and neuronal cell-derived exosomes, decreased ZIKV loads interact with decreased SMPD3 activity and levels upon GW4869 treatment in a dose- and time-dependent manner. These results indicate that SMPD3 enhances ZIKV infection and transmission through neurons derived exosomes in order to spread the infectious viral material. It will be highly intriguing to

understand the mechanism of how SMPD3 assists ZIKV replication in neuronal cells. The immediate future avenues from this study will concentrate on this novel aspect to elucidate the significance of SMPD3 and other neutral Sphingomyelinases in ZIKV infection and neuropathogenesis. The presence of increased ZIKV loads in exosomes in comparison to neuronal cells indicated that ZIKV infectious material is properly abundantly been packaged and maintained to spread through neuronal communication. It was assumed that a larger amount of GW4869 inhibitor is crucial in decreasing the ZIKV loads in neuronal cells. It was also suggested that longer incubations and increased amounts of the inhibitor indicated dramatic effects in decreasing ZIKV loads in neurons derived exosomes. The presence of increasing loads of ZIKV infectious material in exosomes may cause increased transmission causing neuropathogenesis and ultimately death/loss of cortical neurons. The future research efforts will address the underlying molecular mechanisms of SMPD3 and other neutral Sphingomyelinases in manipulating the transmission of ZIKV and its detrimental influence in causing microcephaly in neonatal brains.

Considering the importance of SMPD3 in mediating transmission of ZIKV through neurons-derived exosomes and GW4869 in inhibiting the viral loads in both neurons and neuronal exosomes, it was assumed both as possible therapeutic applicants for controlling ZIKV infection and transmission in developing brains. The long-term future avenues will also define the schemes that depends on neutral Sphingomyelinases including SMPD3, that cause enhanced cortical neuronal cells death, and the underlying molecular mechanisms for ZIKV-induced microcephaly in developing/neonatal brains. The diminished size in the microcephalic brains of ZIKV infected neonates is provoked by a gradual decrease in neuron generation or due to the fast loss of dendritic connections (Ming et al., 2017; Wen et al., 2017). Higher release and transport of infectious exosomes via axonal transport may spread ZIKV infectious viral material to the dendritic branches of the neuronal recipients, thereby reducing the dendritic branching or arborization. Additionally, if ZIKV uses exosomes for transmission in the CNS, it could disseminate the infectious viral RNA and proteins to neural stem cells and thereby mediate the progenitor cells. Both these scenarios would ultimately cause decreased neuron cells numbers and act as a factor responsible for ZIKV-induced

neuronal cell death and microcephaly. Delineating the significance of exosomes and exosomes-associated host molecules that manipulate and assist ZIKV transmission would unravel the molecular mechanism(s) of infection by this neurotropic virus.

3.4 EXPERIMENTAL PROCEDURE

Isolation and Culture of Murine Cortical Neurons and ZIKV Infection

C57BL/6 wild-type female mice with gestation period (day 13) were purchased from Charles River Laboratories and allowed to reacclimatize in our animal facility. Following ethical rules and regulations in accordance with the Institutional Animal Care and Use Committee, primary cultures of murine cortical neurons as disassociated cells were isolated from embryonic day-16 (E16) brains (Sultana et al., 2009; Zhou et al., 2018b). Murine cortical neuronal cells (2×10^5) were seeded in a 12-well plate and cultures were established in complete neurobasal medium with 10% FBS. One day post-plating (DIV; Day in vitro 1), half of the medium was replaced with FBS-free media, to control the growth of glial cells. After 48 h of plating, initiation of neuritogenesis was observed, and cortical neurons were infected with ZIKV (MOI 5 or with different MOI 1, 2.5 or 5; in dose-response experiments) at 72 h post-plating. Neurons were collected at either different time points (24, 48, 72, 96 or 120 h p.i., in infection kinetics and inhibitor treatment assays) or at 72 h p.i., in case of dose-response and other in vitro assays (as indicated in respective Figures and Figure legends). Following collection of neuronal cells and isolation of exosomes, samples were proceeded for RNA extractions and Real-Time Quantitative PCR (QRT-PCR). All culture medium and required supplements for neuronal culture isolation and maintenance were purchased from Invitrogen/ ThermoScientific Inc. ZIKV PRVABC59 strain was obtained from BEI Resources (catalog number: NR-50240) and propagated as per the instructions from the distributor. Due to increased viral loads in cortical neurons at 72 h p.i., this time point was considered for further analysis. Details for infection studies corresponding to the data shown in different figures are mentioned in the respective figure legends. Briefly, for reinfection experiments with infectious exosome fractions, 2×10^5 neurons were co-incubated with 20 µl of neuronal cell-derived exosomal fractions. 400 µl (same ratio) of

the exosome-depleted supernatant fraction (collected from the step before PBS wash during exosome isolation) from neuronal cells was used to process for isolation of exosomes. Neuronal cells were harvested at different time points (24, 48, 72 and 96 h p.i.) and processed for RNA extractions followed by QRT-PCR.

Immunofluorescence, Phase Contrast and Fluorescent Microscopy

2-5 × 10^5 neuronal cells were plated in complete neurobasal medium and allowed to adhere overnight. Two days post-plating neuritogenesis was observed, cortical neurons were infected with ZIKV (MOI 5; in time point samples or with different MOI's 1, 2.5, 5 in dose-response experiment) at either 72 or 120 h post-plating. Immunofluorescence (IFA) was performed as described (Vora et al., 2018). Briefly, cortical neuronal cells were fixed with 4% PFA, permeabilized, blocked (3% BSA) and stained with MAP-2 antibody (Santa Cruz Biotechnology, Inc.) followed by detection with Alexa-Fluor 488 secondary antibody. Sequentially neurons were further stained for either GFAP antibody (Santa Cruz Biotechnology, Inc.) or 4G2 monoclonal antibody (that detects ZIKV E-protein) followed by detection with Alexa-Fluor 594 secondary antibody, respectively. Neuronal cell nuclei were detected with DAPI staining. Fluorescent images were obtained from 72 or 120 h p.i. cortical neuronal cells. Phase-contrast images were collected from both uninfected and ZIKV-infected cells at different days or time points (24, 48, 72, and 96 h p.i.) or at 72 h p.i. in neurons infected with different MOI (infection with dose-response or virus dilution assays). For neutralization assays with ZV-2, ZV-16 or ZV-54, ZV-67 antibodies (Zhao et al., 2016), neurons were fixed and processed as described above, and immune-stained with 4G2 monoclonal antibody, followed by detection with Alexa Fluor 594 secondary antibody. Untreated cells represent no antibody treatments but were incubated either with infectious exosomes or with viral stocks (of known titers as described above). All cells were treated with DAPI to show cell nuclei in addition to bright field images that served as controls. Images were obtained using the EVOS Fluorescence System (Invitrogen/ ThermoScientific Inc.) and 10X or 20X (in Figures 25 and 33) or at 10X magnification (in Figure 26). Representative images are shown for each time point or group. Scale bar is shown on each representative image in the respective groups.

MTT Assays

MTT [3-(4,5-dimethythiazol-2-yl)-2,5-diphenyl-2Htetrazolium bromide] assay was used to measure viability, which served as an index of living neuronal cells. Briefly, 5 mg/ml of stock solution was prepared by completely dissolving MTT (Sigma) in DMSO (100%) and followed by filter sterilizing (0.22 µm filter; Nalgene). Primary cultures of cortical neuronal cells were plated at the density of 1×10^4 cells per well in a 96-well plate. The confluence of the cells was less than 100% in all wells. For infection, neuronal cells were infected with ZIKV (MOI = 5) and at different time points (24, 48, 72, 96, and 120 h) post-infection, then all medium from each well was removed, and added 90 µl of fresh medium to each well. 100 µl of PBS was added to empty wells for background estimation. 10 µl of prepared MTT solution was added to all the wells including PBS containing wells that served as blank controls. Plates were covered in aluminum foils and incubated at 37°C for 2-4 hours (until a purple precipitate was visible). 100 µl of DMSO solvent was added and plates were incubated at 37°C for another 15 min. Absorbance was read at 560 nm and reference plates were read at 650 nm. The uninfected control maintained for 120 h post-plating was considered to calculate the percentages of cell viability. Values from 650 nm reference read were subtracted from the values obtained at 560 nm to determine the neuronal cell viability numbers. Higher absorbance values indicated an increase in cell viability.

RNA Extraction, cDNA Synthesis and QRT-PCR Analysis

Following manufacturer's instructions, total RNA was extracted using Aurum Total RNA Mini Kit (BioRad). RNA was extracted from cortical neurons or neuronal cell-derived exosomes infected (5 MOI) at indicated time points (24, 48, 72, 96 h p.i.) or with various doses (MOI 1, 2.5, 5) of ZIKV-infected group or uninfected controls. RNA was converted to cDNA using the BioRad iScript cDNA synthesis kit. The generated cDNA was used as a template for the amplification and determination of viral burden. For the detection of ZIKV replication, published forward and reversed primers for *NS5* or *E*-gene region were used (Dutta et al., 2018). For SMPD3 gene expression analysis, the following forward and reversed primers were used from published study (Khavandgar et al., 2011). To normalize the amounts of templates, mouse actin amplicons were quantified

with published primers (Zhou et al., 2018b). Primers for *beta-actin* were used in parallel for QRT-PCR normalization. The *gapdh* primer sequences were designed based on the published study (Xu et al., 2014). Equal amounts of mouse cDNA samples were used in parallel for *beta actin*, *gapdh* and ZIKV *E-gene* or *NS5-gene*. The ratio of ZIKV E-gene or *NS5* amount/*beta actin* amount was used as an index to determine the rate of infection in each analyzed sample. QRT-PCR was performed using iQ-SYBR Green Supermix and CFX96 instrument (BioRad, USA). Standard curves were prepared using 10-fold serial dilutions starting from standard 1-6 of known quantities of actin or *gapdh* or ZIKV *E-gene* or *NS5-gene* fragments and QRT-PCR reactions were performed as described (Zhou et al., 2018b). For RNase A treatment, fresh exosomes were isolated from either uninfected or ZIKV infected neuronal cells (2×10^7), distributed the infected exosomes as treated (5 µg/ml RNase A, 37°C for 15 min) or untreated groups. Uninfected exosomes (as similar volumes used in infected groups) treated with RNase A were used as control. For ZIKV laboratory viral stocks (5 MOI), the viral supernatants were treated directly with RNase A and incubated these samples on naïve primary cultures of murine cortical neurons. Non/poorly neutralizing antibodies ZV-2, ZV-16, or 4G2 (Clone D1-4G2-4-15) were obtained from BEI Resources. The highly potent neutralizing antibodies ZV-54 and ZV-67 (Zhao et al., 2016) were a kind gift from Dr. Michael S. Diamond's laboratory, at the Washington University School of Medicine, Saint Louis, MO. For ZV-2, ZV-16 or ZV-54, ZV-67 or 4G2 antibodies treatments or neutralization studies, either 3 µg (of ZV-2, ZV-16 or ZV-54, ZV-67) or 5 µg (of 4G2 antibody) of antibodies was treated for 4 h at 37°C with either freshly isolated exosomes (20 µl of PBS suspension of exosomes from ZIKV infected cells, 72 h p.i., 5 MOI) or with ZIKV laboratory viral stocks (8 MOI as high dose or 0.8 MOI as low dose for ZV-2, ZV-16 or ZV-54, ZV-67 antibodies or 5 MOI for 4G2 antibody treatments). In order to adjust the dose and reflect the infection of recipient cells with infectious exosomes, either high or low doses of viral stocks had been used with known titers for comparison. Exosomes were collected from an independent batch of ZIKV-infected or uninfected cells and were used in this analysis. Neuronal cells were infected through infectious exosomes or viral stocks (pretreated with respective antibodies) for 72 h p.i. and collected for RNA

extractions and processed for QRT-PCR. Untreated samples or neurons incubated with exosomes from uninfected cells served as experimental internal controls.

Immunoblotting and Densitometry Analysis

Briefly, 2 × 10^7 cortical neuronal cells were seeded on to six well-dishes for overnight incubation. The next day, half of the complete media was changed to no-FBS containing medium. Cells were infected with ZIKV (MOI 5) at 72 h post-plating and collected at different time points of 24, 48, 72, and 96 h p.i. or with different doses, of 1, 2.5 and 5 MOI. Cell culture supernatants were collected from the same cells at different time points (24, 48, 72, and 96 h p.i.) of infection or at 72 h p.i. (from different MOI samples) and processed for exosome isolation. Exosome fractions were collected after PBS wash (two times), and adherent cells were collected from the same plates (washed twice with 1 × PBS), and resuspended in modified RIPA buffer. Total protein amounts were estimated using the BCA kit (Pierce/ThermoScientific, Inc.). Whole cell and exosomal lysates (10-30 µg) were separated on 12% SDS-PAGE gels. After gel electrophoresis, blots were blocked with 5% milk buffer and probed with either 4G2 (obtained from Millipore, Sigma or BEI Resources) or HSP70 (Cell Signaling Technologies, Inc) or CD63 or CD9 monoclonal antibodies or SMPD3 polyclonal antibody (Santa Cruz Biotechnologies, Inc), followed by mouse or rabbit HRP-conjugated secondary antibodies (Santa Cruz Biotechnologies, Inc), respectively. Images showing total protein profiles obtained from Coomassie-stained gels served as loading controls. Antibody binding was detected with the WesternBright ECL kit (Advansta, BioExpress). Blots were imaged using Chemidoc MP imaging system and processed using Image Lab software obtained from the manufacturer (BioRad). Densitometry analysis from total cell and exosomal lysates (from both the time point and dose-response immunoblot analysis) between the ZIKV infected (MOI 5) and uninfected controls was performed considering their respective total profile gel images and the respective band.

Isolation of Exosomes from Cell Culture Supernatant

Exosomes were isolated by differential ultracentrifugation method (Théry et al., 2006). Isolation procedure and modifications are shown in chapter 2. Briefly, 1-2 × 10^7 cortical

neuronal cells were seeded for exosome isolation in complete neurobasal medium (overnight). Neurons were infected with ZIKV (MOI 5) for 72 h p.i. Briefly, cell culture supernatants were spun at 100,000 × g for 120 min. Supernatants collected after this spin served as exosome-depleted supernatant (EDS) fractions (used as a control in our study). The pellet containing exosomes and any contaminants were washed with ice-cold PBS (another spin at 100,000 × g, for another 120 min). Resulting exosome pellets is referred to as exosome fractions in our study. Freshly prepared exosome pellets were resuspended in PBS and either frozen at −80°C or used for subsequent evaluations and assays or were resuspended in RNA lysis (Biorad) or modified RIPA buffers (G-Biosciences, BioExpress) for total RNA or protein extractions.

Cryo-Electron Microscopy

The cryo-EM was performed in chapter 2. Briefly, purified concentrated suspensions of ZIKV-infected or uninfected exosomes resuspended in PBS were vitrified on carbon holey film grids and as previously described (Sherman et al., 2006; Sherman et al., 2009). Frozen grids were stored under liquid Nitrogen and transferred to a cryo-specimen holder under liquid Nitrogen before loading into a JEOL 2200FS, or a JEOL 2100 electron microscopes (JEOL Ltd., 3-1-2 Musashino, Akishima, Tokyo 196-8558, Japan). Preliminary screening and imaging of exosomes was done using a 4k × 4k Gatan US4000 CCD camera and final imaging was done at indicated 40,000 × magnification with a 5k × 4k Direct Electron Detector Camera using a low dose imaging procedure. Images were acquired with a ca. 20 electrons/Å2 dose; the pixel size corresponded to 1.5 Å on the specimen scale. A 2.0-2.3 µm defocus range was used for imaging. For exosome size quantitation, the sizes were manually analyzed using scale bar from cryo-EM images and counted exosomes of different sizes per image in each group. Three independent estimations and counting were performed without any bias. Percentages (for size determination) were calculated based on the total number of exosomes in each size range.

OptiPrep™ Density Gradient Exosome (DG-Exo) Isolation

2×10^7 cortical neuronal cells were infected with ZIKV (5 MOI and for 72 h p.i.). Uninfected neurons were used as controls. The detailed protocol for isolation of exosomes on the density gradient is shown in chapter 2. Briefly, supernatants (10 ml) from uninfected/infected cortical neurons were collected and centrifuged at 4°C (480 × g followed by 2000 × g for 10 min each to remove cell debris and dead cells). Cell culture supernatants were concentrated to ~2 ml using the Corning Spin-X UF concentrators or centrifugal filter device with a 5 k nominal molecular weight limit (NMWL) (VWR). Concentrated cultures were processed for OptiPrep™ (DG-Exos) isolation as described in the chapter 2 (Tauro et al., 2012). Six individual fractions were collected from uninfected or infected groups (from top to bottom) manually after 18 h spin at 100,000 × g (with increasing density of iodixanol, and smaller size vesicles on bottom fractions) and diluted with 5 ml of sterile PBS. Fractions were centrifuged at 100,000 × g for 3 h at 4°C, followed by another PBS wash and spin at similar centrifugal forces. DG-Exo fractions were resuspended in 80 µl of PBS and stored at −80°C until further analysis. Exosomal fractions were either processed for Western blotting analysis to detect viral E-protein or the exosomal marker HSP70 or used in infection of naïve primary cultures of murine cortical neurons to determine the infectivity and transmission through infectious exosomal fractions.

Viral Dilution Assay

The virus dilution assay was performed as described in (Schoepp and Beaty, 1984). Briefly, neuronal cells were seeded (at a density of 1×10^5 cells/well in 225 µl of Neurobasal complete medium) on 96 well plates. Neurons were treated with either exosome fraction (20 µl) or with exosome-depleted supernatant fractions (EDS; 400 µl) or with laboratory ZIKV viral stocks (5 MOI) at 72 h post-plating and incubated for additional 5 days. In each group, six different dilutions were used (1-6) and at least eight independent replicates in addition to the uninfected negative controls. Neurons were fixed with the acetone-PBS mixture (3:1, for 20 min at −20°C), and plates were air-dried, washed with 1 × PBS and blocked with 5% FBS-PBS-0.05% Sodium Azide for 15 min at RT. ZIKV E-protein was detected by incubation with a 4G2 monoclonal antibody

(overnight at 4°C), followed by three washes with PBS. Samples were incubated with Alexa-594 labeled mouse secondary antibody for 1 h at RT, followed by washes (3×) with PBS. Plates were analyzed using the EVOS fluorescence system (Invitrogen/ThermoScientific, Inc.) and cells were scored for fluorescence or the presence or absence of infection in comparison to the infected positive controls (infected with laboratory prepared virus stocks) or uninfected negative controls. Representative images from dilutions 10^6 are shown. The percentage of infected neurons is shown from the same dilution for exosome and supernatant fractions.

Neutral Sphingomyelinase Activity Assay

For determining the activity of neutral Sphingomyelinases, the Colorimetric Sphingomyelinase Assay kit from SIGMA-Aldrich was used and followed the instructions from the manufacturer. Briefly, 1×10^7 cortical neuronal cells were plated and three-day post-plating infected with ZIKV (MOI 5) for either 24 or 72 h p.i. In an independent assay to test if an increase in SMPD3 activity is dependent/independent on cell number and exosome production and/release, mouse cortical neuronal cells were plated at densities of 10^3, 10^4, 10^5 , 10^6 and 10^7 cells per well in replicates and measured the total protein amounts and SMPD3 activity. SMPD3 activity was measured by either considering the same amounts of total protein (estimated by BCA assays), where SMPD3 activity was calculated over the total protein amounts, as shown in Figure 39C and 39D. It was also considered an equal volume of samples for determining the SMPD3 activity (Figures 40A and 40D). The total concentration of proteins estimated from uninfected or ZIKV infected neurons or exosomes derived from these neurons are shown in Figures 40B and 40C for cells or Figures 40E and 40F for exosomes. At different time points post-infection, cell culture supernatants were collected and processed for exosome isolation. Both cell and exosomal lysates were resuspended in 1 × PBS and were frozen at −80°C. 50 µl was used for each time point sample (uninfected or ZIKV infected) as 6 replicates. Absorbance from assay samples were measured at 655 nm. Calculations were performed using the Zero blank sphingomyelinase standard that is considered as background blank. All readings were subtracted from the background values. Standard curves were plotted using the

standard values and the amount of active sphingomyelinase present in the samples was determined based on the standard curve.

Small Interfering RNA Transfections and Inhibitor Treatments

For siRNA transfections and silencing of *smpd3*, 1×10^6 of cortical neurons were plated in complete neurobasal medium, allowed to adhere overnight, and changed to half of the medium without FBS on next day. For the silencing of smpd3, specific siRNA (from Santa Cruz Biotechnologies, Inc.) were purchased and transfections were performed as per the manufacturer instructions and protocols. Cells were infected with ZIKV (MOI 5, at 72 h post-plating) and collected at 72 h p.i. Followed by RNA extractions and cDNA synthesis. The silencing efficiency of *smpd3* was analyzed by QRT-PCR. For inhibition of exosome release from neuronal cells, the selective inhibitor (GW4869) was used for Neutral Sphingomyelinase 2 (nSMase2 or SMPD3) (Santa Cruz Biotechnologies, Inc.) dissolved in DMSO. Cytotoxicity of the inhibitor was first analyzed; Neurons did not show any toxicity at tested doses (of 1-20 μM). For inhibitor studies, neurons (2×10^5 for RNA and 1×10^7 for protein extractions) were plated in complete neurobasal medium. Cortical neurons were treated with GW4869 inhibitor (5, 10 or 20 μM) for 4 h at 72 h post-plating, followed by ZIKV infection (5 MOI) at indicated time points (24, 48 and 72 h p.i., for both RNA and protein extractions). Cells treated with similar volume (the volume used was considered for 20-μM GW4869) of DMSO were considered as control groups. Viral loads were determined at all tested time points followed by QRT-PCR analysis. Both whole cells and exosomal lysates (30 μg) were processed for immunoblotting with 4G2 monoclonal antibody, followed by a secondary antibody to detect ZIKV E-protein.

Statistics

Using GraphPad Prism6 software and Microsoft Excel, the statistical significance of the difference observed in data sets were analyzed. Non-paired, two-tail Student *t*-test was used for the entire analysis. Error bars represent mean (+SD) values; P values of <0.05 were considered significant in all analyses. Statistical tests and P values are indicated for significance in all figures.

Ethics Statement

All animal work in this study was carried out in strict accordance with the recommendations in the Guide for the Care and Use of Laboratory Animals of the National Institute of Health. The approved protocol from the Institutional Animal Care and Use Committee (Animal Welfare Assurance Number: A3172-01) (permit number: 16-017) and the approved IBC protocol (number 12-014) were used in this study.

CHAPTER 4

CONCLUSION

Since it is poorly understood on molecular determinants and mechanisms of arthropod-borne *Flavivirus* transmission from vector to the vertebrate, our studies have been focused on this direction. LGTV and ZIKV were used as experimental models and the results showed for the first time that a cell line from medically significant arthropods, such as ticks and mosquitoes, secrete Extracellular Vesicles (EVs) including exosomes that mediate transmission of *Flavivirus* RNA and proteins to the human cells. With transmission via exosomes, infectious organisms such as LGTV and ZIKV, could invade host immune response and directly infect neighboring cells by endocytosis, resulting in causing severe damage to the host. For example, the harmful effects of ZIKA virus (ZIKV) infection is reflected by severe neurological manifestations, including microcephaly in neonates and other complications associated with Guillain-Barré syndrome in adults.

This study is the first to show that tick-borne Langat virus (LGTV), a model pathogen firmly related to tick-borne encephalitis virus (TBEV), profusely uses arthropod exosomes for the dissemination of viral material to the human-skin keratinocytes (HaCaT) and blood endothelial cells (HUVEC). Cryo-electron microscopy indicated the presence of purified arthropod/neurons-derived exosomes with the size range of 30 to 200 nm in diameter. Both positive- and negative-sense strands of LGTV RNA and viral envelope-protein were found inside exosomes derived from arthropod, murine and human cells. Detection of Nonstructural 1 (NS1) protein in arthropod and neuronal exosomes further indicated that exosomes enclose viral proteins. Viral RNA and proteins in exosomes derived from tick and mammalian cells were protected, highly infectious and replicative in all evaluations. Treatment with GW4869, a selective inhibitor that blocks exosome secretion, could affect LGTV loads in both arthropod and mammalian cell-derived exosomes. Trans-well-migration assays addressed that

exosomes derived from infected-brain-microvascular endothelial cells (served as the constitution of Blood-Brain Barrier) assisted LGTV RNA and protein transmission, crossing of the barriers and infection of neurons. The neuronal infection suggested abundant loads of both tick-borne Langat virus, LGTV and mosquito-borne West Nile virus RNA in exosomes. The result also indicated that exosome-mediated LGTV viral transmission is clathrin-dependent. This study provided a new mechanism of *Flaviviral* transmission and infection approach for researches to investigate and think about. It also provided a novel target, in the form of exosomes, and strategy to counter viral infection, pathogenesis and to develop a therapeutic treatment.

The transmission dynamics of ZIKV in or between neuronal cells, or within the developing brains of the fetus are not fully understood. The second study showed that using primary cultures of murine cortical neurons, ZIKV could use exosomes as mediators of viral transmission to disseminate infectious viral materials between neurons. Cryo-electron microscopy showed a heterogeneous population of neuronal exosomes with a size range of 30-200 nm. Increased formation of exosomes from neuronal cells was obtained upon ZIKV infection. Neuronal exosomes enclosed both ZIKV viral RNA and protein(s) that were severe infectious to naïve cells. Studies implemented with RNase A and neutralizing antibodies treatment studies addressed the presence of viral material inside exosomes. Exosomes derived from time- and dose-dependent incubations suggested increasing viral loads indicating increased packaging and delivery of ZIKV RNA and proteins.

Furthermore, it was noted that ZIKV induced both activity and gene expression of neutral Sphingomyelinase (nSMase)-2/SMPD3, an important molecule that regulates the production and release of exosomes. The silencing of SMPD3 in neuronal cells resulted in decreased viral burden and transmission via exosomes. Treatment with SMPD3 specific inhibitor GW4869, magnificently decreased ZIKV loads in both cortical neuronal cells and in exosomes derived from these neurons. Overall, these data indicate that ZIKV mediates SMPD3 activity in cortical neuronal cells for its infection and transmission via exosomes, perhaps leading to harsh neuronal death that may result in neurological phenomenon such as microcephaly in the developing embryonic brains.

Overall, these studies indicated that *flaviviruses* use arthropod-derived exosomes or exosomes from vertebrate cells as a novel approaches for infectious viral RNA and protein transmission from the vector to the host and dissemination with the host, respectively, that could eventually lead to neuro-invasion and neuropathogenesis.

REFERENCES

Ago, H., Oda, M., Takahashi, M., Tsuge, H., Ochi, S., Katunuma, N., Miyano, M., and Sakurai, J. (2006). Structural basis of the sphingomyelin phosphodiesterase activity in neutral sphingomyelinase from Bacillus cereus. J. Biol. Chem. *281*, 16157-16167.

Albi, E., Cataldi, S., Codini, M., Mariucci, G., Lazzarini, A., Ceccarini, M.R., Ferri, I., Laurenti, M.E., Arcuri, C., Patria, F.*, et al.* (2019). Neutral sphingomyelinase increases and delocalizes in the absence of Toll-Like Receptor 4: A new insight for MPTP neurotoxicity. Prostag. Oth. Lipid M. *142*, 46-52.

Alvarez, M.L., Khosroheidari, M., Kanchi Ravi, R., and DiStefano, J.K. (2012). Comparison of protein, microRNA, and mRNA yields using different methods of urinary exosome isolation for the discovery of kidney disease biomarkers. Kidney Int. *82*, 1024-1032.

Anderson, M.R., Kashanchi, F., and Jacobson, S. (2016). Exosomes in viral disease. Neurotherapeutics *13*, 535-546.

Apte-Sengupta, S., Sirohi, D., and Kuhn, R.J. (2014). Coupling of replication and assembly in *flaviviruses*. Curr. Opin. Virol. *9*, 134-142.

Arenaccio, C., Chiozzini, C., Columba-Cabezas, S., Manfredi, F., and Federico, M. (2014). Cell activation and HIV-1 replication in unstimulated CD4+ T lymphocytes ingesting exosomes from cells expressing defective HIV-1. Retrovirology *11*, 46.

Arthur, D.R. (1962). Ticks and disease (Oxford, England: Pergamon).

Aslan, M., Basaranlar, G., Unal, M., Ciftcioglu, A., Derin, N., and Mutus, B. (2014a). Inhibition of neutral sphingomyelinase decreases elevated levels of inducible nitric oxide synthase and apoptotic cell death in ocular hypertensive rats. Toxicol. Appl. Pharmacol. *280*, 389-398.

Aslan, M., Ozcan, F., Tuzcu, H., Kirac, E., and Elpek, G.O. (2014b). Inhibition of neutral sphingomyelinase decreases arachidonic acid mediated inflammation in liver ischemia-reperfusion injury. Int. J. Clin. Exp. Pathol. *7*, 7814-7823.

Baietti, M.F., Zhang, Z., Mortier, E., Melchior, A., Degeest, G., Geeraerts, A., Ivarsson, Y., Depoortere, F., Coomans, C., and Vermeiren, E. (2012). Syndecan-syntenin-ALIX regulates the biogenesis of exosomes. Nat. Cell Biol. *14*, 677.

Bang, C., and Thum, T. (2012). Exosomes: new players in cell-cell communication. Int. J. Biochem. Cell Biol. *44*, 2060-2064.

Barclay, R.A., Schwab, A., DeMarino, C., Akpamagbo, Y., Lepene, B., Kassaye, S., Iordanskiy, S., and Kashanchi, F. (2017). Exosomes from uninfected cells activate transcription of latent HIV-1. J. Biol. Chem. *292*, 14764.

Bates, M. (1949). The natural history of mosquitoes (New York : Macmillan).

Becker, N., Petric, D., Zgomba, M., Boase, C., Madon, M., Dahl, C., and Kaiser, A. (2010). Mosquitoes and their control (Springer Science & Business Media).

Black IV, W.C., Bennett, K.E., Gorrochótegui-Escalante, N., Barillas-Mury, C.V., Fernández-Salas, I., de Lourdes Muñoz, M.a., Farfán-Alé, J.A., Olson, K.E., and Beaty, B.J. (2002). *Flavivirus* susceptibility in *Aedes aegypti*. Arch. Med. Res. *33*, 379-388.

Bobrie, A., Colombo, M., Raposo, G., and Thery, C. (2011). Exosome secretion: molecular mechanisms and roles in immune responses. Traffic *12*, 1659-1668.

Brasil, P., Pereira Jr, J.P., Moreira, M.E., Ribeiro Nogueira, R.M., Damasceno, L., Wakimoto, M., Rabello, R.S., Valderramos, S.G., Halai, U.-A., and Salles, T.S. (2016). Zika virus infection in pregnant women in Rio de Janeiro. New Engl. J. Med. *375*, 2321-2334.

Brault, J.-B., Khou, C., Basset, J., Coquand, L., Fraisier, V., Frenkiel, M.-P., Goud, B., Manuguerra, J.-C., Pardigon, N., and Baffet, A.D. (2016). Comparative analysis between *flaviviruses* reveals specific neural stem cell tropism for Zika virus in the mouse developing neocortex. EBioMedicine *10*, 71-76.

Budnik, V., Ruiz-Cañada, C., and Wendler, F. (2016). Extracellular vesicles round off communication in the nervous system. Nat. Rev. Neurosci. *17*, 160.

Bukong, T.N., Momen-Heravi, F., Kodys, K., Bala, S., and Szabo, G. (2014). Exosomes from hepatitis C infected patients transmit HCV infection and contain replication competent viral RNA in complex with Ago2-miR122-HSP90. PLoS Pathog. *10*, e1004424.

Campos, G.S., Bandeira, A.C., and Sardi, S.I. (2015). Zika virus outbreak, bahia, brazil. Emerg. Infect. Dis. *21*, 1885.

Chambers, T.J., and Diamond, M.S. (2003). Pathogenesis of *flavivirus* encephalitis. Adv. Virus Res. *60*, 273-342.

Chivet, M., Hemming, F., Fraboulet, S., and Sadoul, R. (2012). Emerging role of neuronal exosomes in the central nervous system. Front. Physiol. *3*, 145.

Clarke, C.J., and Hannun, Y.A. (2006). Neutral sphingomyelinases and nSMase2: bridging the gaps. BBA-Biomembranes *1758*, 1893-1901.

Clements, A.N. (1992). The biology of mosquitoes. Volume 1: development, nutrition and reproduction (London: Chapman & Hall).

Colombo, M., Raposo, G., and Thery, C. (2014). Biogenesis, secretion, and intercellular interactions of exosomes and other extracellular vesicles. Annu. Rev. Cell Dev. Biol. *30*, 255-289.

Columba Cabezas, S., and Federico, M. (2013). Sequences within RNA coding for HIV‐1 Gag p 17 are efficiently targeted to exosomes. Cell Microbiol. *15*, 412-429.

Cosset, F.L., and Dreux, M. (2014). HCV transmission by hepatic exosomes establishes a productive infection. J. Hepatol. *60*, 674-675.

Couzin, J. (2005). Cell biology: The ins and outs of exosomes. Science *308*, 1862-1863.

Crans, W.J. (2004). A classification system for mosquito life cycles: life cycle types for mosquitoes of the northeastern United States. J. Vector Eco. *29*, 1-10.

Cvjetkovic, A., Lötvall, J., and Lässer, C. (2014). The influence of rotor type and centrifugation time on the yield and purity of extracellular vesicles. J. Extracell. Vesicles *3*, 23111.

Di Maio, V. (2008). Regulation of information passing by synaptic transmission: a short review. Brain Res. *1225*, 26-38.

Ding, M., Wang, C., Lu, X., Zhang, C., Zhou, Z., Chen, X., Zhang, C.Y., Zen, K., and Zhang, C. (2018). Comparison of commercial exosome isolation kits for circulating exosomal microRNA profiling. Anal. Bioanal. Chem. *410*, 3805-3814.

Dreux, M., Garaigorta, U., Boyd, B., Decembre, E., Chung, J., Whitten-Bauer, C., Wieland, S., and Chisari, F.V. (2012). Short-range exosomal transfer of viral RNA from infected cells to plasmacytoid dendritic cells triggers innate immunity. Cell Host Microbe *12*, 558-570.

Dutta, S., Celestine, M.J., Khanal, S., Huddleston, A., Simms, C., Arca, J.F., Mitra, A., Heller, L., Kraj, P.J., and Ledizet, M. (2018). Coordination of different ligands to copper (II) and cobalt (III) metal centers enhances Zika virus and dengue virus loads in both arthropod cells and human keratinocytes. BBA. General subjects *1862*, 40-50.

Essandoh, K., Yang, L., Wang, X., Huang, W., Qin, D., Hao, J., Wang, Y., Zingarelli, B., Peng, T., and Fan, G.-C. (2015). Blockade of exosome generation with GW4869 dampens the sepsis-induced inflammation and cardiac dysfunction. BBA. Molecular basis of disease *1852*, 2362-2371.

Faizan, M.I., Abdullah, M., Ali, S., Naqvi, I.H., Ahmed, A., and Parveen, S. (2016). Zika virus-induced microcephaly and its possible molecular mechanism. Intervirology *59*, 152-158.

Feinleib, M. (2001). A Dictionary of Epidemiology, -Edited by John M. Last, Robert A. Spasoff, and Susan S. Harris. Am. J. Epidemiol. *154*, 93-94.

Fevrier, B., and Raposo, G. (2004). Exosomes: endosomal-derived vesicles shipping extracellular messages. Curr. Opin. Cell Biol. *16*, 415-421.

Fragnoud, R., Flamand, M., Reynier, F., Buchy, P., Duong, V., Pachot, A., Paranhos-Baccala, G., and Bedin, F. (2015). Differential proteomic analysis of virus-enriched fractions obtained from plasma pools of patients with dengue fever or severe dengue. BMC Infect. Dis. *15*, 518.

Golding, N., Wilson, A.L., Moyes, C.L., Cano, J., Pigott, D.M., Velayudhan, R., Brooker, S.J., Smith, D.L., Hay, S.I., and Lindsay, S.W. (2015). Integrating vector control across diseases. BMC Med. *13*, 249.

Greenhill, C. (2013). Hepatitis: New route of HCV transmission. Nat. Rev. Gastroenterol Hepatol. *10*, 504.

Gritsun, T., Lashkevich, V., and Gould, E. (2003). Tick-borne encephalitis. Antivir. Res. *57*, 129-146.

Hannun, Y.A., and Obeid, L.M. (2002). The ceramide-centric universe of lipid-mediated cell regulation: stress encounters of the lipid kind. J. Biol. Chem. *277*, 25847-25850.

Haslwanter, D., Blaas, D., Heinz, F.X., and Stiasny, K. (2017). A novel mechanism of antibody-mediated enhancement of *flavivirus* infection. PLoS Pathog. *13*, e1006643.

Huang, Y., Li, Y., Zhang, H., Zhao, R., Jing, R., Xu, Y., He, M., Peer, J., Kim, Y.C., and Luo, J. (2018). Zika virus propagation and release in human fetal astrocytes can be suppressed by neutral sphingomyelinase-2 inhibitor GW4869. Cell Discov. *4*, 19.

Janas, A.M., Sapoń, K., Janas, T., Stowell, M.H., and Janas, T. (2016). Exosomes and other extracellular vesicles in neural cells and neurodegenerative diseases. BBA-Biomembranes *1858*, 1139-1151.

Johnstone, R.M. (2006). Exosomes biological significance: A concise review. Blood Cells Mol. Dis. *36*, 315-321.

Jongejan, F., and Uilenberg, G. (2004). The global importance of ticks. Parasitology *129*, S3-S14.

Jung, S.Y., Suh, J.H., Park, H.J., Jung, K.M., Kim, M.Y., Na, D.S., and Kim, D.K. (2000). Identification of multiple forms of membrane‐associated neutral sphingomyelinase in bovine brain. J. Neurochem. *75*, 1004-1014.

Kanninen, K., and Malm, T. (2016). Exosomes in cerebral diseases-novel form of intercellular communication. Duodecim *132*, 1957-1963.

Keller, S., Rupp, C., Stoeck, A., Runz, S., Fogel, M., Lugert, S., Hager, H.-D., Abdel-Bakky, M., Gutwein, P., and Altevogt, P. (2007). CD24 is a marker of exosomes secreted into urine and amniotic fluid. Kidney Int. *72*, 1095-1102.

Keller, S., Sanderson, M.P., Stoeck, A., and Altevogt, P. (2006). Exosomes: from biogenesis and secretion to biological function. Immunol. Lett. *107*, 102-108.

Khavandgar, Z., Poirier, C., Clarke, C.J., Li, J., Wang, N., McKee, M.D., Hannun, Y.A., and Murshed, M. (2011). A cell-autonomous requirement for neutral sphingomyelinase 2 in bone mineralization. J. Cell Biol. *194*, 277-289.

Kooijmans, S.A., Vader, P., van Dommelen, S.M., van Solinge, W.W., and Schiffelers, R.M. (2012). Exosome mimetics: a novel class of drug delivery systems. Int. J. Nanomedicine *7*, 1525-1541.

Kuhn, R.J., Dowd, K.A., Post, C.B., and Pierson, T.C. (2015). Shake, rattle, and roll: impact of the dynamics of *flavivirus* particles on their interactions with the host. Virology *479*, 508-517.

Labuda, M., Austyn, J.M., Zuffova, E., Kozuch, O., Fuchsberger, N., Lysy, J., and Nuttall, P.A. (1996). Importance of localized skin infection in tick-borne encephalitis virus transmission. Virology *219*, 357-366.

Labuda, M., and Randolph, S.E. (1999). Survival strategy of tick-borne encephalitis virus: cellular basis and environmental determinants. Zentralbl. Bakteriol. *289*, 513-524.

Lagunas-Rangel, F.A., Viveros-Sandoval, M.E., and Reyes-Sandoval, A. (2017). Current trends in Zika vaccine development. J. Virus Erad. *3*, 124.

Lang, J.K., Young, R.F., Ashraf, H., and Canty Jr, J.M. (2016). Inhibiting extracellular vesicle release from human cardiosphere derived cells with lentiviral knockdown of nSMase2 differentially effects proliferation and apoptosis in cardiomyocytes, fibroblasts and endothelial cells in vitro. PloS one *11*, e0165926.

Lenassi, M., Cagney, G., Liao, M., Vaupotič, T., Bartholomeeusen, K., Cheng, Y., Krogan, N.J., Plemenitaš, A., and Peterlin, B.M. (2010). HIV Nef is secreted in exosomes and triggers apoptosis in bystander CD4+ T cells. Traffic *11*, 110-122.

Li, H., Saucedo-Cuevas, L., Regla-Nava, J.A., Chai, G., Sheets, N., Tang, W., Terskikh, A.V., Shresta, S., and Gleeson, J.G. (2016). Zika virus infects neural progenitors in the adult mouse brain and alters proliferation. Cell Stem Cell *19*, 593-598.

Li, J., Liu, K., Liu, Y., Xu, Y., Zhang, F., Yang, H., Liu, J., Pan, T., Chen, J., and Wu, M. (2013). Exosomes mediate the cell-to-cell transmission of IFN-α-induced antiviral activity. Nat. Immunol. *14*, 793.

Li, L., Lok, S.-M., Yu, I.-M., Zhang, Y., Kuhn, R.J., Chen, J., and Rossmann, M.G. (2008). The *flavivirus* precursor membrane-envelope protein complex: structure and maturation. Science *319*, 1830-1834.

Lin, J., Li, J., Huang, B., Liu, J., Chen, X., Chen, X.-M., Xu, Y.-M., Huang, L.-F., and Wang, X.-Z. (2015). Exosomes: novel biomarkers for clinical diagnosis. Sci. World J. *2015*.

Liu, Z., Zhang, X., Yu, Q., and He, J.J. (2014). Exosome-associated hepatitis C virus in cell cultures and patient plasma. Biochem. Biophys. Res. Commun. *455*, 218-222.

Longatti, A. (2015). The Dual Role of Exosomes in Hepatitis A and C Virus Transmission and Viral Immune Activation. Viruses *7*, 6707-6715.

Madison, M.N., and Okeoma, C.M. (2015). Exosomes: Implications in HIV-1 Pathogenesis. Viruses *7*, 4093-4118.

Maxian, O., Neufeld, A., Talis, E.J., Childs, L.M., and Blackwood, J.C. (2017). Zika virus dynamics: When does sexual transmission matter? Epidemics *21*, 48-55.

Mellman, I. (1996). Endocytosis and molecular sorting. Annu. Rev. Cell Dev. Biol. *12*, 575-625.

Menck, K., Sönmezer, C., Worst, T.S., Schulz, M., Dihazi, G.H., Streit, F., Erdmann, G., Kling, S., Boutros, M., and Binder, C. (2017). Neutral sphingomyelinases control extracellular vesicles budding from the plasma membrane. J. Extracell. Vesicles *6*, 1378056.

Ming, G.-l., Song, H., and Tang, H. (2017). Racing to uncover the link between Zika virus and microcephaly. Cell Stem Cell *20*, 749-753.

Mitzel, D.N., Wolfinbarger, J.B., Long, R.D., Masnick, M., Best, S.M., and Bloom, M.E. (2007). Tick-borne *flavivirus* infection in Ixodes scapularis larvae: development of a novel method for synchronous viral infection of ticks. Virology *365*, 410-418.

Miyauchi, S., Kitagaki, J., Masumoto, R., Imai, A., Kobayashi, K., Nakaya, A., Kawai, S., Fujihara, C., Asano, Y., Yamashita, M*., et al.* (2017). Sphingomyelin Phosphodiesterase 3 Enhances Cytodifferentiation of Periodontal Ligament Cells. J. Dent. Res. *96*, 339-346.

Moreira, J., Peixoto, T.M., Siqueira, A.M.d., and Lamas, C.C. (2017). Sexually acquired Zika virus: a systematic review. Clin. Microbiol. Infec. *23*, 296-305.

Moudy, R.M., Zhang, B., Shi, P.-Y., and Kramer, L.D. (2009). West Nile virus envelope protein glycosylation is required for efficient viral transmission by Culex vectors. Virology *387*, 222-228.

Mukhopadhyay, S., Kuhn, R.J., and Rossmann, M.G. (2005). A structural perspective of the *flavivirus* life cycle. Nat. Rev. Microbiol. *3*, 13.

Musso, D., Roche, C., Robin, E., Nhan, T., Teissier, A., and Cao-Lormeau, V.-M. (2015). Potential sexual transmission of Zika virus. Emerg. Infect. Dis. *21*, 359.

Narayanan, A., Iordanskiy, S., Das, R., Van Duyne, R., Santos, S., Jaworski, E., Guendel, I., Sampey, G., Dalby, E., Iglesias-Ussel, M*., et al.* (2013). Exosomes derived

from HIV-1-infected cells contain trans-activation response element RNA. J. Biol. Chem. *288*, 20014-20033.

Nasci, R.S., Savage, H.M., White, D.J., Miller, J.R., Cropp, B.C., Godsey, M.S., Kerst, A.J., Bennett, P., Gottfried, K., and Lanciotti, R.S. (2001). West Nile virus in overwintering Culex mosquitoes, New York City, 2000. Emerg. Infect. Dis. *7*, 742.

Neal, J. (2014). *Flaviviruses* are neurotropic, but how do they invade the CNS? J. Infection *69*, 203-215.

Neelakanta, G., and Sultana, H. (2015). Transmission-blocking vaccines: focus on anti-vector vaccines against tick-borne diseases. Arch. Immunol. Ther. Ex. *63*, 169-179.

Nene, V., Wortman, J.R., Lawson, D., Haas, B., Kodira, C., Tu, Z.J., Loftus, B., Xi, Z., Megy, K., and Grabherr, M. (2007). Genome sequence of *Aedes aegypti*, a major arbovirus vector. Science *316*, 1718-1723.

Nuttall, P., and Labuda, M. (2003a). Dynamics of infection in tick vectors and at the tick-host interface. Adv. Virus Res. *60*, 233-272.

Nuttall, P.A., and Labuda, M. (2003b). Dynamics of infection in tick vectors and at the tick-host interface. Adv. Virus Res. *60*, 233-272.

Oh, Y., Zhang, F., Wang, Y., Lee, E.M., Choi, I.Y., Lim, H., Mirakhori, F., Li, R., Huang, L., and Xu, T. (2017a). Zika virus directly infects peripheral neurons and induces cell death. Nat. Neurosci. *20*, 1209.

Ohno, S., Ishikawa, A., and Kuroda, M. (2013). Roles of exosomes and microvesicles in disease pathogenesis. Adv. Drug Deliv. Rev. *65*, 398-401.

Olagnier, D., Muscolini, M., Coyne, C.B., Diamond, M.S., and Hiscott, J. (2016). Mechanisms of Zika virus infection and neuropathogenesis. DNA Cell Biol. *35*, 367-372.

Oliver, J.D., Chávez, A.S.O., Felsheim, R.F., Kurtti, T.J., and Munderloh, U.G. (2015). An Ixodes scapularis cell line with a predominantly neuron-like phenotype. Exp. Appl. Acarol. *66*, 427-442.

Organization, W.H. (2006). Pesticides and their application: for the control of vectors and pests of public health importance (Geneva: World Health Organization).

Organization, W.H. (2012). Handbook for integrated vector management (Geneva: World Health Organization).

Pant, S., Hilton, H., and Burczynski, M.E. (2012). The multifaceted exosome: biogenesis, role in normal and aberrant cellular function, and frontiers for pharmacological and biomarker opportunities. Biochem. Pharmacol. *83*, 1484-1494.

Patz, J.A., Epstein, P.R., Burke, T.A., and Balbus, J.M. (1996). Global climate change and emerging infectious diseases. Jama *275*, 217-223.

Qian, X., Nguyen, H.N., Jacob, F., Song, H., and Ming, G.-l. (2017). Using brain organoids to understand Zika virus-induced microcephaly. Development *144*, 952-957.

Randolph, S.E., Gern, L., and Nuttall, P.A. (1996). Co-feeding ticks: Epidemiological significance for tick-borne pathogen transmission. Parasitol. Today *12*, 472-479.

Raposo, G., and Stoorvogel, W. (2013). Extracellular vesicles: exosomes, microvesicles, and friends. J. Cell Biol. *200*, 373-383.

Regev-Rudzki, N., Wilson, D.W., Carvalho, T.G., Sisquella, X., Coleman, B.M., Rug, M., Bursac, D., Angrisano, F., Gee, M., Hill, A.F.*, et al.* (2013). Cell-cell communication between malaria-infected red blood cells via exosome-like vesicles. Cell *153*, 1120-1133.

Roberts, L.S., and Janovy, J. (2009). Gerald D. Schmidt & Larry S. Roberts' Foundations of Parasitology (Boston : McGraw-Hill).

Rumyantsev, A.A., Murphy, B.R., and Pletnev, A.G. (2006). A tick-borne Langat virus mutant that is temperature sensitive and host range restricted in neuroblastoma cells and lacks neuroinvasiveness for immunodeficient mice. J. Virol. *80*, 1427-1439.

Russo, F.B., and Beltrao-Braga, P.C.B. (2017). The impact of Zika virus in the brain. Biochem. Biophys. Res. Commun. *492*, 603-607.

Sampey, G.C., Saifuddin, M., Schwab, A., Barclay, R., Punya, S., Chung, M.C., Hakami, R.M., Zadeh, M.A., Lepene, B., Klase, Z.A.*, et al.* (2016). Exosomes from HIV-1-infected Cells Stimulate Production of Pro-inflammatory Cytokines through Trans-activating Response (TAR) RNA. J. Biol. Chem. *291*, 1251-1266.

Samuel, M.A., and Diamond, M.S. (2006). Pathogenesis of West Nile Virus infection: a balance between virulence, innate and adaptive immunity, and viral evasion. J. Virol. *80*, 9349-9360.

Schageman, J., Zeringer, E., Li, M., Barta, T., Lea, K., Gu, J., Magdaleno, S., Setterquist, R., and Vlassov, A.V. (2013). The complete exosome workflow solution: from isolation to characterization of RNA cargo. Biomed. Res. Int. *2013*, 253957.

Schey, K.L., Luther, J.M., and Rose, K.L. (2015). Proteomics characterization of exosome cargo. Methods *87*, 75-82.

Schmidt, K., Dressel, K., Niedrig, M., Mertens, M., Schüle, S., and Groschup, M. (2013). Public Health and Vector‐Borne Diseases-A New Concept for Risk Governance. Zoonoses Public Hlth. *60*, 528-538.

Schoepp, R.J., and Beaty, B.J. (1984). Titration of dengue viruses by immunofluorescence in microtiter plates. J. Clin. Microbiol. *20*, 1017-1019.

Schuler-Faccini, L. (2016). Possible association between Zika virus infection and microcephaly—Brazil, 2015. MMWR Morb. Mortal. Wkly. Rep. *65*.

Shapoval, A., Kamalov, I., Denisova, E., Sokolova, E., Luzin, P., Shamarina, A., Gusmanova, A., and Pinaeva, N. (1989). Study of the distant consequences of immunizing people with a live vaccine against tick-borne encephalitis. Tr. Inst. Im. Pastera *65*, 133.

Sherman, M.B., Freiberg, A.N., Holbrook, M.R., and Watowich, S.J. (2009). Single-particle cryo-electron microscopy of Rift Valley fever virus. Virology *387*, 11-15.

Sherman, M.B., Guenther, R.H., Tama, F., Sit, T.L., Brooks, C.L., Mikhailov, A.M., Orlova, E.V., Baker, T.S., and Lommel, S.A. (2006). Removal of divalent cations induces structural transitions in red clover necrotic mosaic virus, revealing a potential mechanism for RNA release. J. Virol. *80*, 10395-10406.

Smith, C.G. (1956). A virus resembling Russian spring-summer encephalitis virus from an ixodid tick in Malaya. Nature *178*, 581-582.

Sonenshine, D.E., and Roe, R.M. (2013). Biology of ticks, Vol 2 (New York: Oxford University Press).

Stanek, G., Burger, I., Hirschl, A., Wewalka, G., and Radda, A. (1986). Borrelia transfer by ticks during their life cycle: studies on laboratory animals. Zentralblatt für Bakteriologie, Mikrobiologie und Hygiene Series A: Medical Microbiology, Infectious Diseases, Virology, Parasitology *263*, 29-33.

Stoffel, W., Hammels, I., Jenke, B., Binczek, E., Schmidt‐Soltau, I., Brodesser, S., Schauss, A., Etich, J., Heilig, J., and Zaucke, F. (2016). Neutral sphingomyelinase (SMPD3) deficiency disrupts the Golgi secretory pathway and causes growth inhibition. Cell Death Dis. 7, e2488.

Stoffel, W., Jenke, B., Blöck, B., Zumbansen, M., and Koebke, J. (2005). Neutral sphingomyelinase 2 (*smpd3*) in the control of postnatal growth and development. P. Natl. Acad. Sci. USA *102*, 4554-4559.

Suen, W.W., Prow, N.A., Hall, R.A., and Bielefeldt-Ohmann, H. (2014). Mechanism of West Nile virus neuroinvasion: a critical appraisal. Viruses *6*, 2796-2825.

Sultana, H., Foellmer, H.G., Neelakanta, G., Oliphant, T., Engle, M., Ledizet, M., Krishnan, M.N., Bonafé, N., Anthony, K.G., and Marasco, W.A. (2009). Fusion loop peptide of the West Nile virus envelope protein is essential for pathogenesis and is recognized by a therapeutic cross-reactive human monoclonal antibody. J. Immunol. *183*, 650-660.

Sultana, H., Neelakanta, G., Foellmer, H.G., Montgomery, R.R., Anderson, J.F., Koski, R.A., Medzhitov, R.M., and Fikrig, E. (2012). Semaphorin 7A contributes to West Nile virus pathogenesis through TGF-β1/Smad6 signaling. J. Immunol. *189*, 3150-3158.

Sultana, H., Neelakanta, G., Kantor, F.S., Malawista, S.E., Fish, D., Montgomery, R.R., and Fikrig, E. (2010). Anaplasma phagocytophilum induces actin phosphorylation to selectively regulate gene transcription in Ixodes scapularis ticks. J. Exp. Med. *207*, 1727-1743.

Tauro, B.J., Greening, D.W., Mathias, R.A., Ji, H., Mathivanan, S., Scott, A.M., and Simpson, R.J. (2012). Comparison of ultracentrifugation, density gradient separation, and immunoaffinity capture methods for isolating human colon cancer cell line LIM1863-derived exosomes. Methods *56*, 293-304.

Thery, C. (2011). Exosomes: secreted vesicles and intercellular communications. F1000 Biol. Rep. *3*, 15.

Théry, C., Amigorena, S., Raposo, G., and Clayton, A. (2006). Isolation and characterization of exosomes from cell culture supernatants and biological fluids. Curr. Proto. Cell Biol. *30*, 3.22. 21-23.22. 29.

Thery, C., Zitvogel, L., and Amigorena, S. (2002). Exosomes: composition, biogenesis and function. Nat. Rev. Immunol. *2*, 569-579.

Vader, P., Breakefield, X.O., and Wood, M.J. (2014). Extracellular vesicles: emerging targets for cancer therapy. Trends Mol. Med. *20*, 385-393.

Van den Pol, A.N., Mao, G., Yang, Y., Ornaghi, S., and Davis, J.N. (2017a). Zika virus targeting in the developing brain. J. Neurosci. *37*, 2161-2175.

Van Niel, G., Porto-Carreiro, I., Simoes, S., and Raposo, G. (2006). Exosomes: a common pathway for a specialized function. J. Biochem. *140*, 13-21.

Villarroya-Beltri, C., Baixauli, F., Gutierrez-Vazquez, C., Sanchez-Madrid, F., and Mittelbrunn, M. (2014). Sorting it out: regulation of exosome loading. Semin. Cancer Biol. *28*, 3-13.

Vora, A., Taank, V., Dutta, S.M., Anderson, J.F., Fish, D., Sonenshine, D.E., Catravas, J.D., Sultana, H., and Neelakanta, G. (2017). Ticks elicit variable fibrinogenolytic activities upon feeding on hosts with different immune backgrounds. Sci. Rep-UK *7*, 44593.

Vora, A., Zhou, W., Londono-Renteria, B., Woodson, M., Sherman, M.B., Colpitts, T.M., Neelakanta, G., and Sultana, H. (2018). Arthropod EVs mediate dengue virus transmission through interaction with a tetraspanin domain containing glycoprotein Tsp29Fb. P. Natl. Acad. Sci. USA *115*, E6604-E6613.

Vreysen, M.J., Saleh, K.M., Ali, M.Y., Abdulla, A.M., Zhu, Z.-R., Juma, K.G., Dyck, V.A., Msangi, A.R., Mkonyi, P.A., and Feldmann, H.U. (2000). Glossina austeni (Diptera: Glossinidae) eradicated on the island of Unguja, Zanzibar, using the sterile insect technique. J. Econ. Entomol. *93*, 123-135.

Wang, A., Thurmond, S., Islas, L., Hui, K., and Hai, R. (2017a). Zika virus genome biology and molecular pathogenesis. Emerg. Microbes. Infect. *6*, e13.

Wen, Z., Song, H., and Ming, G.-l. (2017). How does Zika virus cause microcephaly? Gene Dev. *31*, 849-861.

Xiao, D., Ohlendorf, J., Chen, Y., Taylor, D.D., Rai, S.N., Waigel, S., Zacharias, W., Hao, H., and McMasters, K.M. (2012). Identifying mRNA, microRNA and protein profiles of melanoma exosomes. PLoS One *7*, e46874.

Xu, C.R., Li, L.C., Donahue, G., Ying, L., Zhang, Y.W., Gadue, P., and Zaret, K.S. (2014). Dynamics of genomic H3K27me3 domains and role of EZH2 during pancreatic endocrine specification. EMBO J. *33*, 2157-2170.

Zhang, J., Li, S., Li, L., Li, M., Guo, C., Yao, J., and Mi, S. (2015). Exosome and exosomal microRNA: trafficking, sorting, and function. GPB *13*, 17-24.

Zhao, H., Fernandez, E., Dowd, K.A., Speer, S.D., Platt, D.J., Gorman, M.J., Govero, J., Nelson, C.A., Pierson, T.C., and Diamond, M.S. (2016). Structural basis of Zika virus-specific antibody protection. Cell *166*, 1016-1027.

Zhou, W., Woodson, M., Neupane, B., Bai, F., Sherman, M.B., Choi, K.H., Neelakanta, G., and Sultana, H. (2018a). Exosomes serve as novel modes of tick-borne *flavivirus* transmission from arthropod to human cells and facilitates dissemination of viral RNA and proteins to the vertebrate neuronal cells. PLoS Pathog. *14*, e1006764.

APPENDIX

RIGHTS AND PERMISSIONS

Chapter 2

The content used in chapter 2 is published in PLOS Pathogen (PLOS), Title: *Exosomes serve as novel modes of tick-borne flavivirus transmission from arthropod to human cells and facilitates dissemination of viral RNA and proteins to the vertebrate neuronal cells* (https://doi.org/10.1371/journal.ppat.1006764). Some content and figures were modified to fit according to the chapter format. This article is published with open access under the terms of the Creative Common Attribution 4.0 International License (https://creativecommons.org/licenses/by/4.0/) which permits unrestricted use, distribution, and reproduction in any medium.

Chapter 3

The content used in chapter 3 is published in Emerging Microbes & Infections (Taylor & Francis Group), Title: *Exosomes mediate Zika virus transmission through SMPD3 neutral Sphingomyelinase in cortical neurons* (https://doi.org/10.1080/22221751.2019.1578188). Some content and figures were modified to fit according to the chapter format. This article is published with open access under the terms of the Creative Common Attribution 4.0 International License (https://creativecommons.org/licenses/by/4.0/) which permits unrestricted use, distribution, and reproduction in any medium.

VITA

WENSHUO ZHOU

Department of Biological Sciences, 110 Mills Godwin Life Science Building,
Old Dominion University, Norfolk VA-23529.

EDUCATION

- **Bachelor of Engineer, Bio-engineering: August 2011,** China Pharmaceutical University, Nanjing, P.R. China-211198.

CERTIFICATE AND TRAINING

- Poster presentation on “Exosomes Act as Novel Modes of Tick-Borne *Flavivirus* Transmission and Mediators of Neuroinvasion and Neuropathogenesis in Vertebrate Host”, American Society for Virology (ASV-2016).
- Poster presentation on “Exosomes Serve as Novel Modes of Tick-Borne *Flavivirus* Transmission from Arthropod to Human Cells and Facilitate Dissemination of Viruses to Vertebrate Neuronal Cells”, Extracellular RNA Communication Consortium (ERCC9-2017).

PEER-REVIEWED PUBLICATIONS

- **Zhou, W.,** Woodson, M., Neupane, B., Bai, F., Sherman, M.B., Choi, K.H., Neelakanta, G., Sultana, H. (2018) Exosomes serve as novel modes of tick-borne *flavivirus* transmission from arthropod to human cells and facilitates dissemination of viral RNA and proteins to the vertebrate neuronal cells. PLoS Pathog. 14 (1): e1006764.
- Vora, A., **Zhou, W.,** Londono-Renteria, B., Woodson, M., Sherman, M.B., Colpitts, T.M., Neelakanta, G., Sultana, H. (2018) Arthropod EVs mediate dengue virus transmission through interaction with a tetraspanin domain containing glycoprotein Tsp29Fb. Proc Natl Acad Sci USA.115 (28): E6604-E6613.
- Taank, V., **Zhou, W.,** Zhuang, X., Anderson, J.F., Pal, U., Sultana, H., Neelakanta, G. (2018) Characterization of tick organic anion transporting polypeptides(OATPs) upon bacterial and viral infections. Parasite Vectors. 11(1): p. 593.
- **Zhou, W.,** Woodson, M., Sherman, M.B., Neelakanta, G., Sultana, H., (2019) Exosomes mediate Zika virus transmission through SMPD3 neutral Sphingomyelinase in cortical neurons. Emerging Microbes & Infections. 8:1, 307-326.